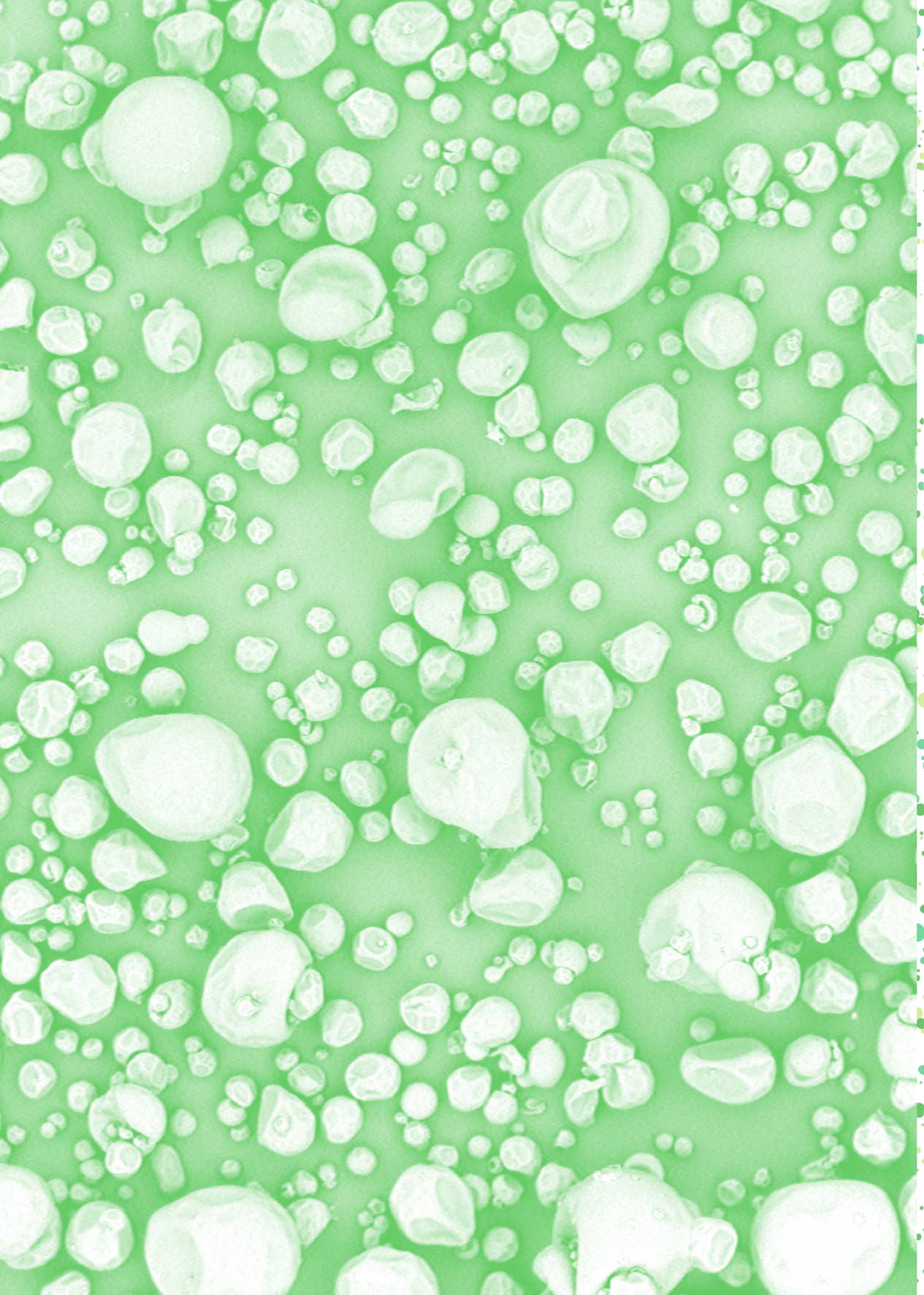

POWDER MORPHOLOGY DEVELOPMENT DURING SPRAY DRYING

POWDER MORPHOLOGY DEVELOPMENT DURING SPRAY DRYING

ELINE M. BOTH

ELINE M. BOTH

Powder Morphology Development during Spray Drying

Eline M. Both

Thesis committee

Promotors

Dr Maarten A.I. Schutyser
Associate professor, Food Process Engineering
Wageningen University & Research

Prof. Dr Remko M. Boom
Professor of Food Process Engineering
Wageningen University & Research

Other members

Prof. Dr E. van der Linden, Wageningen University & Research
Prof. Dr P. Först, Technical University München, Germany
Dr J. Schröder, Danone, Utrecht
Dr V. van Steijn, Technical University Delft

This research was conducted under the auspices of the Graduate School VLAG (Advanced studies in Food Technology, Agrobiotechnology, Nutrition and Health Sciences).

Powder Morphology Development during Spray Drying

Eline M. Both

Thesis

submitted in fulfilment of the requirements for the degree of doctor
at Wageningen University
by the authority of the Rector Magnificus,
Prof. Dr A.P.J. Mol,
in the presence of the
Thesis Committee appointed by the Academic Board
to be defended in public
on Friday 5 July 2019
at 1:30 p.m. in the Aula

Eline M. Both

Powder Morphology Development during Spray Drying

130 pages

PhD thesis, Wageningen University, Wageningen, the Netherlands (2019)

With references, with summary in English

ISBN 978-94-6343-992-3

DOI 10.18174/477793

Contents

Chapter 1	General introduction	7
Chapter 2	Morphology development during sessile single droplet drying of mixed maltodextrin and whey protein solutions	17
Chapter 3	Morphology development during single droplet drying of mixed component formulations and milk	35
Chapter 4	The role of viscosity in morphology development during single droplet drying	53
Chapter 5	Drying kinetics and viscoelastic properties of concentrated thin films as a model system for spray drying	73
Chapter 6	General Discussion	91
	References	107
	Summary	117
	Acknowledgements	123
	About the author	125
	Publications	127
	Training activities	129

1

General introduction

1.1. Introduction

Drying is a major unit operation in many industries; among these are the food, feed, ceramics, wood, paper, and waste water industry. Drying provides extended shelf-life to products, contributes to the functional product properties, and facilitates storage and transportation. About 85% of the currently applied drying technologies rely on convective drying, during which a wet product is usually dried by exposure to hot air (Mujumdar, 2015). Other, less applied drying technologies rely on heat transfer by conduction or radiation. The most frequently used convective dryers in the food industry are tunnel dryers, spray dryers, and fluidized bed dryers. Tunnel dryers are used for drying of larger solid foods, for example fruit and vegetable pieces, where the products move on a tray or conveyer belt through a tunnel with hot air. Spray dryers are used for drying of liquid formulations: here, the liquid is atomized in small droplets, ~10 to 100 µm in diameter, and dried by exposure to hot air. Because of the small droplet size, the drying time is usually short, 5 to 30 seconds. In fluidized bed dryers, a product is dried in a fluidized bed by hot air, and is therefore only suitable for solid products with a small particle size. Fluidized bed dryers are often applied after spray drying to remove the last bits of moisture and cool the spray-dried powder to room temperature.

Spray drying is frequently applied in the dairy industry. About 50% of the produced milk in for example France is converted into spray dried products and the worldwide production of spray-dried whole milk powder exceeds 5 million ton per year (Schuck et al., 2016). During many ingredient manufacturing processes, aqueous (by)streams are concentrated and spray dried into a storage stable powder to be further used in food or feed applications. Spray dried ingredients are for example plant protein concentrates that can be used to prepare meat analogues, starch to be used in soups and sauces, and milk and egg powder used to make cookies or ice cream. Spray-dried formulations can also be directly sold to consumers; examples are infant formula and coffee creamer, while spray dried amorphous lactose is used as a matrix material in many pharmaceutical tablets.

Spray dried powders have superior quality due to, amongst others, the limited exposure to heat and the high and controllable degree of agglomeration. Although typical inlet air temperatures are 180-220°C, the product temperature remains relatively low due to evaporative cooling. Therefore, there is only limited product degradation during drying. Moreover, the reconstitution and flowability of spray-dried powders can be excellent. Rapid

reconstitution properties are a necessity for instant beverages aimed at consumers, while good flowability is important for handling and filling packages with the powder. Besides the degree of agglomeration, also the morphology of the primary powder particle influences the reconstitution behavior and flowability (Bumiller et al., 2002; X. Fu et al., 2012; Takeiti et al., 2010). However, the morphology development, especially as function of material composition and drying conditions, has not yet been the subject of in-depth scientific study. Due to the currently limited mechanistic understanding, developing novel spray-dried product formulations with desired quality properties is still often a very empirical endeavor. Since the drying behavior of a new product is currently hard to predict, inefficient trial-and-error approaches are used to establish optimum drying conditions.

Better understanding of the morphology development is expected not only to contribute to improved powder quality, but can also improve the efficiency of spray drying operations. Specifically, lack of control on the particle formation and stickiness behavior increases the risk of fouling in spray drying towers, which leads to unnecessary downtime and loss of material. Narrowing windows of operation by having a better grip on the process could facilitate more efficient drying operations.

A disadvantage of spray drying is its relatively large energy use, having a thermal efficiency between 20% and 51% (RVO, 2015). The Dutch food and beverage industry uses annually ~60 PJ fossil fuel energy for drying operations, contributing to ~30% of the total fossil fuel energy use (Berenschot, 2017). The energy efficiency of a spray dryer may be improved by recovering heat from the outgoing moist air, for example by dehumidification of the outgoing air by zeolite wheels and thus recovering the latent heat otherwise emitted into the environment (Moejes et al., 2018); however the regeneration of the zeolites is energy intensive. The recovered heat can be upgraded in quality and used again for drying by using heat pump technology. Recent developments in heat pump technology make application of heat pumps in combination with spray drying realistic (Moejes et al., 2018).

An alternative approach to realize more energy efficient drying operations is to replace the existing technology with different or intensified drying technology. Though still an immature technology, a recent development is vortex chamber spray drying (Tourneur et al., 2018). In this technology, droplets are dried in a rotating fluidized bed, where high-G conditions enhance heat and mass transfer and agglomerated powders may be created. Another approach is to replace spray drying by a conductive drying technology, which has a higher

efficiency, but operates at the boiling temperature, which increases the thermal load on a product. Conductive technologies such as agitated thin film drying can be operated at reduced pressure, which make the drying process milder (Qiu et al., 2018), but this makes the process also more capital intensive. Finally, many other drying technologies such as infrared drying or microwave assisted drying have been proposed for drying of foods, but these are not always suitable for drying of liquid formulations nor have sufficient capacity to facilitate large-scale production. In addition, the use of electricity for heating purposes is not efficient.

Even though spray drying is a well-established technology for drying of liquid food formulations, the scientific understanding of the development of the particle morphology during spray drying is lacking. This knowledge is highly relevant for the powder product properties and for improving the efficiency of spray drying operations. In the following sections, the morphology development mechanisms during spray drying will be discussed in more detail (1.2). Different methods to study the morphology are reviewed (1.3). Finally, the research objective and an overview of this thesis are provided (1.4).

1.2. Morphology development during spray drying

In general, solid or solidifying components during spray drying can be classified into three types (Walton and Mumford, 1999):

I. Components that form a skin at the surface durig drying, for example milk or gelatin;
II. Components that crystallize during drying, for example several types of salt;
III. Components that agglomerate during drying; insoluble, suspended materials such as silica.

Most food components are skin-forming, and therefore only these mechanisms are described in detail here. As water evaporates, the surface of the droplet recedes, leading to an increasing solute concentration near the surface. This results in a driving force for diffusion of solutes away from the surface, where smaller components, such as lactose, have a faster diffusion rate than larger components, such as proteins (Meerdink and van't Riet, 1995). The ratio between the evaporation of water and the diffussion of components is defined in the Peclet number $Pe = \frac{\kappa}{8\,D}$, with κ the evaporation rate and D the diffusion coefficient (Vehring et al., 2007). If Pe >> 1, the evaporation dominates, the concentration

near the surface increases over time and a skin is formed. When more water evaporates, the skin grows thicker and denser and eventually the particle starts to solidify.

The differences between the morphologies of spray dried powders can be large (Fig. 1.1). Casein powder particles are wrinkled spheres, lactose particles are partially crystallised and fragmented, maltodextrin particles are fragmented and whey protein particles are hollow spheres. More complex solutions like skim and whole milk form porous spherical and agglomerated particles.

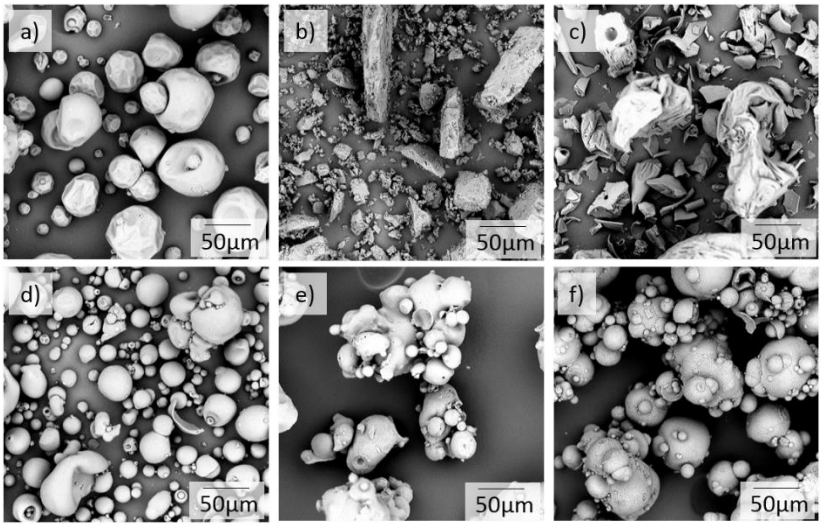

Fig. 1.1. Morphology of industrial dried powders, with a) micellar casein, b) lactose, c) maltodextrin DE12, d) whey protein, e) skim milk, f) whole milk.

1.3. Single droplet drying as a research approach

Droplets dried in a spray dryer have a wide particle size distribution and are exposed to varying drying trajectories, i.e. air temperature and residence time. Furthermore, the fast drying kinetics makes it impractical to follow the drying process over time; only the final powder can be analyzed. Therefore single droplet drying methods are employed to monitor droplet drying in time, with controlled drying conditions. Understanding the morphology development during single droplet drying can help to develop knowledge-based guidelines for spray drying.

Although the first single droplet drying experiment to understand spray drying originates from 1952 by Ranz and Marshall, the topic regained interest in the last decades. Several

Table 1.1. An overview of research on morphology development using single droplet drying (adapted from Schutyser et al., 2018).

	Author	Studied component	Set-up	Parameter range	Effect on morphology
Composition	Sadek et al., 2014	Micellar casein and whey protein	Sessile pendant droplet	Different protein ratios	Casein: wrinkled, whey: vacuole
	Tran et al, 2017	Lactose, whey protein, skim milk	Suspended droplet	Different protein / lactose ratios	More rigid crust with high protein
Initial dry matter (DM)	Bouman et al., 2016	Whey protein	Sessile droplet	5 to 30 % (w/w)	Lower DM wrinkled, higher DM vacuole
	Wu et al., 2014	Skim milk	Free-flying droplet	33 to 54 % (w/w)	Lower DM wrinkled, higher DM vacuole
	Rogers et al., 2012	Skim milk	Free-flying droplet	4% to 40%	More extensive buckling at low DM
Air temperature (T)	Bouman et al., 2016	Whey protein	Sessile droplet	20°C, 40°C, 60°C, and 80°C	No effect on morphology
	Rogers et al., 2012	Fresh skim milk	Free-flying droplet	120 to 140°C	Low T wrinkled, high T vacuole
	Tran et al., 2017	Lactose	Suspended droplet	60 to 180 °C	Low T, shriveled with small cavities High T, larger single cavity
Air humidity	Sadek et al., 2016	Micellar casein	Sessile pendant droplet	2% and 40%	No effect on morphology
	Griesing et al., 2016	Mannitol	Acoustic levitation	1%, 5%, 10% and 15%	Increasing air humidity led to a decrease in porosity

single droplet drying methods are used, for example using acoustic levitation, pendant droplet, free-flying droplet, and sessile droplet. However, due to the larger droplet size (~ 1-2 mm) and lower drying temperatures employed during single droplet drying, the drying usually takes several minutes. This is a major difference with industrial spray drying processes where drying occurs within a few seconds.

Single droplet drying studies have been carried out on measuring the drying kinetics (e.g. Adhikari et al., 2000) and on the phase separation dynamics of solutes during drying (e.g. Nuzzo et al., 2015). The development of the morphology has been studied with single droplet drying (SDD), in which the effect of the composition, the initial dry matter content, the air temperature, and the air humidity, on the morphology development was studied (Table 1.1).

In this thesis a sessile single droplet dryer is used (Fig. 1.2a), which was originally developed by Perdana to study the inactivation of bacteria and enzymes during drying (Perdana et al., 2011). This SDD approach is well suitable to study the development of the morphology, as the droplet can be positioned in the focal plane of a camera and the drying of the droplet is not disturbed by the presence of an acoustic field or filament. The influence of the conductive heat transfer via the contact area during drying was estimated to be less than 5% of the total heat transfer (Perdana et al., 2011) and thus has only minor influence.

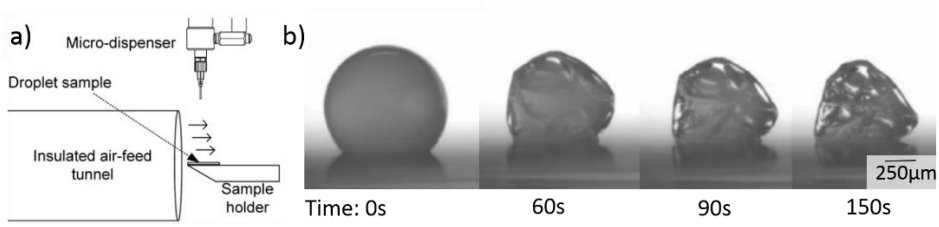

Fig. 1.2. Sessile single droplet drying as developed by Perdana, with a) a schematic overview of the set-up, and b) a time lapse of a drying maltodextrin droplet with an initial dry matter content of 20% (w/w), dried with hot air of 80°C and 0 g/kg humidity with a velocity of 0.2 m/s (image adapted from (Perdana et al., 2013b, 2011).

1.4. Objective and outline of the thesis

The main objective of the research in this thesis was to create mechanistic understanding of the development of the morphology of drying droplets. This was divided into two main research questions:

1. By what mechanisms do the drying conditions and product composition determine the skin formation and subsequent morphology development?
2. Can the rheological properties of components at high concentration explain the morphology development during drying?

To answer these research questions multiple methods were employed (Fig. 1.3). Single droplet drying was used to observe the development of the morphology, thin film drying was used to study the skin formation and its effect on the drying kinetics, and rheology was used to measure the properties of model formulations. In the following paragraphs a detailed description of the approach per chapter is given.

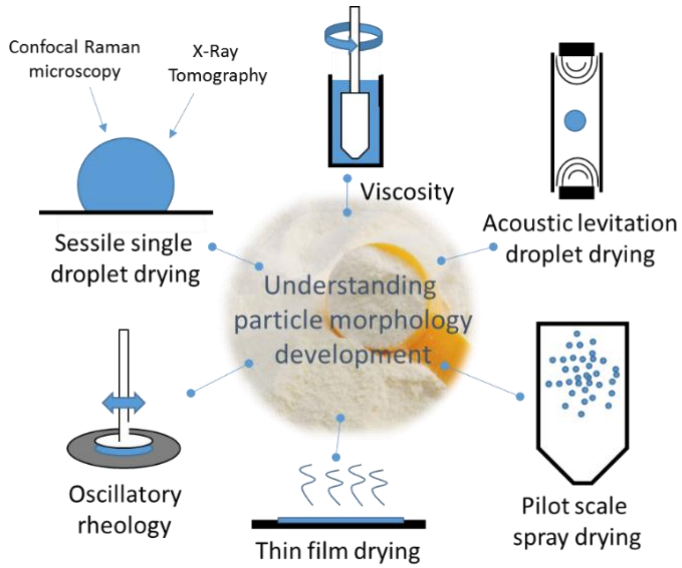

Fig. 1.3. Schematic overview of the methods used in this thesis. Images not drawn to scale.

In **chapter 2** the influence of the drying temperature and droplet composition on the formed particle morphology is studied. For mixtures of maltodextrin DE12 and whey protein, the drying of a single droplet is followed in time. First the evaporation rate during the constant drying rate period is evaluated, followed by the locking point and subsequent morphology development. Finally, the internal structure of the dried particles is analyzed using X-ray tomography and confocal Raman microscopy.

This is extended with the drying of micellar casein and lactose, and eventually to the drying of whole milk in **chapter 3**, which shows that understanding the drying behavior of model components provides insight on the drying of more complex solutions. Furthermore, a short comparison between two single droplet drying methods is provided, i.e. sessile single droplet drying and acoustic levitation drying.

Chapter 4 continues with maltodextrin and whey protein, however, this time the effects of the initial droplet size and dry matter content are studied. Especially the latter provides insight on the skin formation during drying, and therefore these results are combined with rheological experiments. The viscosity profile upon concentration gives insight on the critical solids concentrations needed for skin formation.

In **chapter 5** a different approach is chosen to study the drying behavior, using thin films as a model system. First, the drying kinetics are measured using a specially developed thin film dryer. Subsequently, the viscoelastic properties of nearly dried films are studied. These two methods combined, provide insight in the relation between the rheology and the morphology development during single droplet drying.

A general discussion on the results of this thesis is presented in **chapter 6**. Furthermore, the results from this thesis are compared with the particle morphology obtained with a pilot scale spray dryer, and the effect of the morphology on the final powder characteristics is analyzed. This shows the importance of looking at drying from a combined product and process perspective, and shows the industrial relevance of the project.

2

Morphology development during sessile single droplet drying of mixed maltodextrin and whey protein solutions

This chapter has been published as Both, E.M., Karlina, A.M., Boom, R.M., Schutyser, M.A.I., 2018. Morphology development during sessile single droplet drying of mixed maltodextrin and whey protein solutions. Food Hydrocolloids 75, 202–210.

Abstract

A sessile single droplet drying method is employed to gain understanding on spray drying behavior of mixed maltodextrin and whey protein solutions. Skin formation and subsequent locking of the skin and morphology development were the main aspects studied. Droplets of initial solids content of 30% (w/w), containing maltodextrin DE12 and whey protein in varying ratios were dried at temperatures ranging between 40°C and 90°C at a sessile droplet drying platform. The droplet composition did not influence the initial drying rate or locking point, but had major influence on the morphology of the final particle. Particles with high amount of whey protein and/or dried at low temperatures were smooth and spherical with one large vacuole, whereas high maltodextrin concentrations and/or high temperature particles gave a wrinkled surface and multiple vacuoles. Results suggest that composition and drying temperature have a strong influence on particle morphology, and can be altered to steer morphology. Skin formation being a determining factor in morphology development in whey protein-rich systems is explained by sol-gel transition and in maltodextrin-rich systems by reaching a viscosity value that leads to critical skin rigidity.

2.1. Introduction

Spray drying is a commonly used technique in the food and pharmaceutical industry to produce powdered products. It is a relatively mild technique that allows for high throughput. A spray dried powder virtually always features a complex, porous matrix, in which immiscible materials are finely distributed. The particle morphology is the result of a very complex and dynamic process during which the components migrate and removal of the water becomes increasingly difficult over time, because the matrix from which the water is removed becomes more and more concentrated. It is challenging to study particle morphology development on an industrial scale, due to the scale of the equipment, the fast-drying kinetics, and polydispersity of the droplets. Therefore, single droplet drying is often used as a technique to study drying at a particle level. The main disadvantage of the method is the larger droplet size than in spray drying, and therefore the drying kinetics are slower. However, several studies have shown the relevance of single droplet drying for studying spray drying, regarding to drying kinetics and particle morphology (N. Fu et al., 2012a; Sadek et al., 2015b).

There are several methods available to study single droplet drying, namely levitation drying methods, free flight drying methods and sessile droplet drying methods (Schutyser et al., 2012). We here use a sessile single droplet drying platform that allows careful monitoring of the evolution of the drying droplet into a powder particle as a function of time. The droplet is dried with a convective air flow, of which the speed is comparable to the relative speed of the droplet and the air during spray drying. The main disadvantage of sessile single droplet drying is the contact of the droplet with the platform. To minimize the contact area, the droplet is deposited on a hydrophobic membrane. The effect of conductive heat transfer between the platform and the droplet on the drying process is estimated to be less than 5% of the total heat transfer, and therefore most heat transfer occurs through convection (Perdana et al., 2011).

The particle morphology of a powder is an important characteristic to study, since it influences the bulk density, particle size, particle surface area and porosity. Therefore, it can influence the reconstitution behavior of a powder (Takeiti et al., 2010). The particle morphology has been studied in detail before, for example by Walton and Mumford, who distinguish three types; i.e. materials with a skin-like structure, a crystalline structure, and an agglomerate structure (Walton and Mumford, 1999). Skin-forming materials lead to the

formation of solid, hollow, shriveled or porous particles, depending on the drying temperature and materials. Several parameters have an influence on the morphology development during drying, namely the droplet size, the composition of the original solution (Bylaitë et al., 2001; Sadek et al., 2014), the initial solids content (Bouman et al., 2016; Wu et al., 2014), air temperature (Alamilla-Beltrán et al., 2005; Maas et al., 2011), and air humidity (Griesing et al., 2016; Sadek et al., 2016). While several parameters have been examined independently of each other, their correlations have not been studied in detail.

The objective of the current study is to extend the previous work by studying the combined effects of component ratio and drying temperature on the drying kinetics and final morphology in a model system of maltodextrin with a dextrose equivalent (DE) of 12 and whey protein. The effect of component ratio is relevant if it is desired to translate the acquired insight to more realistic product formulations. Most previous studies focused on drying behavior of only whey protein or maltodextrin solutions. For whey protein solutions it was found that both single droplet drying and laboratory spray drying led to formation of hollow particles with a so-called vacuole (Bouman et al., 2016; Sadek et al., 2014). Several studies reported that drying of maltodextrin solutions below 100°C yields a wrinkled particle morphology (Alamilla-Beltrán et al., 2005; Perdana et al., 2013a), where drying at higher temperatures leads to a smooth particle morphology (Alamilla-Beltrán et al., 2005). In practice for industrially processed maltodextrin powders various types of morphologies can be found, e.g. spherical, cylindrical, wrinkled, or irregular, depending on molecular weight distribution of the formulation and applied process conditions such as type of atomizer and air temperatures (Takeiti et al., 2010).

2.2. Materials and methods

2.2.1. Solutions

Protein solutions were prepared by adding whey protein isolate (WP) powder (~94% protein, <1% fat, <1% lactose, ~4% ash, Friesland Campina, the Netherlands) to demineralized water and subsequent stirring overnight. Sugar solutions are prepared by adding maltodextrin (MD) with a dextrose equivalent of 12 (Roquette, France) to demineralized water and stirring for 30 minutes. Both solutions have a concentration of 30% (w/w) and are mixed in the following mass ratios; 100:0, 75:25, 50:50, 25:75, 10:90,

5:95 or 0:100 (WP:MD). Compositions are given on a dry matter basis. The ratios 90:10 and 95:5 were not included in this study, since the influence of whey protein on the morphology is larger than the effect of maltodextrin DE12. The viscosities of the prepared component solutions were measured using a double-gap measuring system (DG26.7, MCR301, Anton Paar GmbH, Germany) at a shear rate gradient of 1 to 100 s^{-1} at 20°C. The solutions all behaved Newtonian with viscosity values of 0.016 Pa.s (0:100), 0.016 Pa.s (5:95), 0.018 Pa.s (50:50), 0.022 Pa.s (75:25), and 0.026 Pa.s (100:0 WP:MD).

2.2.2. Drying of droplets

A sessile droplet drying platform (Fig. 2.1), as described by Perdana et al. (2011), is used to study the morphology during drying (Perdana et al., 2011). The droplet is deposited by a pneumatic micro-dispenser (Nordson Engineering Dispensing, USA) on a hydrophobic membrane to retain the spherical shape (Polypropylene, Akzo Nobel Faser Ag., The Netherlands). The droplet is dried in a heated air flow (RH = 0%) of a temperature between 40°C and 90°C and a velocity of 0.3 m/s. Experiments were stopped one minute after the last visible morphology change, which ranged from 2 minutes when drying at 90°C to 10 minutes when drying at 40°C. Droplet size and shape are recorded by a µEye 1480ME CCD camera (Imaging Development systems GMBH, Germany) at a frame rate of 0.5 fps. Six replicates were dried for each composition-temperature combination, however only droplets with an initial radius of 500 µm +/- 50 µm were included in the data analysis to exclude initial droplet size effects. Therefore, the morphology pictures and data analysis correspond to 2 to 5 duplicates (table 2.1).

Table 2.1. The number of replicates per composition (WP:MD) and air temperature (°C)

		Composition (WP:MD)						
		100:0	75:25	50:50	25:75	10:90	5:95	0:100
Air temperature (°C)	40		3	5	3	4	5	
	50		3	5	3	3	3	
	60		2	6	4	3	4	
	70	4	3	4	5	3	4	5
	80		4	3	2	3	4	
	90		2	5	3	3	3	

2.2.3. Particle analysis

Droplet size evolution during the constant drying rate period was extracted from the recorded video using the image processing toolbox from Matlab (Mathworks, USA). The scale was determined by correlating the number of pixels of the needle to its actual size, which is 225µm. The image was then converted to a binary image to facilitate automatic boundary recognition by the software. In the binary image a circle was fitted to the boundary between the droplet and air. The base of the droplet, i.e. the boundary between membrane and droplet, was manually inserted in the software (Fig. 2.2). From the fitted circle and baseline, the droplet height, radius and base length was calculated. Assuming a spherical droplet, the droplet volume was calculated by the spherical cap formula:

$$V = \frac{\pi h^2}{3}(3R - h) \qquad [2.1]$$

With V the volume of the droplet (µm^3), h the height of the droplet (µm), and R the droplet radius (µm).

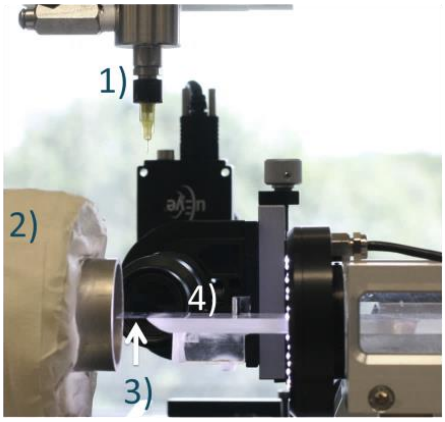

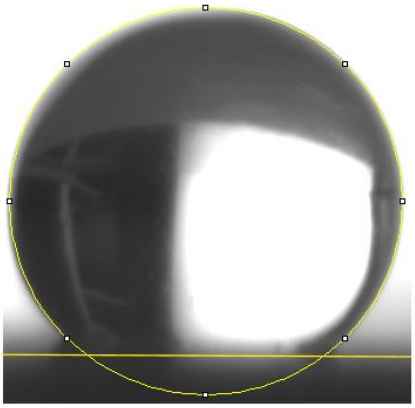

Fig. 2.1. (left) Sessile droplet platform with (1) microdispenser with a needle tip, (2) Insulated air tunnel, (3) Sample holder, (4) µEye camera.
Fig. 2.2. (right) Automatic boundary detection with an image analysis routine implemented in Matlab. The detected circumference of the droplet and the manually inserted boundary between droplet and membrane are visualized in yellow.

Selected dried particles were visualized with X-ray tomography (XRT), scanning electron microscopy (SEM), and/or confocal Raman microscopy (CRM). The drying conditions of the selected particles are specified below the figures. For XRT and SEM one representative particle was used, where for CRM two particles were scanned at two locations to ensure

reproducibility. The XRT scans were performed with an X-ray microfocus CT system (Phoenix v[tome]x m, General Electric, USA). 3D structures were calculated via back projection (Phoenix datos|x reconstruction software, General Electric, USA) and images were reconstructed with Avizo software (version 8.0, FEI, USA). For SEM analysis, samples were fixed on the sample holder by carbon adhesive tabs and sputter coated with 15 nm of tungsten. SEM images were taken at 2 KV, 6.3 pA, using a Magellan 400 field emission scanning electron microscope (FEI, Eindhoven, the Netherlands). CRM was performed with a WITec alpha300 system in combination with a 785 nm laser for excitation and a 100x objective with an NA of 0.95 (WITec, Germany). This resulted in a lateral resolution of 500 µm and a vertical resolution of 600 µm. The scan size of the images was 25µm (width) by 25µm (depth). The integration time per Raman spectrum was 100 milliseconds.

2.3. Results and discussion

This section is subdivided into three parts, starting with (I) initial drying behavior, (II) skin formation, and (III) final particle morphology, followed by a more detailed study of internal composition.

2.3.1. Part I: Initial drying behavior

Drying starts with external, air-side limitation to mass and heat transfer; this is referred to as the ideal drying or constant drying rate period. Because mass transfer is externally limited, it is expected that the composition does not influence the water evaporation rate at this point. The constant drying rate can be described by the "radius squared law" given by (Jakubczyk et al., 2012):

$$r^2(t) = r_0^2 - \kappa\, t \qquad [2.2]$$

With r the droplet radius (m), r_0 the initial droplet radius (m) and κ the drying rate ($m^2.s^{-1}$). The squared radius has a linear relationship with time when the drying is constant, and therefore analysis was stopped when deviating from linearity. The calculated drying rates for each composition at each drying temperature are plotted in Fig. 2.3. Per temperature, a one-way ANOVA was performed to examine the effect of composition on the evaporation rate. There were no significant differences found (α=0.05) between droplets of different composition dried at the same temperature, except for the droplets with ratio 5:95 (WP:MD) dried at 50°C, which were found to have a significantly larger evaporation rate that is most likely due to experimental errors. Given this almost constant evaporation rate

regardless of the composition, we can assume that indeed ideal drying was observed at the beginning of drying. The standard deviation of the measurements became larger with higher air temperature, since the duration of the initial ideal drying period decreases and thus less data points were obtained to accurately determine κ. The drying rate can only be indirectly determined in the set-up used, i.e. by monitoring the decrease in particle size via image analysis. This is acceptable during initial drying, but becomes unreliable after skin formation when diffusion-limited drying starts.

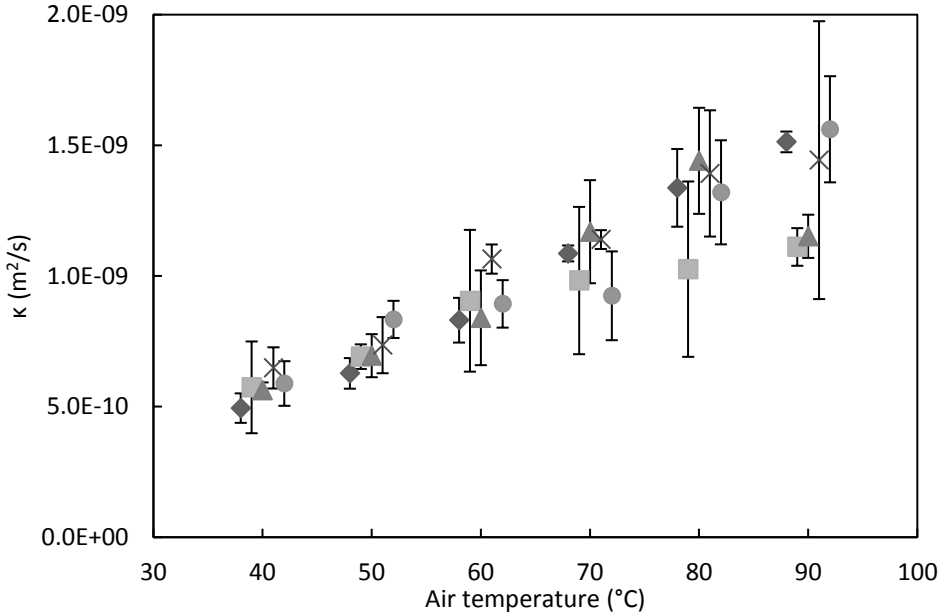

Fig. 2.3. Drying rate κ during the constant drying rate period, as a function of drying air temperature for different droplet compositions: (◆) 75:25, (■) 50:50, (▲) 25:75, (✕) 10:90, (●) 5:95 (WP:MD). To enhance visibility the temperatures on the x-axis were shifted with a maximum of 2°C. The drying rate κ was calculated according to the "radius squared law" as given by Jakubczyk et al. (2012).

2.3.2. Part II: Skin formation

The dimensionless Péclet number is defined as the ratio of the drying rate and the solute diffusivity in the droplet, and describes whether drying is uniform or not (Vehring et al., 2007). The Péclet number of drying droplets can be calculated by:

$$Pe = \frac{\kappa}{8\,D} \qquad [2.3]$$

With κ the drying rate ($m^2.s^{-1}$), and D the diffusion coefficient of the solute in the liquid phase ($m^2.s^{-1}$). When drying at Pe>>1, as is the case in this study, the evaporation of water leads to a gradual increase of the solids concentration near the surface, which eventually leads to skin formation. The time at which the skin starts to hinder the evaporation marks the transition point from the constant drying rate regime to the falling drying rate regime. For the understanding of drying after skin formation, it is important to consider the temperature of the drying air. With air temperatures above the boiling temperature of the solvent, then vapor formation can cause bubble nucleation during the falling rate period. This will lead to a pressure increase in the droplet followed by a so-called 'blow hole", i.e. vacuole formation from inside to outside (Bouman et al., 2016), or particle inflation/deflation cycles (Tran et al., 2016). In this study air temperatures did not exceed 90°C, and the pressure in the droplet progressively decreases due to a decrease in solvent volume internally by evaporation through the skin. However, bubble formation inside a drying droplet during the falling rate regime may occur as well below the atmospheric boiling temperature due to the reduced internal pressure (Pauchard and Couder, 2004). During drying the formed skin will develop in time and will eventually reach a point, referred to as the locking point, where shrinking comes to an arrest due to the strength of the developed skin. The strength of this developed skin will determine to what extent it can resist the difference between the internal pressure and the atmospheric pressure, and thus what kind of morphology is formed. The degree of bending of the skin can vary from small invaginations to formation of complete vacuoles, depending on the skin properties (Vehring, 2008). For weak skins, the skin will bend and buckle under the pressure, creating a wrinkled particle. Particles with a fully rigid skin cannot bend under external pressure, but will develop a defect at the weakest point of the skin and to subsequent vacuole formation from this defect (Sadek et al., 2014; Sugiyama et al., 2006). A theoretical study showed that vacuole formation reduces the elastic energy of the skin (Meng et al., 2014).

In Fig. 2.4 three time series of drying droplets with different component ratios are shown, which were dried with air of 70°C. Fig. 2.4a shows a drying droplet containing only whey protein (MD:WPI 0:100). At first ideal shrinking could be observed; however the drying was not symmetrical up to the locking point. In the set-up used, the airflow was coming from one side since the droplet is fixed. The upstream side of the droplet experienced a slightly higher air temperature, which led to more local water evaporation. Therefore at the upstream side the critical skin concentration was attained faster in comparison to the

downstream side. The moment at which the critical skin concentration was reached at the upstream side is referred to as the partial locking point and occurred for particle in Fig. 2.4a after approximately 45 seconds. After 60 seconds the downstream side of the droplet locked as well and a vacuole started to form; this point is referred to as the overall locking point. This occurred at the bottom of the downstream side, where the skin was weakest due to the slowest evaporation, and then bent under the external pressure. Fig. 2.4c is an example of a time series of a wrinkling droplet (WP:MD 10:90). In this case we did not observe pronounced asymmetric drying, but instead after approximately 60 seconds the first morphological change was wrinkling at the downstream side of the airflow. Eventually, due to the deformable skin a fully wrinkled particle was formed. To demonstrate the effect of mixed components, in Fig. 2.4b an example is given of a droplet containing maltodextrin and whey protein in equal ratios. After a period of asymmetric drying, both wrinkling of the skin and vacuole formation were observed, although the latter less pronounced compared to pure whey protein. Vacuole formation started 60 seconds after the onset of drying which indicated that despite the excess protein, the maltodextrin had an important influence on the morphology development.

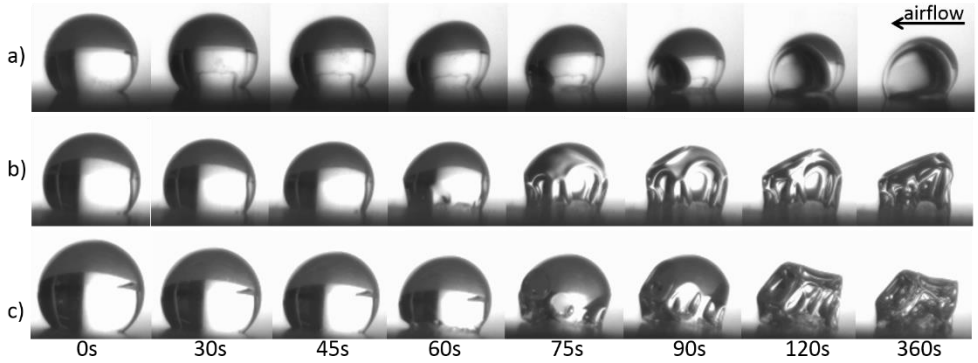

Fig. 2.4. Morphology development in time for three droplets with different composition; a) 100:0, b) 50:50, c) 10:90 (WP:MD). All droplets were dried at 70°C. The air flow came from the right side as indicated by an arrow.

From the time series, three important events could be distinguished during formation of particle morphology; the partial locking point, the overall locking point and the development of the final particle morphology. Depending on the set-up used, the locking point can be identified in different ways, e.g. the time when the evaporation rate starts to decrease, when the droplet diameter becomes constant or visually from camera images

(Tran et al., 2016). In this study, the partial locking point is defined as the point where the droplet becomes asymmetric and the overall locking point is defined as the starting point of morphology development. Both could be best determined visually from camera images. Droplets dried at 70°C were analyzed on their partial and overall locking point (Fig. 2.5), and the remaining droplet volume at that point respectively (Fig. 2.6). Droplets with more protein tend to reach the partial locking point earlier in the drying process and at a larger radius, relative to the droplets that were higher in maltodextrin. These droplets eventually attained locking slightly later, but with the same relative remaining volume as the other droplets. For the droplets high in maltodextrin there seemed not to be a partial locking point, and immediately full locking occurred. These results suggested that in the period before locking, the evaporation rates already started to differ, and hence that the locking point was not equal to the transition point from constant to falling evaporation rates. However, due to the high variance between the droplets and the small differences, these trends were not unambiguous.

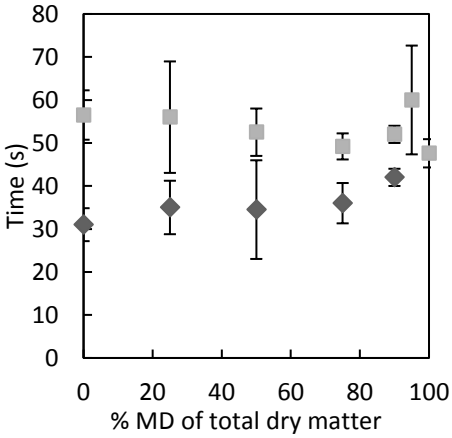

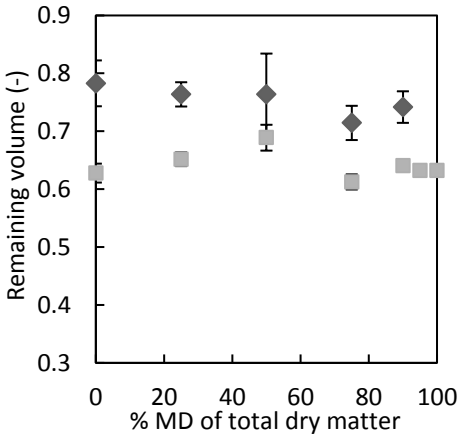

Fig. 2.5. (left) Partial locking point time (◆) and overall locking point time (■).
Fig. 2.6. (right) Remaining volume relative to the original volume (R/R_0) at the partial locking point (◆) and at the overall locking point (■). The droplets had varying composition, dried at 70°C. The partial locking point was not observed for compositions 5:95 and 0:100 (WP:MD) and are therefore not included in the graph. Composition is annotated on the x-axis as % MD of total dry matter, i.e. 25% corresponds to a composition of 75:25 (WP:MD).

The overall locking point was investigated for different combinations of composition and temperature (Fig. 2.7). For the samples dried at low temperatures, i.e. 40°C, 50°C, and 60°C

the droplets with a high protein content had a later overall locking point time. The lines converged at higher air temperatures, and no differences could be discerned between the different compositions anymore. In part III of this paper, it is shown that samples with a later locking point, also showed different final morphology, where samples with a later locking point were likely to have a smooth and hollow morphology.

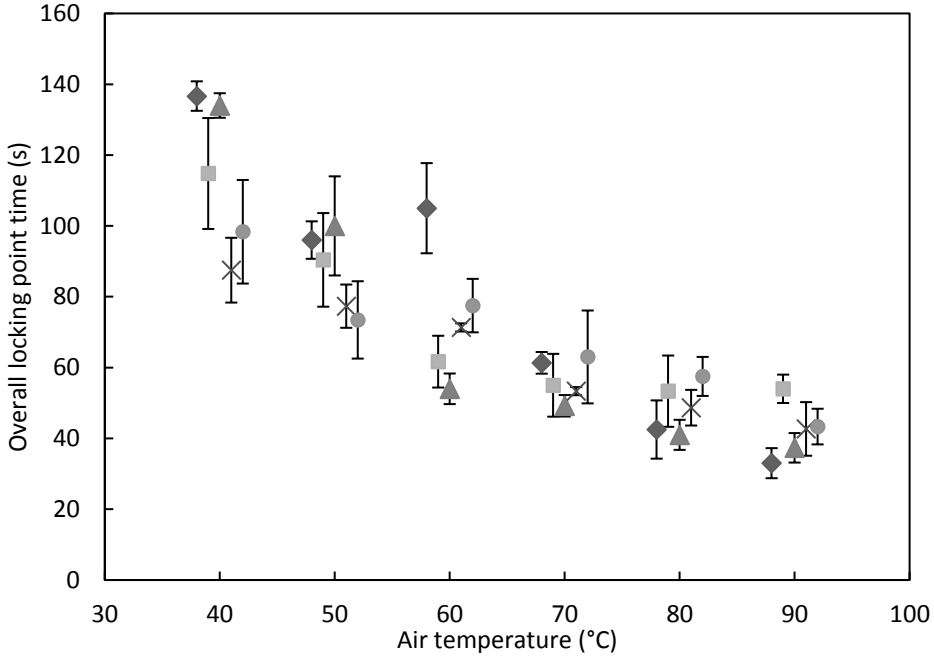

Fig. 2.7. Overall locking point time (seconds) as a function of the drying temperature and droplet composition; (◆) 75:25, (■) 50:50, (▲) 25:75, (✕) 10:90, (●) 5:95 (WP:MD). The temperature on the x-axis is shifted with maximum 2°C to enhance visibility. The overall locking point time is defined as the moment of first visible skin formation.

2.3.3. Part III: Final particle morphology development

After the overall locking point of the droplet, a pressure difference builds up between the inside and outside of the droplet due to the continued evaporation of water and the skin properties determine the morphological changes. The final particle morphology is an indicator for the typical rigidity of the skin during drying, which is expected to be a function of the drying temperature and the droplet composition. In Fig. 2.8 the final particle morphologies are shown for several drying temperatures (vertical-axis) and different component ratios (horizontal-axis). Solutions containing higher concentrations of protein

(left hand side) formed particles with a single large vacuole, whereas solutions with more maltodextrin yielded wrinkled particles, which corresponds to earlier observations in laboratory spray drying experiments (Bylaitë et al., 2001).

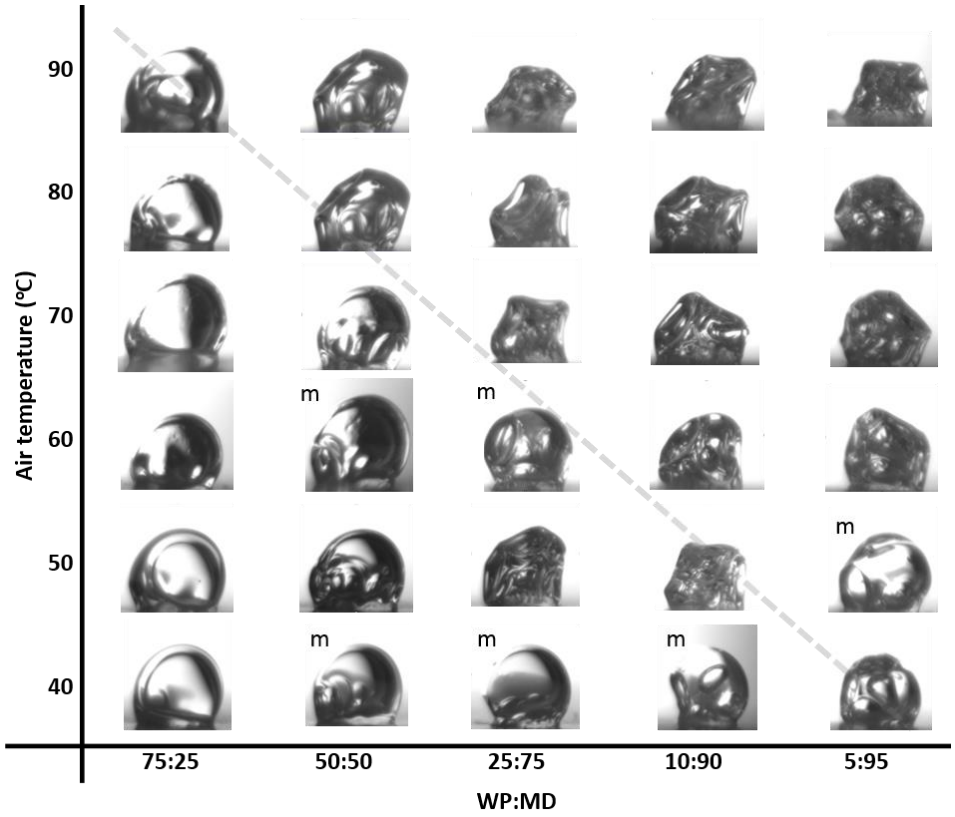

Fig. 2.8. Morphology diagram. The final particle morphology is depicted as a function of the drying temperature (°C) and composition (WP:MD). (m) indicates multiple morphologies were observed, with the most prevalent morphology pictured. The line is drawn to guide the eye.

The effect of temperature can be observed clearly for droplets with a component ratio of 50:50 (WP:MD), which formed hollow particles when dried at low temperatures (up to 70°C) and wrinkled particles when dried at higher temperatures (80°C and 90°C). For the solutions richer in MD we also observed a temperature effect, although all particles were wrinkled; at higher drying temperatures particles became less transparent which suggests heterogeneity in the matrix. Generally speaking, we found smooth particles and clear samples dried at low temperature and/or with high protein ratio and more turbid wrinkled

particles when dried at high temperature and/or high maltodextrin ratio. For some conditions we observed that both types of morphology occurred for different particles dried at the same conditions (indicated with the letter m in Fig. 2.8). We hypothesize that these conditions were close to the transition, and that small variations in for example initial size, contact angle with the membrane, and drying conditions may gave rise to sufficiently different skin properties during drying and therefore different particle morphology. In future the insight on morphology development may be used for better operation of industrial spray drying processes, where both drying conditions and product composition are variables to control morphology.

For colloidal suspensions the mechanism behind skin formation is assumed to consist of a sol-gel transition of the colloidal particles in the skin (Sugiyama et al., 2006; Tsapis et al., 2005). Continuous evaporation of water leads to increased pressure drop across the capillaries that exist in the gel phase. Initially, the shrinkage of a drying droplet will be isotropic, where the viscous nature of the skin still dominates. However, when the skin thickens at some point the pressure drop overcomes the repulsive forces between the colloidal particles leading to sol-gel transition. At this point the skin will start to lock. Sadek et al. (2015) conclude that whey proteins behave as small hard colloidal spheres upon drying and will form brittle plastic skins after the sol-gel transition.

The morphology development of drying maltodextrin droplets is found highly dependent on the maltodextrin chain length (Takeiti et al., 2010). Maltodextrin DE12 molecules have on average an ovoid-like shape in solution (Avaltroni et al., 2004) and will not gel, since the chain length is sufficiently small (Chronakis et al., 1996). During the drying of maltodextrin the viscosity in the droplet becomes higher due to an increase in concentration (Dokic et al., 1998), which will reduce the diffusion of water towards the surface (Adhikari et al., 2005; Perdana et al., 2014). This means that the evaporation rate goes down and thus the effect of evaporative cooling goes down. This will cause an increase in droplet temperature, which leads to a decrease in viscosity (Dokic et al., 1998). Due to this decrease in viscosity the diffusion will increase again, and the drying continues. This continuous cycle effectively causes the droplet temperature to slowly rise with increasing viscosity. At a certain viscosity, the skin is no longer capable to shrink and a locking point is observed. However, we hypothesize that the skin was still deformable, contradictory to whey protein skins, since it did not undergo glass transition or sol-gel transition at this point. When whey protein and

maltodextrin mixtures were dried, the interaction of the two components is of interest. It is hypothesized that the maltodextrin polymers disturb the sol-gel transition of the colloidal proteins, thus weakening the matrix, which will result in wrinkled particles. Only high amounts of protein, and/or slow drying rates give the protein opportunity to form a gel network, which can provide strength to the matrix and lead to the formation of hollow particles.

The mechanisms behind skin formation determine the resistance that the skin can provide against deformation. However, measuring the skin strength during droplet drying is complex and has not been attempted by many authors yet. Only Sadek *et al.* (2015) have investigated the relationship between particle morphology, concentration at the time of buckling, and indentation resistance of film layers for native casein and whey protein solutions. Their single droplet drying experiments showed wrinkled particles for casein and hollow particles for WPI, where the concentrations of proteins in the skin at the moment of buckling were found to be 156 $g.L^{-1}$ for casein and for WPI 414 $g.L^{-1}$, respectively. Lastly, in their study films were prepared with an a_w of 0.4 and thickness of 5 mm showing stiffer material and higher relaxation time for native caseins than whey proteins (Sadek et al., 2015a). On the one hand the results suggested that both the mechanical properties of the skin and the skin thickness are of importance upon buckling. On the other the indirect approach of this study in measuring skin strength made it difficult to correlate these properties at the appropriate conditions.

2.3.4. 3D analysis of the morphology

Fig. 2.8 shows a wide array of different morphologies, from which six particles with a distinct morphology were selected to visualize the internal structure by X-ray tomography (Fig. 2.9). Three different internal morphologies were observed, i.e. one large vacuole with opening to the outside, one large vacuole without opening to the outside, and multiple smaller vacuoles. Generally speaking, increasing temperature and MD content did lead to the formation of more, but smaller vacuoles without connection to the outside. Previous research on drying of whey protein droplets showed particles with large vacuoles always connected to the outside air (Bouman, 2016), which is here occasionally found for droplets high in whey protein (e.g. Fig. 2.9b), but not exclusively. This type of vacuole develops when the skin is pulled in from the weakest spot. Also large vacuoles without connection to the outside are observed (e.g. Fig. 2.9a and 2.9c). The low internal pressure will facilitate an air

flow inwards, which will result in bubble growth inside the droplet (Pauchard and Couder, 2004). However, if the connection to the outside is present, but small, it may not have been detected by XRT having a resolution of ~10µm. The particles with a very rigid skin, thus a hollow morphology (Fig. 2.9a and 2.9b), showed a uniform skin thickness, which was independent of air flow direction. Lastly, particles dried at high temperature and containing more maltodextrin tended to have multiple smaller vacuoles. The viscosity of the maltodextrin bulk solution might be high enough to prevent extensive bubble coalescence. Also, many of the high maltodextrin samples were cracked, which indicates that the pressure difference was higher than the dry shell could withstand.

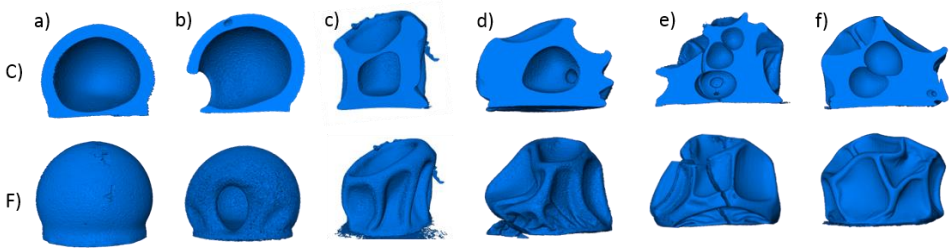

Fig. 2.9. XRT images of final particle morphologies with (C) cross-section, (F) front view, with varied air temperature and composition (WP:MD); (a) 75:25 at 40°C (1 vacuole), (b) 50:50 at 50°C (2 vacuoles), (c) 50:50 at 70°C (1 vacuole), (d) 25:75 at 60°C (3 vacuoles), (e) 10:90 at 70°C (5 vacuoles), and (f) 1:99 at 90°C (6 vacuoles). Between brackets is the number of vacuoles observed with XRT, not all are visible in the current cross-section.

2.3.5. Phase separation

When drying multi-component systems, the skin properties will be influenced by phase separation of the components. Phase separation causes the skin properties to differ from the bulk properties, and it can be influenced by initial composition and the drying temperature. From the morphology images, we have observed that different drying temperatures, and thus different drying rates, led to various morphologies for the same composition. Confocal Raman microscopy was used as a tool to visualize the influence of drying temperature. CRM shows the clearest pictures when the sample shows a high extend of phase separation. Therefore droplets with a ratio of 5:95 (WP:MD) were visualized, since they were most likely to fully phase separate. The droplets were dried with air of 40°C, 50°C and 90°C to investigate the phase separation at different drying temperatures. The particle dried with air of 40 °C showed a transition particle which is mostly smooth with small wrinkles (Fig. 2.10a), whereas the particles dried with air of 50°C and 90°C were wrinkled

(Fig. 2.10b and 2.10c). The droplet dried slowest with air of 40 °C showed a phase separated system, with spots of protein in a maltodextrin matrix and enriched protein at the surface. At an air temperature of 50°C the drying was faster and allowed for less phase separation, although still protein enriched zones could be observed. For the sample dried with air of 90°C no phase separation was visible.

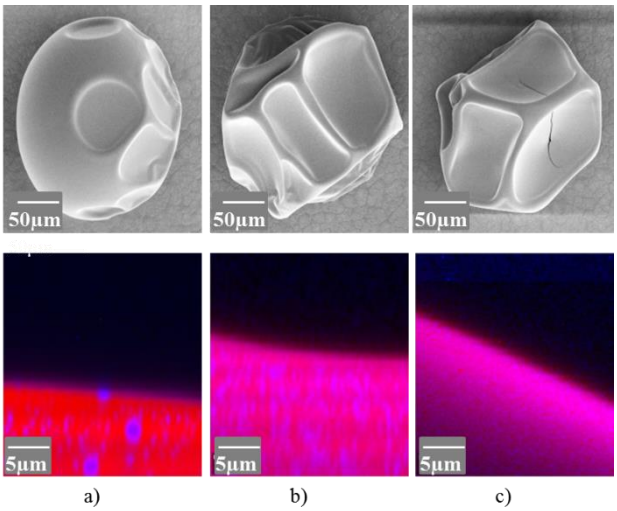

Fig. 2.10. Scanning electron microscope (top) and confocal Raman (bottom) images of particles with a component ratio of 5:95 (WP:MD) which were dried at (a) 40°C (b) 50°C and (c) 90°C. The confocal Raman images show the distribution of WPI (blue) and maltodextrin (red).

Protein enrichment at the surface is often attributed to the surface activity of the protein (Adhikari et al., 2009; Fäldt et al., 1993; Nuzzo et al., 2015b). The extent of protein enrichment at the surface is also influenced by the drying rate, where lower drying rates allow more phase separation (Chew et al., 2014). In general, molecules with a larger hydrodynamic radius have a slower diffusion rate (Wu et al., 2014), which is in this case whey protein (~17kDa) compared to maltodextrin DE12 (Mn = 1500 $g.mol^{-1}$, Mw = 15000 $g.mol^{-1}$, (Castro et al., 2016)). Furthermore, the high viscosity of the droplet reduces the diffusion rate, and therefore phase separation is slow. Besides the drying speed, the temperature itself may also affect phase separation since higher temperatures lead to better miscibility of components. However, this effect is assumed to be small since the droplet temperature is uniform and at the wet bulb temperature, which is 14°C, 19°C or 29°C when drying at 40°C, 50°C or 90°C at 0% RH. The confocal Raman microscopy results

confirmed that slower drying resulted in more extensive phase separation, and it is hypothesized that proteins dominate the skin properties and morphology at slow drying due to phase separation, despite the low initial amounts.

2.4. Conclusion

Particle morphology is often seen as an inevitable result of drying, however in this research we show that it can be influenced by processing conditions. Therefore, the effect of particle composition and drying temperature on particle morphology were investigated by drying droplets having different ratios of maltodextrin and whey protein at several temperatures. Although the initial drying kinetics were only a result of drying temperature, the particle morphologies evolve in interaction with droplet composition and drying temperature. Droplets with a high concentration of protein yielded smooth and hollow particles, whereas particles with more maltodextrin were wrinkled and had multiple smaller vacuoles. Particles dried at lower temperatures were more likely to form hollow particles, whereas particles dried at higher temperature had the tendency to become wrinkled with fixed ratio of maltodextrin to whey protein. Skin formation and subsequent morphology development in drying whey protein solutions is explained to arise from jamming and a subsequent sol-gel transition in the colloidal whey protein system and for maltodextrin from reaching a viscosity value that leads to critical skin rigidity. Morphology development arising from skin formation in mixed systems of whey protein and maltodextrin was extensively characterized in this study and provides a thorough basis for understanding the complex drying behavior. Underlying skin formation mechanisms, influenced by the interactions between whey protein and maltodextrin in relation to drying conditions are however not yet understood and require further characterization of mixed systems. The gained insight in this study should ultimately allow industry to better control particle morphology and thus particle functionality in spray drying processes. This will lead to better products with enhanced functionalities.

3

Morphology development during single droplet drying of mixed component formulations and milk

This chapter has been published as Both, E.M., Nuzzo, M., Millqvist-Fureby, A., Boom, R.M., Schutyser, M.A.I., 2018. Morphology development during single droplet drying of mixed component formulations and milk. Food Res. Int. 109, 448–454.

Abstract

We report on the influence of selected components and their mixtures on the development of the morphology during drying of single droplets and extend the results to the morphology of whole milk powder particles. Sessile single droplet drying and acoustic levitation methods were employed to study single droplet drying. The influence of carbohydrates (lactose and maltodextrin DE12) and proteins (micellar casein or whey protein) on morphology development is very different, since upon concentration protein systems will jam and undergo a colloidal glass transition, whereas carbohydrate systems will gradually increase in viscosity as a consequence of the concentration. Whey protein gives relatively rigid shells due to jamming of the 'hard sphere' proteins, while casein micelles behave as 'soft spheres' that can deform after jamming, which gives flexibility to the shell during drying. The influence of the carbohydrates on the final morphology was found much larger than the influence of the proteins. Caseins influenced morphology only in mixtures with lactose at higher concentrations due to its high voluminosity. Similar observations were done for whole milk, where fat appeared to have no influence. With maltodextrin the influence of the casein was again observed in the shape and smoothness of wrinkles. Both sessile and levitated droplet drying methods provide a similar and consistent view on morphology development.

3.1. Introduction

During spray drying, a powdered product is formed by dehydration of droplets of a solution. The physical properties of powders that result from this process, such as the bulk density and particle size influence the application behavior of the powders, such as the reconstitution (Takeiti et al., 2010) or the flow properties (Fu et al., 2012). Therefore, understanding the drying behavior of ingredient formulations is of crucial importance for producing high quality powdered products.

A common approach to study spray drying in detail is single droplet drying. Various single droplet drying techniques are available and described in several reviews (Fu, Woo, & Chen, 2012; Sadek et al., 2015; Schutyser, Perdana, & Boom, 2012). Single droplet drying has been applied to obtain more insight on drying kinetics (Che, Li, & Chen, 2012; Fu, Woo, Selomulya, et al., 2012; Malafronte, Ahrné, Schuster, Innings, & Rasmuson, 2015), the stickiness of a drying particle (Adhikari et al., 2017), the surface composition of a dried particle (Fu, Woo, & Chen, 2011; Nuzzo, Millqvist-Fureby, Sloth, & Bergenstahl, 2015), and development of the morphology (Both, Karlina, Boom, & Schutyser, 2018; Sadek, Tabuteau, & Schuck, 2013). The morphology of single component solutions has been studied extensively before, e.g. maltodextrin and casein form wrinkled particles, and whey protein forms smooth particles with a large internal vacuole (Both et al., 2018; Bouman, Venema, de Vries, van der Linden, & Schutyser, 2016; Sadek et al., 2014). However, it is not yet known how these components interact to form the final morphology of powder particles from complex mixtures, and why. Therefore we here concentrate on extending the mechanisms of particle formation for single ingredients towards understanding of the morphology obtained from complex systems.

Selected components were lactose and maltodextrin DE12 as carbohydrates, and micellar casein and whey protein as proteins. Lactose, casein and whey protein are major milk components, while maltodextrin was included to investigate the effect of carbohydrate chain length on morphology. The ratios between the selected carbohydrates and proteins were varied to systematically study the influence on morphology of the different components in the mixed systems. Subsequently, whole milk droplets were dried to gain understanding in the morphology development of complex systems. Here two single droplet drying techniques were evaluated, namely sessile droplet drying and acoustic levitation. Both methods have their pros and cons in mimicking droplet drying during actual

spray drying. For example, the acoustic field during acoustic levitation is known to influence the shape of the droplets and the drying kinetics, leading to higher heat and mass transfer coefficients compared to free-falling droplets (Yarin et al., 1999). In sessile droplet drying contact between the platform and the droplet affects the spherical shape and air flow around the droplet, although the estimated influence of the conduction between the platform and the droplet was maximum 5% of the total heat transfer (Perdana, Fox, Schutyser, & Boom, 2011). In the comparison between the methods also the effect of the initial droplet size and the applied air velocity on the development of the morphology was evaluated. This is relevant since all single droplet drying methods employ droplet sizes (100-1000 µm) that are an order of magnitude larger than during spray drying (10-100 µm). This lengthens the drying time significantly, since the drying time scales quadratically with the initial droplet radius, and therefore the translation of single droplet drying results to spray drying should be done with caution.

3.2. Materials and methods

3.2.1 Materials

3.2.1.1 Model solutions

Protein solutions were prepared by adding whey protein isolate (WP, 94% protein, Friesland Campina, The Netherlands) or micellar casein (Cas, 88% protein, Friesland Campina, The Netherlands) to demineralized water and stirred overnight. Subsequently the selected carbohydrate, maltodextrin with a dextrose equivalent of 12 (MD12, Roquette, France) or lactose (Lac, Friesland Campina, the Netherlands), was added to the protein solution and stirred for 30 minutes. Solutions containing maltodextrin were stirred at room temperature, while solutions with lactose were heated to 50°C while stirring and cooled down before use. The final solutions had a dry matter concentration of 30% (w/w) and a composition of 0:100, 10:90, 20:80, or 30:70 (protein:carbohydrate on a dry basis).

3.2.1.2 Milk solution

Whole milk spray dried powder (Arla Food Ingredients, Denmark) was dissolved in cold MilliQ water to a dry matter content of 30% (w/w), and stirred for 30 minutes. Subsequently, the solution was heated to 70°C to ensure complete dissolution.

3.2.2 Single droplet drying methods

3.2.2.1 Sessile single droplet platform

The sessile single droplet drying platform (SSDD, Fig. 3.1a) has been developed by Perdana et al. (2011). A pneumatic micro-dispenser (Nordson Engineering Dispensing, USA) deposits a droplet on a hydrophobic membrane (Polypropylene, Akso Nobel Faser Ag., the Netherlands) in the focus of a CCD camera (μEye 1480ME, Imaging Development systems GMBH, Germany). The movable air tunnel is placed over the droplet and the droplet is then dried with dry, hot air at 80°C or 90°C (T_{air}) with a velocity of 0.3, 0.4 or 0.5 m/s (ϕ_{air}). Initial droplet radius was varied between 400 and 600μm (R_0). The insert in Fig. 3.1a shows a droplet on the membrane with the radius (R) and height (H) indicated. The ratio R/H is used to describe the roundness of a droplet. The standard deviations given are based on 4 replicates, except for 3 samples where only 3 replicates were used (WP:Lac 30:70, Cas:MD12 30:70, and Cas:Lac 10:90). The sample holder can be operated in two modes: stagnant or rotating (at 15rpm). Unless otherwise specified the sample holder was in the stagnant mode. The specific drying conditions are given in the caption of the figure.

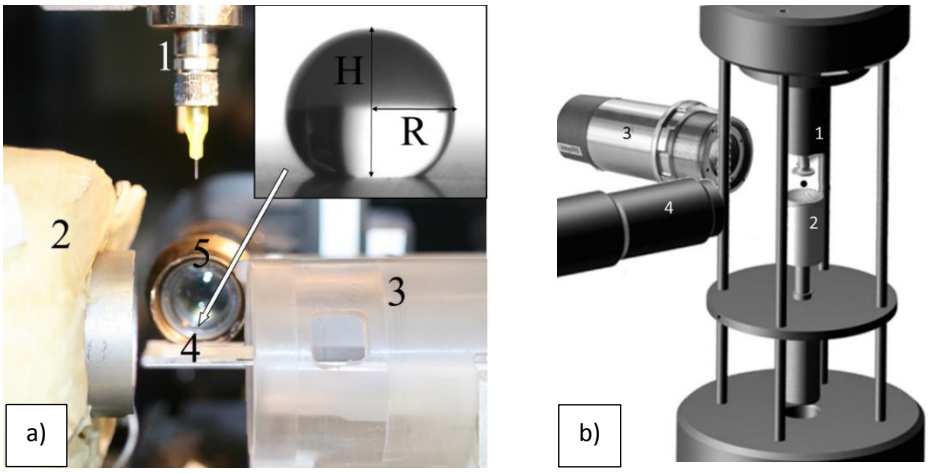

Fig. 3.1. Single droplet drying methods, with a) Sessile single droplet drying platform with (1) micro-dispenser with a needle tip, (2) Insulated air tunnel, (3) movable air tunnel, (4) sample holder with hydrophobic membrane, (5) camera. The insert shows a droplet on the membrane with the radius (R) and height (H), and b) the Drying Kinetics Analyser, with (1) transmitter, (2) reflector, (3) infrared thermometer, (4) CCD camera. Image was adapted from (Brask et al., 2007).

3.2.2.2 Drying Kinetics Analyzer

The Drying Kinetics Analyzer (DKA, GEA Niro, Denmark) has been described in detail before and therefore will be only briefly described here (Brask et al., 2007; Ullum et al., 2017). A single droplet is levitated by an ultrasonic field (Fig. 3.1b), while drying it with hot air of 80°C and 7% RH at an airspeed of 0.4 m/s. The drying is monitored with a CCD camera and an infrared thermometer to measure the droplet temperature. The initial droplet radius was varied between 590 and 820µm (R_0). The standard deviations given are based on 4 replicates.

3.2.3 Particle analysis

The droplets dried with SSDD were analyzed on the initial droplet size, final droplet size and the locking point size via image analysis of the recorded movie using ImageJ (National Institute of Health, USA). The scale to determine the exact dimensions of the droplet during image analysis was derived from the fixed needle size (225µm). Similarly, the droplet size was obtained during acoustic levitation by the image analysis methods that are integrated in the DKA software. The locking point, which represents the onset of morphology development, was defined as the first visual observation of shape deviation of the drying sessile droplet. Selected dried particles were visualized with Scanning Electron Microscopy (SEM), and/or Confocal Raman Microscopy (CRM). The drying conditions of the selected particles are specified below the figures. For SEM analysis, one representative sample was visually selected and fixed on the sample holder by carbon adhesive tabs and sputter coated with 15 nm of tungsten. SEM images were taken at 2 KV, 6.3 pA, using a Magellan 400 field emission scanning electron microscope (FEI, Eindhoven, the Netherlands). CRM was performed with a WITec alpha300 system in combination with a 532 nm laser for excitation and a 100x objective with an NA of 0.95 (WITec, Germany). This resulted in a lateral resolution of 250nm and a vertical resolution of 500nm. The scan size of the images was 25µm (width) by 25µm (depth). The integration time per Raman spectrum was 100 milliseconds. The images were analyzed using the instrument software.

3.3. Results and discussion

3.3.1 Morphology development of model systems

Protein-carbohydrate mixtures were dried at 90°C to study the effect of the composition on the morphology. The ratios of selected components, i.e. whey protein, micellar casein,

lactose and maltodextrin DE 12 were varied between 10:90, 20:80 and 30:70 (protein:carbohydrate). Further increase of the amount of casein was not possible as its maximum solubility was reached. The drying temperature of 90°C was chosen as a typical outlet temperature of an industrial spray drying process. Droplet drying time series visualizing the morphology development of droplets with a protein to carbohydrate ratio of 30:70 are presented in Fig. 3.2.

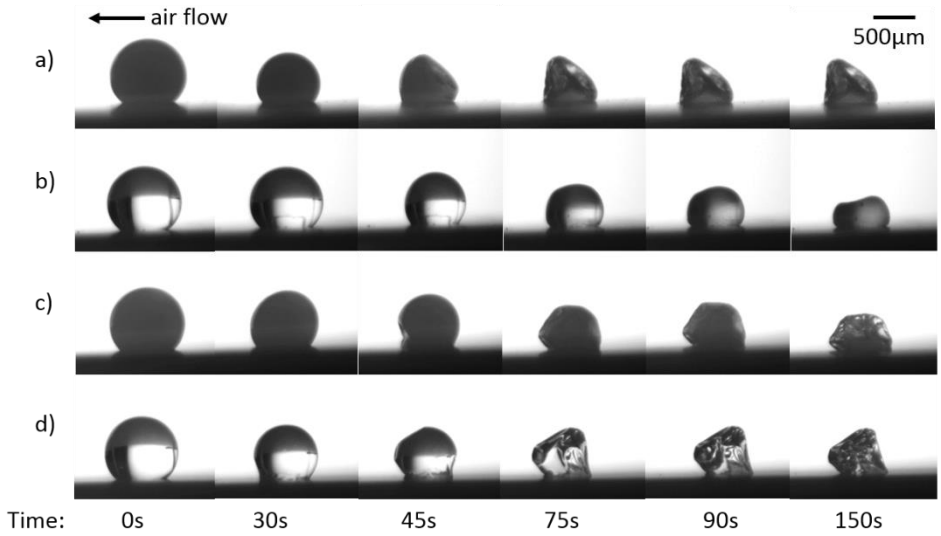

Fig. 3.2. Time series of morphology development during sessile single droplet drying of a) Casein:lactose, b) Whey protein:lactose, c) Casein:maltodextrin, and d) Whey protein:maltodextrin. The protein:carbohydrate ratio was 30:70, R_0 was 550±20µm, T_{air} was 90°C at a φ_{air} of 0.3 m/s. The air flow was from right to left.

- Series 3.2a shows the drying of a mixture of casein and lactose. Initially, ideal shrinkage was observed, followed by a large indentation in the direction of the air flow. At a later stage another indentation occurred, opposite to the air flow direction.
- Series 3.2b shows a mixture of lactose and whey protein. The duration of the ideal shrinkage period was longer than for the lactose-casein mixture. After locking, further shrinkage from the top of the droplet occurred, but no longer from the sides of the droplet. Additionally, the transparency of the solution changed from

clear to opaque, which has been observed previously but could not be explained by differences in crystallinity (Fu, Woo, Moo, & Chen, 2012).

- Series 3.2c represents a drying droplet of casein and maltodextrin, which showed again initial ideal shrinkage followed by a small indentation at the downstream side of the air flow. Next, the droplet started wrinkling from all sides and thus a completely wrinkled particle was obtained.
- Series 3.2d represents a drying droplet of whey protein and maltodextrin, which dried similarly to series 3.2c. The only difference was that the period of ideal drying was slightly shorter than in series 3.2c.

All droplets in Fig. 3.2 exhibit a period of ideal shrinkage where most probably no skin is formed and no internal mass transfer limitations occur. However, at the moment that a discernible skin develops this may be assumed to be related to hindered evaporation and the onset of morphology development. This moment is defined as the locking point and was determined visually from the onset of shape deformation of the droplet. These locking points and the corresponding droplet sizes were determined for each sample (Fig. 3.3). The locking point of droplets with mixtures of protein-lactose was around 55 seconds, whereas the protein-maltodextrin samples had a locking point of 30 seconds. Correspondingly, protein-lactose droplets shrank more before their locking point, locking at a radius around 79% of their initial radius, while the protein-maltodextrin droplets locked at 88% of their initial radius. The evaporation rate of water during the constant rate drying regime was determined equal for both samples (data not shown). The later locking point for the lactose systems therefore necessarily leads to more shrinkage until the locking point. Similar observations were made for lactose and sodium caseinate solutions, where the time to reach the locking point for a sodium caseinate-lactose solution (40:60) took twice as long compared to a pure sodium caseinate solution (Fu et al., 2011).

The particles were nearly spherical until their locking point and therefore the radius of the particle can be used to describe the morphology of the particles. However, after locking the radius is not an appropriate measure anymore. Therefore the sphericity of particles was calculated, which is defined by the ratio of the droplet radius and the droplet height (R/H). As mentioned, the droplets remain nearly spherical during the initial, ideal shrinkage, with a R/H ratio of ~ 0.6. After that, the R/H ratio changes depending on the components in the solution (Fig. 3.4). The height of the droplets with lactose rapidly decreased while the

droplet radius did not decrease any further. Therefore the R/H ratio of these droplets increased to ~0.8 - 1.0. In contrast, the particles containing maltodextrin maintained a R/H ratio of ~0.6, even though their morphology was wrinkled. This ratio means that the droplet remained nearly spherical throughout the drying process, indicating that the presence of the hydrophobic membrane was of limited influence to the formed morphology.

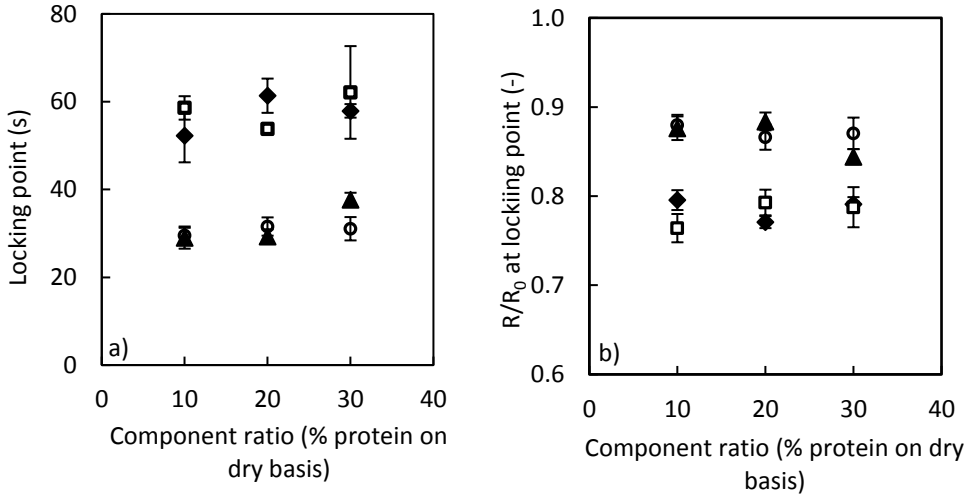

Fig. 3.3 with a) Locking point time and b) normalised radius (R/R_0) at the locking point of droplets with different protein:carbohydrate ratios. With: (♦) WP:Lac, (□) Cas:Lac, (○) WP:MD, (▲) Cas:MD. R_0 was 550 ± 20 µm and T_{air} was 90 °C at a φ_{air} of 0.3 m/s in the SSDD.

The final particle morphologies for the different component combinations are demonstrated in Fig. 3.4. The most distinct differences observed are between particles with lactose and maltodextrin. Particles with lactose were smaller; particles with maltodextrin were larger and more wrinkled. These differences may be explained by the different physical properties of maltodextrin DE12 and lactose. Most importantly, the viscosity of a lactose solution is much lower than the viscosity of a maltodextrin solution. A lower viscosity in the lactose solutions imposes less constraints on internal flow in partially liquid droplets and may thus lead to collapse followed by development of the solid round morphology (Che et al., 2012). Another difference between the carbohydrates is the possibility of crystallization during drying. Lactose might crystallize, whereas maltodextrin will not due to its higher glass transition temperature, i.e. 138°C versus 98°C (Avaltroni et

al., 2004; Schuck et al., 2005). Crystallization may especially occur at the center of the particle where drying proceeds more slowly, while the skin layer remains more amorphous (Fu, Woo, Moo, et al., 2012). The internal crystallization may enhance the transfer of water since it removes lactose from the solution, facilitating diffusion through the matrix during drying (Perdana, van der Sman, Fox, Boom, & Schutyser, 2014). However, it is well known that crystallization of lactose is delayed in the presence of protein (Haque and Roos, 2004). Detailed analysis on the crystallization process was beyond the scope of the current study.

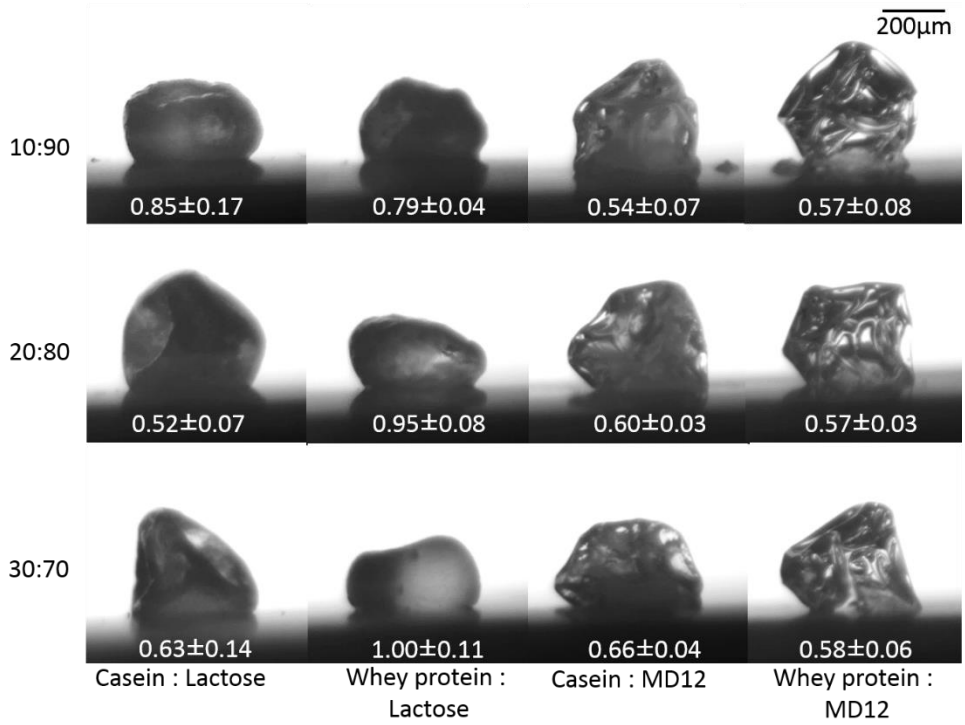

Fig. 3.4. Final particle morphology of dried droplets with varying composition (horizontal) and varying ratio of protein and carbohydrate (vertical). The droplets were dried in the SSDD at T_{air} was 90°C at a φ_{air} of 0.3 m/s, with an R_0 of 550±20µm. The air flow was from right to left. In each picture the average ratio of the radius and height (R/H) of the droplet is indicated.

The effect of the two proteins on morphology was less pronounced. The combination of lactose and whey protein yield smooth, opaque particles. There appears no clear influence of the increasing ratio of whey protein on final particle morphology, which suggests that lactose dominates the morphology development. This observation is not in agreement with

a previous study of Nuzzo et al. (2015), who observed changes in morphology for spray-dried lactose-bovine serum albumin (BSA) particles at increasing amounts of BSA. The difference between this and the previous study may be due to the lower initial solids concentrations in the study of Nuzzo et al., which increases the drying time and thus the chance of phase separation that again affects morphology. In contrast to whey protein or BSA, small amounts of casein drastically affected the particle morphology for casein-lactose solutions (Fig. 3.4). While particles with 10% casein showed similar morphology compared to that of whey protein-lactose particles, particles with 20% or 30% casein (on dry basis) showed a larger final particle with two large dents on each side.

The particle morphologies with the two proteins and maltodextrin as presented in Fig. 3.4 do not differ very much, i.e. both show showed wrinkled particles and their morphologies are still dominated by the carbohydrate. However, from SEM microscopy analysis a clear difference in the depth of the wrinkles being formed at the surface can be observed between the two different proteins. In Fig. 3.5a a dried maltodextrin droplet is shown as reference, which shows large rims and smooth indentations. The particles with whey protein-maltodextrin showed similar morphologies (Fig. 3.5b), whereas the casein-maltodextrin particles had rougher, wrinkled indentations with more fine structure features (Fig. 3.5c). Surprisingly, not all casein-maltodextrin particles showed similar morphology: 1 out of 4 droplets had shallower wrinkles and remained more or less spherical (Fig. 3.5d). The limited effect of the protein on the morphology of maltodextrin droplets corresponds to earlier results presented by Both et al., 2018, who showed that whey protein only influences the morphology at low drying temperatures and/or high protein content. These conditions can both be interpreted as allowing a higher protein content at the surface of the particles at locking, where the protein is present as a more densely packed surface layer and/or a thicker surface layer. The difference in influence on particle morphology of the two proteins may be explained by their different colloidal structure and their behavior at the air-water interface. First of all, the caseins are organized into porous, larger micellar structures, leading to high voluminosity. Whey protein has a voluminosity factor of ~1.5 m^3/kg, while this is ~4.4 m^3/kg for casein, leading to higher volume fractions of casein at the same mass fraction. Furthermore, whey protein is a globular protein, which is assumed to behave as a hard sphere upon concentrating. As soon as the protein in the shell becomes more concentrated, the whey proteins jam and form a highly viscous shell, which provides strength against deformation. At the same time protein molecules at the air-water interface

are assumed to undergo conformational changes and unfolding of their initial globular structure to expose hydrophobic domains. This gives rise to non-covalent bonds between protein molecules to create a cohesive film with a high surface elastic modulus (Lucassen-Reynders et al., 2010). These effects will result in a morphology with a smooth surface and a larger internal vacuole (Bouman et al., 2016). However, casein micelles will only show hard sphere behavior up to a volume fraction of 0.54. When the micelles are further concentrated, the kappa-brushes of the micelles will start to overlap increasing the proximity of the casein micelles. Subsequently, the micelles are in contact, will exhibit hard-sphere behavior and ultimately jam at a volume fraction of 0.69 (Dahbi et al., 2010). When the kappa-brushes start overlapping, the casein micelles act as soft deformable spheres with entanglement to neighbors. These interactions and soft film formation give rise to the formation of a wrinkled morphology. When drying mixed systems with proteins and maltodextrin, we can observe the influence of the two proteins in the wrinkles formed, i.e. more smooth for whey protein and more wrinkled for casein (Fig. 3.5).

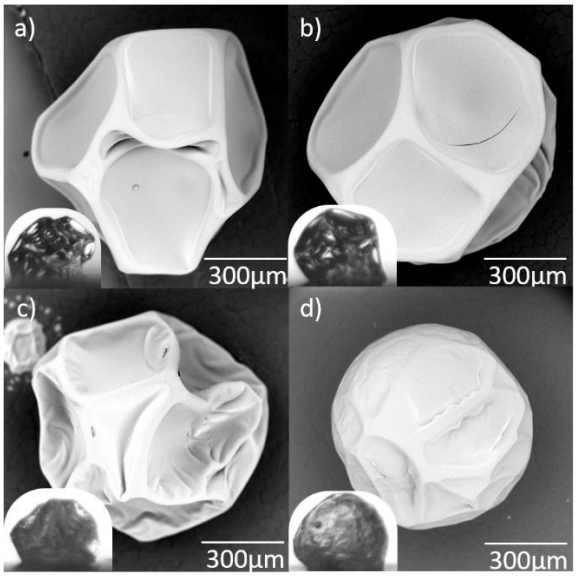

Fig. 3.5. SEM pictures corresponding to the images of Fig. 3.4, with a) MD without protein, b) WP:MD 20:80, and c&d) Cas:MD 20:80 with in c) the most prevalent morphology (75% of all droplets) and in d) the alternative morphology (25% of all droplets). The inserts are the same particles but imaged by the video camera on the SDD platform.

3.3.2 Morphology development of milk

Single droplet drying of mixtures of components as presented in the previous section generated insight on the contribution of individual components to the final morphology. Practically relevant spray dried formulations, such as milk, are much more complex. Therefore, our investigation continued on morphology development during drying of whole milk. In this further investigation two highly relevant process parameters were varied, i.e. initial droplet size and air speed. Additionally, the drying results of two different single droplet drying methods were compared on morphology development.

3.3.2.1 Influence of process parameters

From Fig. 3.6 it can be clearly seen that the morphology of dried milk particles is very similar to the observed morphology of casein and lactose (30:70) in Fig. 3.2. The bulk composition of whole milk is Lactose:Casein:Whey:Fat ~40:20:5:35, so the amount of casein relative to lactose is slightly higher than for the model solutions. Interestingly, the presence of a high amount of fat appeared not to influence the particle morphology. It may be explained by the emulsification of the fat, which minimizes the exposure of fat at the droplet surface. The observations in this study are in in contrast with observations by Malafronte et al. (2015) who found that skim milk showed a more shriveled morphology than whole milk (Malafronte et al., 2015). We speculate that this may be related to the higher initial dry matter content of the droplets in this study (i.e. ~45% (w/w)). The initial dry matter content has been before related to differences in morphology development (Bouman et al., 2016).

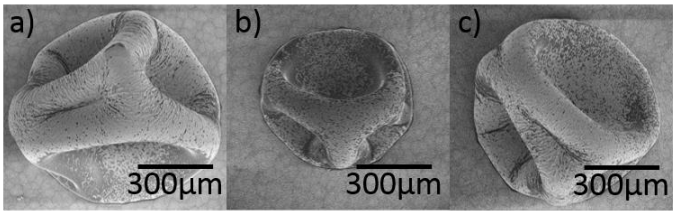

Fig. 3.6. SEM pictures of final particle morphologies of milk droplets dried at different conditions, with a) φ_{air}=0.5 m/s and R_0=450µm, b) φ_{air}=0.4 m/s and R_0=400µm, c) φ_{air}=0.4 m/s and R_0=500µm. Droplets were dried in the SSDD at T_{air} of 80°C.

There was no effect of the drying parameters, i.e. initial size and air speed, on the final morphology. However, we do see a clear influence on the locking point and the particle size at locking in Fig. 3.7a and 3.7b. A larger initial radius increases the time till locking (Fig. 3.7a),

while the relative size at the locking point remains similar (Fig. 3.7b). Increasing the air speed reduced the locking point, probably due to faster mass transfer, but there is no effect of the air velocity on the relative size at the locking point. The effects of the air speed are much smaller than the effect of the initial droplet size.

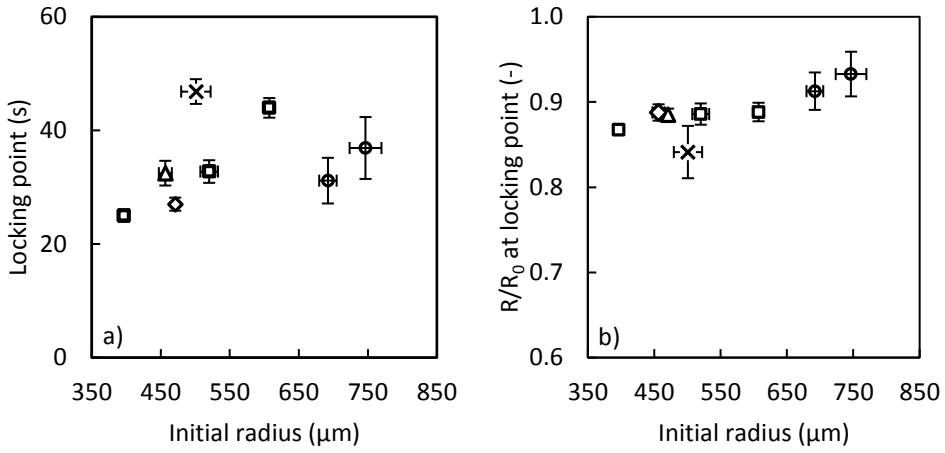

Fig. 3.7. a) Locking point time and b) normalized radius (R/R_0) at the locking point of droplets dried with varying initial radius and drying conditions: (△) SSDD at φ_{air} = 0.3 m/s, (□) SSDD at φ_{air} = 0.4 m/s, (◇) SSDD at φ_{air} = 0.5 m/s, (×) rotating SSDD at φ_{air} = 0.4 m/s, (○) DKA at φ_{air}=0.4 m/s. All droplets were dried at 80 °C.

Confocal Raman microscopy images were made to visualize the component distribution near and below the particle surface (Fig. 3.8a-c). A very thin layer of protein is visible at the surface (in red). Below that lactose-protein enriched domains (in purple) and fat enriched domains (in yellow) are visible. The effect of a smaller initial radius (Fig. 3.8b vs 3.8a), or a higher drying speed (Fig. 3.8c vs 3.8a) on the phase separation is very limited. Only in Fig. 3.8a a small lactose enriched zone is visible below the surface, whereas the faster dried droplets (Fig. 3.8b and 3.8c) do not have this zone. Phase separation is influenced by the drying time, and therefore larger droplets are expected to show more phase separation. This was also shown in a comparison between single droplet dried and spray dried whole milk, where less phase separation was visible in the spray dried particles (Nuzzo et al., 2017). Phase separation near the droplet surface during drying is governed by differences in diffusivity and surface activity of components (Fäldt et al., 1993; Meerdink and van't Riet, 1995). In addition, phase separation is driven by repulsive forces between the protein and

other components (maltodextrin) (Manoj et al., 1996). Furthermore, during spray drying the atomization processes may contribute to phase separation or even coalescence, leading to for example an increase of fat at the surface (Foerster et al., 2016).

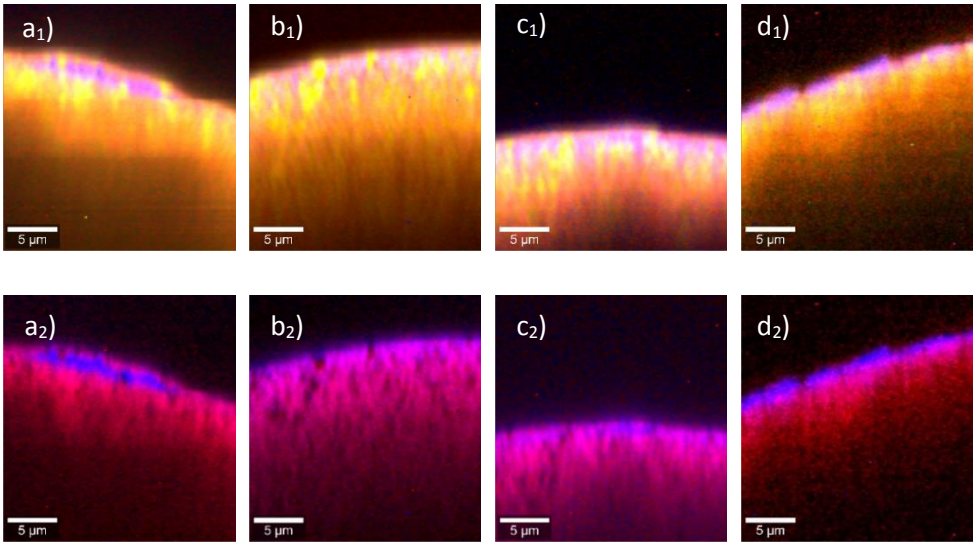

Fig. 3.8. Confocal Raman microscopy images of dried milk droplets at different conditions, with a) SSDD with φ_{air}=0.4 m/s and R_0=500µm, b) SSDD with φ_{air}=0.4 m/s and R_0=400µm, c) SSDD with φ_{air}=0.5 m/s and R_0=450µm and d) DKA with φ_{air}=0.4 m/s and R_0=750µm. All droplets were dried at 80°C. Top row: distribution of lactose, casein and fat. Bottom row: distribution of lactose and casein only. Lactose is pictured in blue, casein in red and fat in yellow. The scale bar represents 5µm.

3.3.2.2 Effect of single droplet drying method

Different single droplet drying methods have been employed by researchers, of which the most popular are the pendant drop, the acoustic levitator and the sessile droplet method. We here compare the latter two methods. Additionally, the sessile droplet dryer was used in two modes: stagnant and rotating. The SSDD platform in rotating mode mimics the spin of a droplet during spray drying, which is caused by momentum transfer and the relative motion of the droplet to the drying air (Schutyser et al., 2012).

In Fig. 3.9 three time series of drying droplets of whole milk are presented.

- The first series represents the stagnant sessile single droplet drying. After initial uniform drying, at around 60 s, a large indentation is formed from the left side,

which is downstream of the air flow. Later, another indentation is formed at the right side.

- The second time series represents a slowly rotating sessile droplet (Fig. 3.9b). A disadvantage of the rotation is the poorer quality of the images, since the droplet was not always in the focal plane of the camera. Again, morphology development started with an indentation at one side, followed by multiple indentations from other sides.
- The third time series represents a droplet dried in the acoustic levitator (Fig. 3.9c). Also here the first indentation was coming from one side, in this case the top, and was later followed by a second indentation from the bottom.

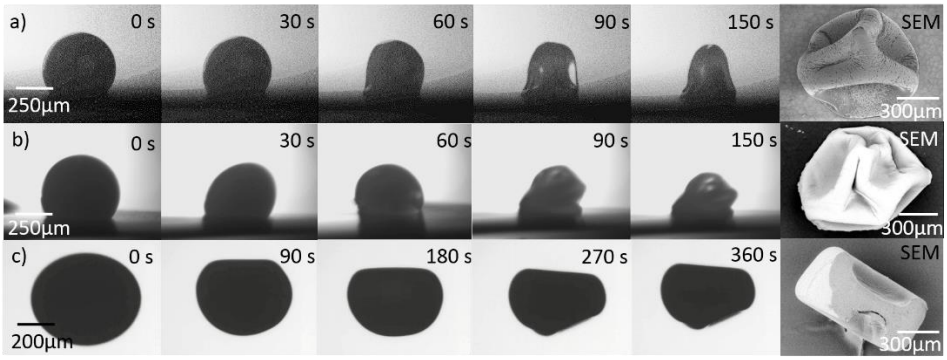

Fig. 3.9. Times series of single droplets dried with three different single droplet dryers, with a) SSDD with R_0=500µm, b) rotating SSDD with R_0=500µm, c) DKA with R_0=690µm. Droplet were dried at φ_{air} of 0.4 m/s and T_{air} of 80°C. The last image corresponds to the last picture of the time series made by SEM.

Both the acoustic levitator and the sessile platform yielded large indentations. However, the sessile droplet is fixed to the droplet holder, and indentation from the bottom is not possible, Thus a triangle shaped morphology resulted. Still, we conclude that the methods give quite similar results. The acoustic levitator allows indentation from all sides, including the side not visible to the camera. This means that one in three times, an indented morphology was formed, while for the camera the droplet appeared spherical.

For these drying methods the locking point time and size were determined as well (Fig. 3.7a and 3.7b). When the sessile platform was used in the rotating mode the locking point was later than in the stagnant mode, even though the reduced quality of the images of the

rotating droplet made the detection of the exact onset of morphology development more difficult, giving large uncertainties to this value. We therefore conclude that there is no discernible difference in locking point. When comparing drying in the DKA and stagnant SSDD, it was found that the overall drying times of the particles for the SSDD and DKA were in agreement with the difference in initial droplet size ($t_{drying} \sim R_0^2$), i.e. ~2.5 and ~5 minutes. However, the locking point of the DKA droplets is earlier and at a larger droplet size than expected, which might be due to droplet deformation due to the presence of the acoustic field. During acoustic levitation it can be observed that the droplet shape deviates from an ideal sphere, which makes it hard to identify the exact locking where the droplet starts to deform due to skin formation. This effect may explain the different observation of the locking point. The droplet dried in the acoustic levitator was analyzed with Confocal Raman microscopy to visualize phase separation (Fig. 3.8d). The degree of phase separation appeared slightly larger, which is most likely the result of the larger initial droplet size and subsequently longer time for phase separation to take place. Overall we conclude that both methods provide similar results and thus both methods can be considered for studying morphology development during droplet drying.

3.4. Conclusion

Understanding particle morphology development in relation to drying conditions and composition is key to controlling particle properties in spray-drying. Morphology development was investigated via a two-step approach using single droplet drying: 1) drying of mixtures of components, followed by 2) drying of a complex solution, i.e. milk. Morphology development in model mixtures was found dominated by the carbohydrates rather than the influence of the proteins. Only caseins influenced morphology at increased concentrations in mixtures with lactose and maltodextrin, possibly due to the high water binding of micellar casein, giving it a large voluminosity. The resulting flexibility of the micellar casein allows wrinkling of the formed skin as it gives flexibility to the skin even after locking. With maltodextrin it appeared that the influence of casein was present in the shape and smoothness of the wrinkles. In milk, the presence of high amounts of micellar caseins influenced the morphology of dried milk particles, even though the fat was somewhat enriched near the surface of the droplet. Fat did not provide any structural strength to the skin, but neither did it weaken it, since the fat is present as emulsified droplets. The evaluated single droplet drying methods give similar final particle morphology and thus are all good methods to study droplet morphology development. To really improve industrial

spray drying processes, SDD results should be connected to better insight on drying behavior of droplets inside spray dryers via a multi-scale modelling approach. In this way results from this study may be used in future to develop better powdered products by spray drying.

4

The role of viscosity in morphology development during single droplet drying

This chapter has been published as: Both, E.M., Siemons, I., Boom, R.M., Schutyser, M.A.I., 2019. The role of viscosity in morphology development during single droplet drying. Food Hydrocoll. 94, 510–518.

Abstract

Particle morphology influences the final quality of a powdered product. However, the mechanisms behind morphology formation are not completely understood yet. In this study particle morphology is linked to rheological properties of the concentrated liquid formulations at high concentration. Shear rate sweeps showed jamming of the whey protein at concentrations of ~50% (w/w), whereas maltodextrin remained fluid up to concentrations of ~70% (w/w). The morphology development of the latter components during single droplet drying could be influenced by adapting the initial droplet size and dry matter content. If droplets had a high initial dry matter (50% (w/w) morphology development started immediately, and the formed morphology could be explained by the rheological behavior of the mixture at that concentration. This indicated that measuring the rheological properties at high concentrations can provide insight in morphology development. Gaining insight on morphology development will eventually lead to higher quality powdered products.

4.1. Introduction

Spray drying is a widely used process to convert liquid formulations into powder to facilitate transport and extend their shelf-life. During drying not only water is removed, but the powder will also attain a particular morphology, which is related to quality parameters such as flowability (X. Fu et al., 2012) and reconstitution behavior (Takeiti et al., 2010). The morphology development during spray drying of droplets can be followed using single droplet drying, imposing controlled and monitored conditions (Schutyser et al., 2018). The use of single droplet drying to mimic spray drying has been extensively discussed in reviews (N. Fu et al., 2012a; Sadek et al., 2015b; Schutyser et al., 2018). Although the drying rate during single droplet drying experiments is lower (especially due to difference in droplet size) compared to spray drying, the particle morphologies observed are representative for spray dried particles (Nuzzo et al., 2015a; Sadek et al., 2016, 2014). Some studies report more pronounced morphologies in single droplet drying, while the overall appearance is similar (Nuzzo et al., 2017). This shows that single droplet drying experiments are meaningful for mimicking and studying spray drying processes.

In a previous study on single droplet drying of solutions containing whey protein (WP) and maltodextrin DE12 (MD) we already concluded that the typical morphology varies from particles with a wrinkled surface and small internal vacuoles, to particles with a smooth surface and a large internal vacuole (Both et al., 2018a; Bouman et al., 2016). This morphology could be influenced by altering the drying conditions, which was explained by the combination of the drying rate and the subsequent different skin properties. Depending on the composition, conditions could be identified at which lowering the drying temperature created a transition from wrinkled towards smooth particles. In the current research we will extend this work by investigating the effect of the dry matter content and droplet size on the morphology development, at the conditions identified previously.

To understand the morphology development it is important to gain better insight on the rheological properties of the formed skin. During drying, solutes in the droplet become increasingly concentrated at the droplet surface, which leads to the formation of a viscoelastic skin (Vehring et al., 2007). The rheological properties of the skin contribute to particle morphology development; however, measurement of these properties in-line is very challenging or virtually impossible. Instead, bulk rheological properties of the solutions may be assessed, e.g. viscosity or viscoelastic properties. The viscosity of highly

concentrated solutions has been measured for several model systems (e.g. Avaltroni et al., 2004; Brownsey et al., 2003; Dahbi et al., 2010; Haene and Liederkerke, 1996; Parker et al., 2005) and for whey proteins has been related to morphology by Sadek et al. (2013). The relationship between viscoelastic properties and morphology has not yet been much explored, except for two recent studies via indentation of 5 mm thick dried films (Sadek et al., 2015a), and via oscillatory droplet tensiometry (Andersson et al., 2018). Therefore, in this study we aim to understand the morphology development by analysis of the viscous behavior of mixed formulations at increasing concentrations. This can contribute to better understanding of the morphology development during spray drying, and with that facilitate the production of powders with a higher quality and lower environmental impact.

4.2. Materials and methods

4.2.1. Materials

Solutions of whey protein isolate (94% protein, Friesland Campina, The Netherlands) and maltodextrin with a dextrose equivalent of 12 (Roquette, France) were made with varying mass ratios: 100:0, 75:25, 50:50, 25:75 and 0:100 (WP:MD on a dry basis) and varying dry matter content: 20, 30, 40 and 50% (w/w). First, the whey protein was dissolved in demineralized water and stirred overnight at 4°C to ensure complete hydration. Next, the maltodextrin was added to this solution and stirred for 30 minutes at room temperature. The solutions used in single droplet drying (SDD) were made with a dry matter content of 30, 40 or 50 w/w%, with mass ratios of 25:75 or 50:50 (WP:MD), where the 40 and 50% (w/w) solutions were deaerated for 20 min to remove entrapped air in an ultrasonic bath (5210E-DTH, Branson, USA). The solutions used in rheology could not all be dissolved at the targeted dry matter content, due to the higher protein content and/or dry matter content than the samples used in SDD. Therefore, all solutions were first made at 20% (w/w) and subsequently concentrated using a rotational evaporator at 70 mBar and 50°C. Following this procedure, we ensured that all components remained in solution.

4.2.2. Sessile single droplet drying

The morphology development during the drying of solutions was studied with a sessile droplet drying platform (Fig. 4.1) that was further developed from the platform that was previously described by Perdana et al. (2011). A pneumatic micro-dispenser (Nordson Engineering Dispensing, USA) deposited a droplet on a hydrophobic membrane

(Polypropylene, Akzo Nobel Faser Ag., the Netherlands) in the focus of a CCD camera (µEye 1480ME, Imaging Development systems GMBH, Germany). The droplet was dried with dry, hot air at 60°C (25:75 WP:MD) or 70°C (50:50 WP:MD), which are the transition conditions as identified in Both et al., 2018, with a velocity of 0.3 m/s, and a relative humidity of ~1%. The initial droplet radii varied between 300 and 700 µm and the initial dry matter content was 30, 40 or 50% (w/w). The 40 and 50% (w/w) solutions were deaerated for 20 min to remove entrapped air in an ultrasonic bath (5210E-DTH, Branson, USA). The data analysis is based on 4 replicates. The initial droplet size, final droplet size and locking point size were determined from the recorded movie with ImageJ (National Institute of Health, USA). The scale was determined by correlating the number of pixels of the needle to its actual size, which is 225µm. The locking point was defined as the first visual deviation from the original spherical droplet shape.

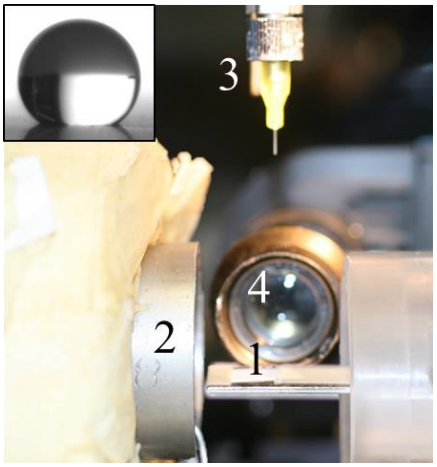

Fig. 4.1. Sessile single droplet drying platform, with (1) sample holder with hydrophobic membrane, (2) insulated air tunnel, (3) robotic dispenser with needle tip, (4) µEye camera. The insert shows a droplet on the hydrophobic membrane.

4.2.3. Rheology measurements

The rheological experiments were carried out with a strain-controlled rheometer (MCR 502, Anton Paar). A shear rate sweep was performed using a concentric cup geometry (CC17, 16,660mm x 24,858mm (width x height), Anton Paar) at 20°C. The shear rate was logarithmically increased from 0.1 to 100s^{-1}, with 15 measuring points with durations that decreased logarithmically from 300 to 1s. Subsequently, the procedure was reversed, i.e.

from 100 to 0.1s^{-1} with 15 measurement points and logarithmically increasing durations of 1 to 300s. With this procedure the absence of loading history and sample fracture were verified. Samples of varying dry matter content were measured in duplicate; once including the reversed procedure, and once without the reversed procedure. A rotational temperature sweep was performed at a constant shear rate of 50s^{-1} using a cone-plate geometry (CP50-4, Anton Paar) with a diameter of 25 mm and 4.000° angle. Samples had a dry matter content of 40% (w/w) and the sample temperature was linearly increased from 15°C to 90°C with a ramp of 2.5°C·min^{-1}, with 121 measuring points and a duration of 15s per point. Paraffin oil was used to avoid any undesired evaporation from the samples during the temperature sweep.

4.2.4. Describing the relation between viscosity and concentration

4.2.4.1. Maltodextrin DE12

The viscosity profile upon concentration of a polymer solution can be described with a series of universal relations. In the semi-dilute regime the combination of the empirical Spurlin-Martin-Tennent's (SMT) model combined with the Mark-Houwink relation has been shown to describe the viscosity of maltodextrin solutions (Avaltroni et al., 2004; Spurlin et al., 1946), being random coil polymers. The intrinsic viscosity of a polymer solution [η] can be described with the Mark-Houwink relation:

$$[\eta] = kM_v{}^{\alpha} \tag{4.1}$$

With M_v the viscosity-averaged molecular weight (10,000 g·mol^{-1} for the maltodextrin used), and k and α constants related to the degree of molecular expansion at 20°C, thus the polymer backbone stiffness and polymer-solvent interactions. For maltodextrin, (Avaltroni et al., 2004) found that k and α are 2.43·10^{-3} (dl·g^{-1}) and 0.337 (-). These parameters are the input parameters for the SMT model, which is based upon the Huggins model:

$$\eta_{sp} = [\eta]ce^{k_H[\eta]c} \tag{4.2}$$

With η_{sp} the specific viscosity $\eta_{sp} = \eta_{eff}^{SMT}/\eta_{water} - 1$ (-), c the concentration (g·dl^{-1}), [η] the intrinsic viscosity (dl·g^{-1}), and k_H the Huggins parameter. The effective viscosity (η_{eff}) is the dynamic viscosity (Pa·s). The Huggins parameter k_H, was in this study used as a fitting parameter and in earlier studies estimated to be 1.34±0.20 or 1.2 (-) for maltodextrins

(Avaltroni et al., 2004; Sman and Meinders, 2012). An average density was used in the semi dilute regime (20 – 40 w/w%) to convert the weight fraction x_{md} (% w/w) to concentration c (g·dl^{-1}), namely 1150 kg·m^{-3} which corresponds to a 30 w/w% solution.

In the concentrated regime, the viscosity of a polymer solution is governed by the amount of free volume. Williams, Landel and Ferry developed a free volume model (WLF) which relates the viscosity of a polymer solution at a specific temperature to the viscosity at the glass transition temperature (Williams et al., 1955):

$$\log\left(\frac{\eta_{eff}^{WLF}}{\eta_g}\right) = -\frac{C_1(T-T_g)}{C_2+T-T_g} \tag{4.3}$$

With η_g the universal viscosity at the glass transition ~10^{11} Pa·s, the universal parameters C_1 = 17.4 and C_2 = 51.6 K (Anese et al., 1996; Soesanto and Williams, 1981), and the glass transition temperature T_g which can be described by the Couchman-Karasz theory (Couchman and Karasz, 1978):

$$T_g = \frac{x_w \Delta C_{p,w} T_{g,w} + x_{md} \Delta C_{p,s} T_{g,s}}{x_w \Delta C_{p,w} + x_{md} \Delta C_{p,s}} \tag{4.4}$$

With $x_w = 1 - x_{md}$ the mass fraction of water, $T_{g,w}$ the glass transition of water (134 K), $\Delta C_{p,w}$ the change in specific heat capacity at the glass transition of water (1.92 J·g^{-1}·K^{-1}), $T_{g,s}$ the glass transition of maltodextrin DE12 (450 K), $\Delta C_{p,s}$ the change in specific heat capacity at the glass transition of maltodextrin DE12 (0.426 J·g^{-1}·K^{-1}) (Avaltroni et al., 2004; van der Sman and Meinders, 2011).

The SMT model is applicable to systems with low concentrations, while the WLF equation is only valid for higher concentrations. Thus we need to combine these two models if we want describe the full range of concentrations. We combine the two model equations using an ordinary smoothed step function:

$$\eta_{eff,md} = \left(1 - \left(\frac{1}{1+e^{-\frac{x_{md}-b}{t}}}\right)\right)\eta_{eff}^{SMT} + \left(\frac{1}{1+e^{-\frac{x_{md}-b}{t}}}\right)\eta_{eff}^{WLF} \tag{4.5}$$

With b and t as fitting parameters, where b represents the transition point from η_{eff}^{SMT} to η_{eff}^{WLF}, and t is a measure of the abruptness of the transition, where a larger t provides a smoother transition.

4.2.4.2. Whey protein and mixtures of whey protein and maltodextrin

Globular proteins such as whey proteins do not exhibit the same rheological behavior as random coil polymers, such as maltodextrins. Whey protein solutions may be considered to behave as hard sphere dispersions upon concentrating (Loveday et al., 2007), and therefore the viscosity can be described by the Krieger-Dougherty relation (KD), which describes the viscosity as a function of the volume fraction of the protein (φ):

$$\frac{\eta_{eff,wpi}}{\eta_{medium}} = \left(1 - \frac{\phi}{\phi_{max}}\right)^{-[\eta]\phi_{max}} \tag{4.6}$$

With φ_{max} the maximum packing density and [η] the intrinsic viscosity. The volume fraction of protein was calculated from the weight fraction multiplied with the voluminosity: $\varphi = x_{wpi} \cdot q$. The voluminosity of whey protein is estimated 1.5 mL·g^{-1} (Walstra et al., 1984) and assumed constant at varying concentration. For whey protein solutions the viscosity of water is used as η_{medium}, whereas for mixed systems the viscosity of the maltodextrin solution was used. Furthermore, in mixed systems a modified weight fraction was used for both maltodextrin and whey protein: $x_{mod,i} = x_i/\left(x_i + x_{H_2O}\right)$. By using a modified fraction it is assumed that the presence of another component has no effect on the viscosity of the component modelled.

4.3 Results and discussion

As drying is essentially a concentration process, we first discuss the effect of concentration on the viscosity of maltodextrin and whey protein mixtures (section 4.3.1 and 4.3.2). Subsequently we will address the effect of temperature for the same mixtures (section 4.3.3). Our observations are then related to the particle morphology development during spray drying (section 4.3.4).

4.3.1 Effect of concentration on viscosity of maltodextrin and whey protein solutions

The viscosity of maltodextrins, whey proteins and mixtures thereof was Newtonian in the measured shear rate range for all compositions (Appendix 4.I). The experimental data for

the effective viscosity of maltodextrins as a function of concentration and the proposed models are shown in Fig. 4.2. At lower concentrations (< 40% w/w), the effective viscosity follows the prediction by the Spurlin-Martin-Tennent (SMT) theory quite closely (Eqn. 4.1 and 4.2). Avaltroni et al. (2004) already showed that the SMT-model gives fair estimations of the viscosity of (semi-)dilute maltodextrin mixtures (from 1-50% w/w) with different dextrose equivalent (Avaltroni et al., 2004). The Huggins parameter (k_H) is influenced by the molecular architecture of the glucose homopolymer, and was found to be 1.34 or 1.2 (-)for maltodextrin in previous work (Avaltroni et al., 2004; Sman and Meinders, 2012). Linear regression on the current data resulted in a value of 1.23±0.02 (-), in line with expectation. Generally, a Huggins parameter value > 1 indicates a poor solvent quality. This is underlying the general tendency of carbohydrate polymers to aggregate (Avaltroni et al., 2004). Upon increasing the concentration (> 40% w/w), the polymer-polymer association becomes more pronounced and maltodextrins are expected to form a percolating network via hydrogen bonding, increasing the mechanical stability of the solution (Molinero et al., 2003). Therefore, the SMT theory cannot predict the viscosity of concentrated solutions.

For higher concentrated solutions the Williams-Landel-Ferry (WLF) theory is better suitable to describe the viscosity of polymers (Williams et al., 1955). This theory can be used to predict the viscosity depending on temperature and the concentration (Eqn. 4.3 and 4.4). From Fig. 4.2 we can conclude that the effective viscosity of highly concentrated (>40% w/w) maltodextrin solutions was well described by the WLF theory. To illustrate, the WLF model was able to accurately describe the rheological behavior of starch hydrolysates in a concentration range between 60 and 85% w/w and for temperatures ranging between 20°C and 80°C (Haene and Liederkerke, 1996), and Sopade et al. (2003) showed that the WLF theory could also more accurately describe the temperature dependency of the viscosity of honey when compared to Arrhenius, Vogel-Tamman-Fulcher and power-law models (Sopade et al., 2003). In general, the WLF theory should not be applied much below the Tg or at very low viscosity levels (<10 Pa.s). However, Haene and Liederkerke (1996) showed that for starch hydrolysis products, the theory could be applied down to viscosity levels of 0.1 Pa·s. Also here we find that the theory can be applied for maltodextrins down to ~0.1 Pa·s, (Fig. 4.2). The viscosity of the maltodextrin solution over the whole range of concentrations can be described by combining the SMT and the WLF theory using a smoothed step function approach (eqn. 4.5), with b = 0.45 and t = 0.03 as the fitting parameters. This generalized equation can aid in for instance predicting the self-diffusivity

of maltodextrins following the generalized Stokes-Einstein equation (Sman and Meinders, 2013).

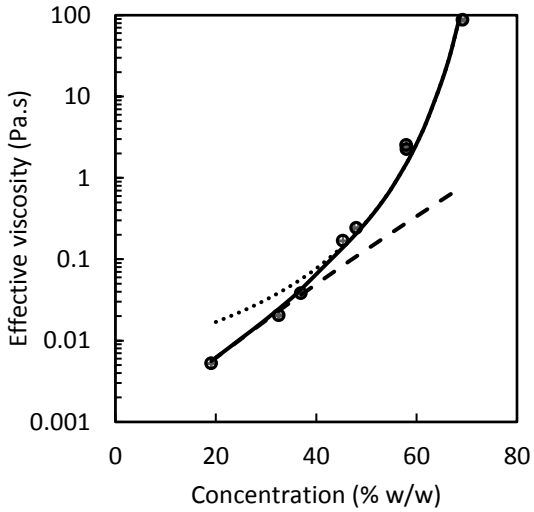

Fig. 4.2. Viscosity of maltodextrin solutions at 20°C as a function of concentration, with (○) experimental data, (- -) SMT model, (···) WLF model, (–) Smoothed step function.

The effective viscosity of whey protein can be described using the commonly applied Krieger-Dougherty relation for dispersions of hard spheres (Fig. 4.3, Eqn. 4.6). This relation assumes that there is a steady state between individual spherical particles and cooperatively moving packets of particles that are constantly formed and dissociated (Loveday et al., 2007). The KD model has already been shown before to describe the viscosity of β-lactoglobulin, which is the major protein present in whey protein isolate (deWit and Klarenbeek, 1984; Loveday et al., 2007). Applying this model to the data presented here, the intrinsic viscosity and maximum packing density of the protein were found to be 4.92±0.41 ($dl \cdot g^{-1}$) and 0.79±0.03 (-), respectively. These values are substantially higher than the theoretical values of 2.5 and 0.62, respectively, for monodisperse, completely rigid spheres (Dörr et al., 2013). However, Loveday et al. found that pure β-lactoglobulin dispersions already have an intrinsic viscosity of 3.6 and a maximum packing density of 0.71 (Loveday et al., 2007). The increased packing density for β-lactoglobulin dispersions may be explained by the formation of dimers. Their shape can be approximated by prolate ellipsoids, which form a denser packing than spheres (Donev et al., 2004; Parker et al., 2005). In the case of our whey protein dispersions, the packing density is even further

increased as it is a mixture of differently sized, shaped and charged molecules, which will allow even denser packing.

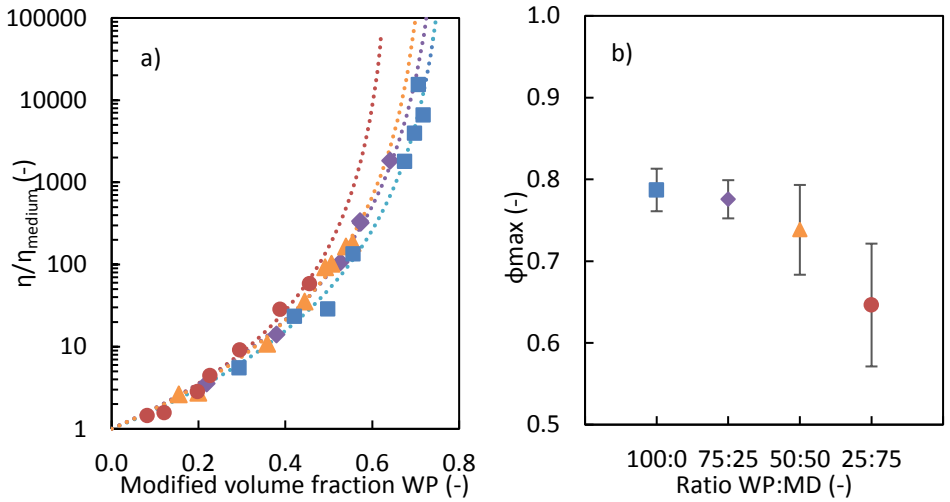

Fig. 4.3. a) η/η_{medium} as a function of modified volume fraction whey protein and composition, where the color of the line of the KD model fit is similar to the corresponding symbol of the experimental data. b) the maximum packing density from KD as a function of composition. With (■) whey protein, (◆) 75:25 WP:MD, (▲) 50:50 WP:MD, (●) 25:75 WP:MD.

4.3.2. Effect of concentration on viscosity of maltodextrin - whey protein mixtures

The viscosity of the mixed maltodextrin-whey protein solutions was analyzed using KD. In the analysis, the viscosity of the medium was described as the viscosity of the modified weight fraction maltodextrin using the SMT/WLF theory and the KD model was fitted on the basis of the modified volume fraction of whey protein (Fig. 4.3, Eqn. 4.6). This approach provided a good fit for 75:25 (WP:MD) with a similar maximum packing density as for pure whey protein. However, when the mixtures were higher in maltodextrin, the modified volume fractions of whey protein and the η/η_{medium} were much lower, which resulted in higher uncertainty of the fitted maximum packing density. Furthermore, the fitted ϕ_{max} of the whey proteins decreased with increasing maltodextrin content (Fig. 4.3b), showing that the presence of maltodextrin influences the packing and jamming of the whey proteins. This implicates that the whey protein solutions high in maltodextrin do not undergo jamming upon concentration, simply because the fraction maltodextrin is too high. This is also illustrated by Fig. 4.4, where the viscosity is plotted against the concentration. Here the

jamming of the whey proteins in the 100:0 and 75:25 (WP:MD) is clearly visible from the asymptote around ~50% (w/w), whereas the solutions higher in maltodextrin have a gradual slope even at high concentration.

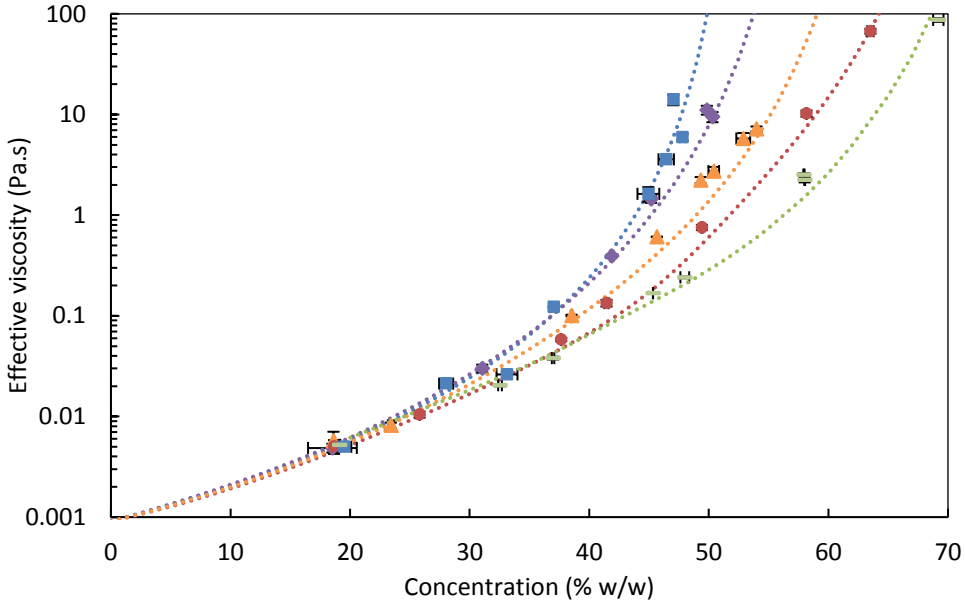

Fig. 4.4. Viscosity of maltodextrin, whey protein and mixtures thereof as a function of concentration. The color of the line of the model fit is similar to the corresponding symbol of the experimental data. With (-) maltodextrin, (■) whey protein, (◆) 75:25 WP:MD, (▲) 50:50 WP:MD, (●) 25:75 WP:MD.

4.3.3. Effect of temperature on viscosity of maltodextrin - whey protein mixtures

The viscosity is influenced by the concentration and the temperature. While initially the droplet temperature settles at the wet bulb temperature, after reaching a critical moisture content the droplet temperature starts to increase while at the same time the skin is being formed. This may lead to a reduction in viscosity, which again can influence the skin formation and thus the morphology development. To assess the temperature dependency, solutions of 40% (w/w) were heated from 15°C to 90°C at a constant shear rate (Fig. 4.5a). The results showed that the influence of the temperature on the viscosity of whey protein solutions was smaller than for maltodextrin solutions. The viscosity of maltodextrin solutions at 50°C was reduced by a factor 4 compared to the viscosity at 15°C, whereas the viscosity of whey protein was reduced by a factor 3. At high temperatures the viscosity

increased again, in the case of whey protein this was around 58°C. This may be related to denaturation of whey proteins, which usually starts around 63-65°C. Sugars can delay protein denaturation (Haque et al., 2015), which explains that the temperature at which denaturation occurs shifts to higher temperatures with higher maltodextrin content (Fig. 4.5b). In the mixture 75:25 (WP:MD) the maltodextrin apparently is not able to delay the protein denaturation, which may be possibly aligned with the limited effect of the maltodextrin on the jamming of whey proteins (Fig. 4.4).

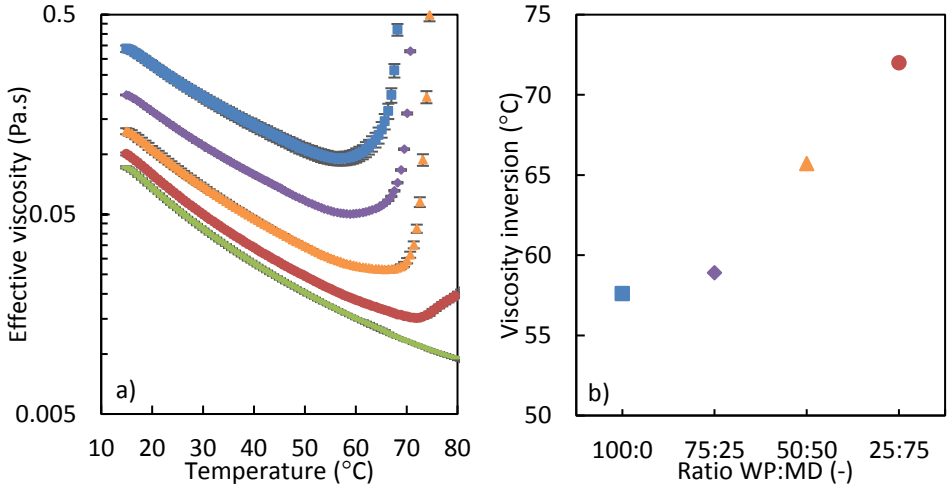

Fig. 4.5. a) Viscosity of maltodextrin, whey protein and mixtures thereof as a function of temperature, and b) Temperature at viscosity inversion as a function of ratio WP:MD. With (-) maltodextrin, (■) whey protein, (◆) 75:25 WP:MD, (▲) 50:50 WP:MD, (●) 25:75 WP:MD. The temperatures indicate the temperature at the viscosity inversion.

4.3.4. Morphology development during single droplet drying

As discussed in the introduction, solutions of mixtures were dried around their transition conditions, because at these conditions, small variations of the drying conditions will cause large differences in morphology. Fig. 4.6 demonstrates that on this transition, the same drying conditions can either result in a smooth, hollow particle, or in a denser, wrinkled particle. In Fig. 4.6a a time series of a drying droplet forming a smooth and hollow morphology is shown. The drying started at a constant drying rate (Both et al., 2018a), while slowly the concentration of components at the surface increased and a skin was formed. When the skin thickened, the morphology started to develop at the so-called locking point. Afterwards, the droplets formed a vacuole which rapidly grew until the droplet was hollow.

In Fig. 4.6b a droplet was dried under the same conditions. The initial drying was similar, but after the locking point a different morphology was formed: the skin was pulled in from multiple sides leading to a fully wrinkled particle surface.

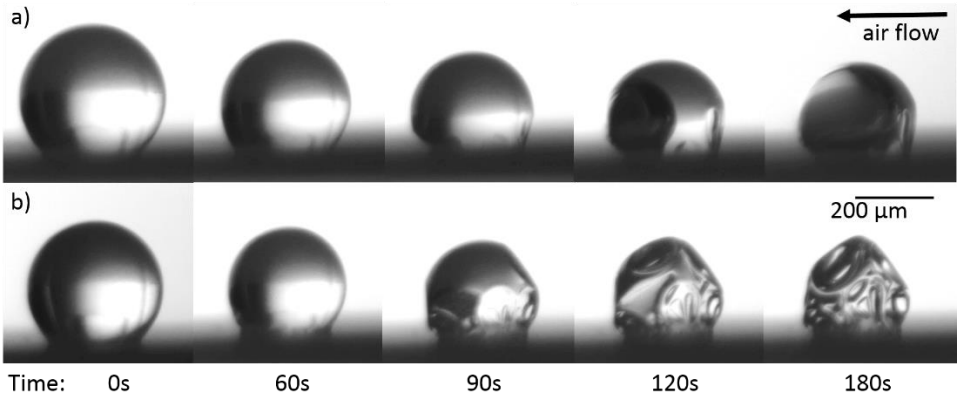

Fig. 4.6. Time series of droplets dried under similar conditions who develop a different type of morphology, with a) vacuole formation and b) wrinkling. Specific conditions: 25:75 (WP:MD), T_{air}: 60°C, R_0: 370µm, DM_0: 30% (w/w). Air flow is from right to left, as indicated by an arrow.

Subsequently, droplet drying experiments were carried out at varying initial size and initial dry matter content at the transition conditions. The effect of both parameters on the final particle morphology is shown in Fig. 4.7a (25:75 WP:MD) and Fig. 4.7b (50:50 WP:MD). The morphology of droplets with an initial dry matter content of 30% (w/w) showed a clear effect of the droplet size; larger droplets tended to result in a smooth and hollow morphology, while smaller droplets were more likely to result in wrinkled particles. The droplets with an initial radius of 370µm (25:75) and 390µm (50:50) were dried at the transition conditions, which provided particles showing either hollow of more wrinkled morphology. Increasing the initial dry matter content to 40% or 50% (w/w), yielded wrinkled particles regardless of the initial size.

The onset of morphology development, the so-called locking point, provides information on the skin formation. Therefore, the locking point time (Fig. 4.8a) and the size at the locking point (Fig. 4.8b) were determined for these samples, to identify the effect of both initial size and initial dry matter content. The droplets with composition 25:75 (WP:MD) showed a later locking point time, and therefore a smaller normalized radius (R/R_0) at the locking point than the 50:50 mixture, due to the lower drying temperature. Generally, larger

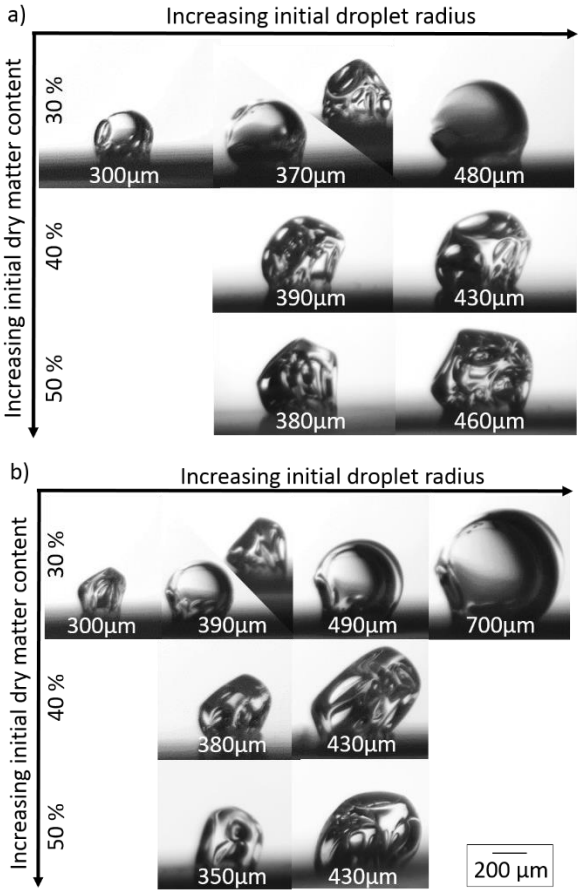

Fig. 4.7. Final particle morphology of dried droplets, with different composition: a) 25:75 (WP:MD) at T_{air} 60°C and b) 50:50 (WP:MD) at T_{air} 70°C, and varying initial dry matter content (vertical) and initial droplet radius (horizontal). The radius given corresponds to the initial droplet radius.

droplets had a later locking point, but the normalized radius (R/R_0) was independent of the initial size. Increasing the dry matter content from 30% to 40% (w/w) decreased the locking point time approximately by half, while further increasing to 50% (w/w) only slightly lowered the locking point time. The same effect was visible for the radius at the locking point: at 30% (w/w) it is ~88% of the initial radius, whereas for 40% and 50% (w/w) it lies around ~96%. These small differences between the 40 and 50% (w/w) samples suggests that only a small amount of water needs to be evaporated before the skin reaches a sufficiently high strength and the morphology starts to form.

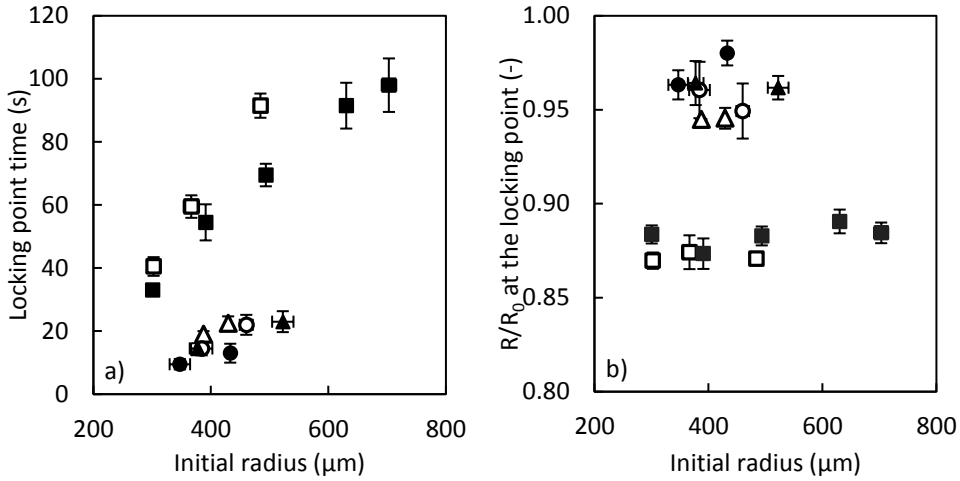

Fig. 4.8.a) Locking point time and b) normalized radius (R/R_0) at the locking point of drying droplets as a function of initial droplet size, with varying composition (□,△,○ WP:MD 25:75; ■,▲,● WP:MD 50:50), and varying initial dry matter content (■,□: 30% (w/w); ▲,△: 40% (w/w); ●,○: 50% (w/w)). The droplets with the composition of WP:MD 25:75 were dried at 60°C and WP:MD 50:50 were dried at 70°C.

A critical phenomenon for morphology development is the formation of a skin at the droplet surface. During drying water evaporates from the surface of the droplet, leading to an increase of concentration of molecules near the surface. If the diffusion rate of the molecules away from the surface is slower than the evaporation rate, a skin is formed that gradually increases in thickness during further drying (Vehring et al., 2007). At a certain skin consistency, the skin will no longer be able to shrink to compensate the volume reduction due to water evaporation. However, water evaporation still continues, and therefore the internal pressure decreases and as a result stresses are building up to deform the droplet skin (Sugiyama et al., 2006). Therefore, the skin consistency determines the type of morphology. A rigid, jammed skin cannot easily deform and the internal pressure continues to decline until a local weak point in the skin will collapse. This creates a defect and initiates a large vacuole to be formed. A viscous and deformable skin can continuously deform leading to a wrinkled particle. The skin strength depends on the rheological properties of the system, i.e. whey protein and maltodextrin DE12 solutions will behave differently upon concentration. Whey proteins act as a 'hard spheres' and therefore jamming will occur at sufficiently high concentrations. Maltodextrin, on the other hand, will slowly increase in viscosity and only undergo glass transition upon cooling. When advancing towards the glass

transition, water diffusion rates will decrease and thus drying will slow down, which allows more time for the skin to deform. These different responses were clearly observed in the rheology measurements (Fig. 4.4). For whey protein jamming occurred at a concentration above ~50% (w/w), forming a rigid skin and subsequent vacuole formation. Maltodextrin solutions were still fluid when concentrated to 70% (w/w), leading to the formation of a weak skin and therefore a wrinkled morphology.

The locking point analysis of the drying droplets (Fig. 4.8) showed that for droplets with an initial dry matter content of 50% (w/w) locking occurs almost instantly. Therefore, this dry matter content can be regarded as a critical concentration in morphology development, and rheological testing at this concentration can provide valuable insights. Mixtures with a 75:25 (WP:MD) ratio are close to maximum packing at this concentration and are expected to form a rigid skin, which was shown in previous research for drying temperatures ranging from 40 to 90°C (Both et al., 2018a). The mixtures with a 50:50 or 25:75 (WP:MD) are not close to maximum packing, and will thus form a weak skin, which may be expected to lead to a wrinkled morphology. However, as showed in Fig. 4.7 vacuole formation was observed during the drying of droplets with a large initial radius (> 350µm at 30% dm). Due to the slow drying, phase separation may occur, leading to whey protein enriched zones. This could provide rigidity to the skin, leading to the formation of hollow particles. Although phase separation was not measured here, it has been previously observed for droplets dried under similar conditions (Both et al., 2018a; Nuzzo et al., 2015b), and is therefore the most likely phenomenon behind the effect of droplet size on morphology. Phase separation may either be entropically induced liquid-liquid phase separation, or be caused by denaturation of the protein (see Fig. 4.5), depending on the conditions during drying, especially on the temperature. Furthermore, whey protein is a surface active component and has a higher molecular weight than maltodextrin. It is therefore likely that relatively more whey protein is present at the air-water interface than maltodextrin (Fäldt et al., 1993; Meerdink and van't Riet, 1995).

4.4. Conclusion

The rheological properties of concentrated aqueous solutions of whey protein isolate and DE12 maltodextrin were investigated and related to the development of distinct particle morphology during drying of single droplets of the same mixtures. The viscosity increase of the mixed whey protein and maltodextrin as function of concentration and temperature

was described with various models. Subsequent droplet drying experiments revealed that morphology development of the whey protein-maltodextrin solutions could be well related to the rheological behavior of the mixtures. The droplets were expected to form wrinkled morphologies, as the viscosity increased only moderately even at high concentrations. However, the morphology appeared highly dependent on drying time, where the 'slower' dried droplets were more likely to form a smooth and hollow morphology. Therefore, it was assumed that phase separation occurred, leading to whey protein enriched zones. If skin formation occurs faster than phase separation, maltodextrin will dominate morphology development and a wrinkled morphology develops.

Rheological analysis of the concentrated mixed systems assisted in gaining insight in morphology development, since the viscosity at high concentration could act as an indicator for morphology of the tested components. Combining single droplet drying with rheology extends the possibilities of interpretation of single droplet drying observations. A wider range of components should be tested to analyze if rheological behavior at high concentrations can be used as an indicator for morphology development. For example, the viscosity profile of micellar caseins gave a good explanation for the formed morphology (Dahbi et al., 2010; Sadek et al., 2016). Also in the case of lactose, the very low viscosity at high concentrations can explain the later locking and the formation of a collapsed morphology (Both et al., 2018b). In future work therefore the relationship between rheology and morphology should be investigated for a wider range of component mixtures, and at higher dry matter contents.

Appendix 4.I. Results from the shear rate sweeps

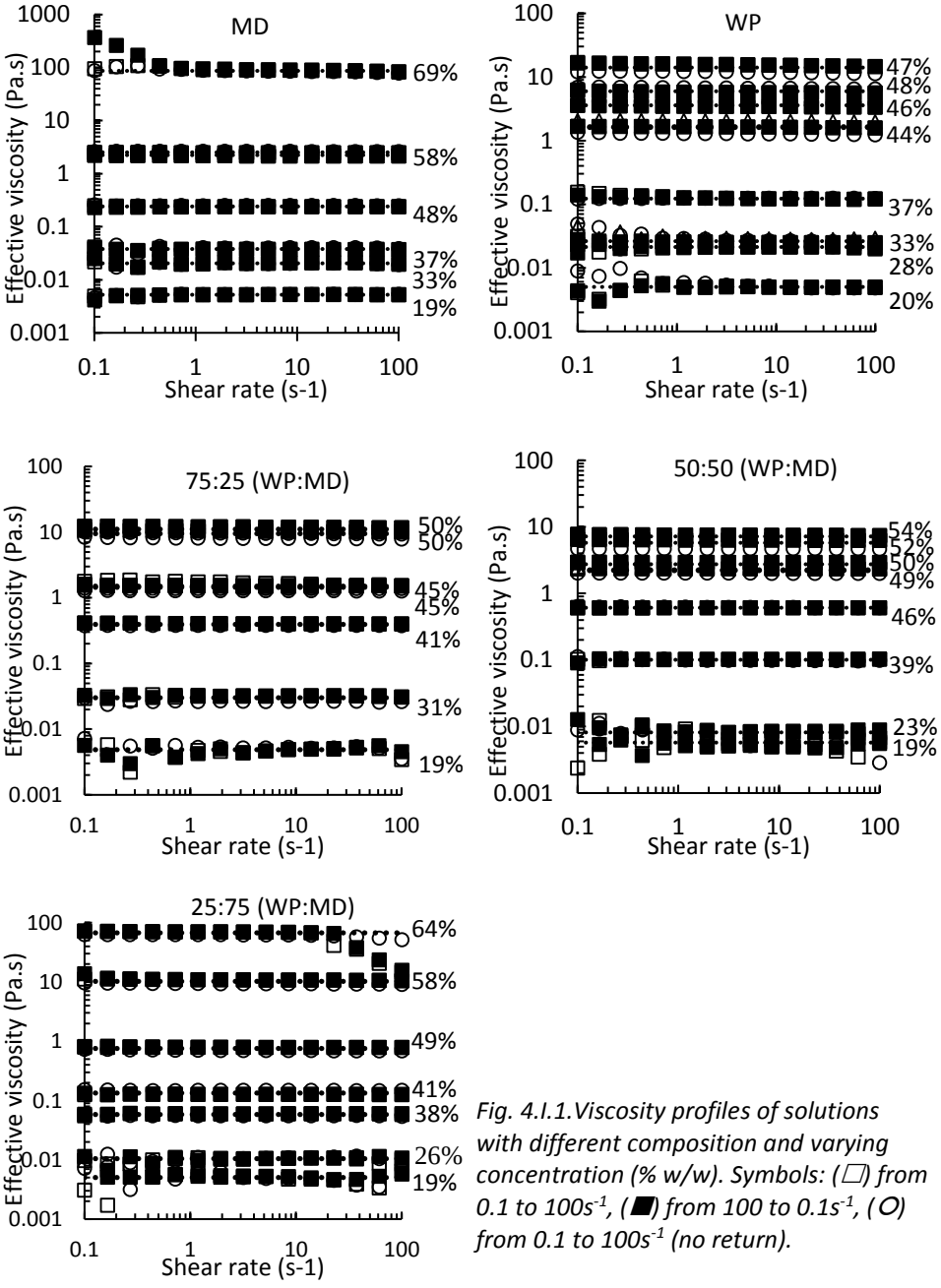

Fig. 4.I.1.Viscosity profiles of solutions with different composition and varying concentration (% w/w). Symbols: (□) from 0.1 to 100s^{-1}, (■) from 100 to 0.1s^{-1}, (○) from 0.1 to 100s^{-1} (no return).

5

Drying kinetics and viscoelastic properties of concentrated thin films as a model system for spray drying

Abstract

Controlling the development of the particle morphology during spray drying is of large importance to obtain high quality powders. During drying of skin-forming materials it is still unknown how the rheological properties of the skin develop as a function of time, moisture content and temperature. We here studied films prepared from whey protein – maltodextrin mixtures as a model system for spray drying. The rheological properties were assessed by oscillatory shear measurements at relevant high dry matter contents (66-82 w/w%). During drying, the films high in whey protein became brittle and had slower evaporation compared to films high in maltodextrin. Rheological analysis showed that for whey protein rich systems (with higher ratio than 25:75 WP:MD) the films were in structural arrest at the dry matter contents measured. Maltodextrin films on the other hand showed typical viscoelastic polymer behavior, although as little as 1% addition of whey protein altered its viscoelastic properties drastically. The viscoelastic properties could be related to vacuole formation during single droplet drying: samples that undergo structural arrest at a lower dry matter content (high in whey protein), form less and larger vacuoles compared to samples that undergo structural arrest only at high concentration (high in maltodextrin).

5.1. Introduction

Spray drying is a commonly used process in food, feed and pharmaceutical industries to produce powdered products with long shelf-life. During spray drying a liquid feed is atomized into hot drying air, which results in rapid dehydration of micron-sized droplets into dried particles. During this dehydration a particle morphology develops, which to a large extent determines the quality of the powders, such as the flowability (Bumiller et al., 2002; X. Fu et al., 2012), and the reconstitution behavior (Takeiti et al., 2010). Hitherto, drying operations are often optimized via trial-and-error approaches. Insight in the morphology development will contribute to a more rational approach towards optimizing the quality of powders and contribute to more efficient spray drying operations by reducing fouling.

During drying, solids concentrate near the surface, which leads to skin formation (Vehring et al., 2007). Subsequently, the mechanical properties of this skin contribute to resistance against deformation, which greatly influences the final morphology. An interesting approach to study skin formation and subsequent morphology development is single droplet drying, where one droplet is dried and monitored under controlled conditions (Perdana et al., 2011; Sadek et al., 2015b; Schutyser et al., 2018). This method was successfully applied to study morphology development as a function of the imposed drying conditions and formulation (Both et al., 2018b; Bouman et al., 2016; Nuzzo et al., 2017; Perdana et al., 2013b; Sadek et al., 2014; Tran et al., 2017). While single droplet drying studies yield especially visual information on morphology development, there is need for further investigating the relation between the drying kinetics and the dynamic rheological properties, and relating these to the observed particle morphology development.

For single droplet drying methods, the monitoring of drying kinetics (i.e. mass decrease) is challenging, although some single droplet drying approaches such as pending droplet drying facilitate this. During single droplet drying, the masses are very small and drying can be influenced by a necessary filament into the pending droplet or by the acoustic field that levitates a drying droplet. The objective of the current study was to understand the relation between the development of the morphology of drying droplets, and the development of the rheological properties of the skin that is being formed, using thin film drying as a model system. Therefore, a convective thin film dryer was developed to accurately assess the drying kinetics for complex matrices dried at relevant drying air temperatures and

velocities. These measurements complement the visual observations during single droplet drying. Understanding the effect of skin formation on the drying kinetics, will lead to more insight in the drying of complex formulations.

Ideally, rheological properties of the skin are assessed in-line during single droplet drying. However, droplet sizes and resulting deformation forces are too small to perform accurate in-line measurement of the rheological behavior. Moreover, during drying, sharp gradients develop in a particle or a film, which complicate the in-line assessment of the rheological properties. Earlier studies used indentation on equilibrated, partially dried films (Sadek et al., 2015a) or viscosity measurements of highly concentrated solutions (Both et al., 2019). In the current study, we used a procedure to prepare equilibrated partially dried whey protein – maltodextrin films with high solids content and performed oscillatory rheology on these. The rheological properties obtained from a frequency sweep test provide information on the resistance against deformation of the prepared film, which is then related to the development of the morphology during drying.

5.2. Materials and methods

5.2.1. Materials

Solutions of whey protein isolate (WP, 94% protein, Friesland Campina, The Netherlands) and maltodextrin with a dextrose equivalent of 12 (MD, Roquette, France) were made with a total dry matter content of 30 w/w% and varying mass ratios; 100:0, 75:25, 50:50, 25:75, 10:90, 5:95, 1:99, and 0:100 (WP:MD on dry basis). For the preparation procedure of different whey protein – maltodextrin mixtures, the whey protein was always first dissolved in demineralized water and stirred overnight at 4°C to ensure complete hydration. Subsequently, the maltodextrin was added to this solution and stirred for 30 minutes at room temperature.

5.2.2. Thin film drying

A thin film dryer (TFD) was designed and built (Fig. 5.1). The air tunnel was 50·14·2.6 cm (L·W·H), through which hot air was blown of 105°C and 1% relative humidity at a speed of 1 m/s. The sample tray (4·9·0.05 cm L·W·H) was situated above a scale in the middle of the drying tunnel (Sartorius Cubis, Germany). The initial sample weight was 2.8 grams, resulting in an initial film thickness of 0.8 mm. Samples were dried in the thin film dryer for 1.5 hour, while every 30 seconds measurements were taken of the sample weight and film

temperature (Infrared, Testo 835-T1, the Netherlands). Detailed pictures were taken of 25:75 (WP:MD) films with a Smartzoom 5 (Zeiss, Germany) after 15 and 30 minutes of the middle of the film and the right side of the film. Films were prepared from solutions following either the normal dissolution procedure or the normal dissolution procedure with an additional vacuum degasification for 10 minutes at 70mBar in a rotary evaporator.

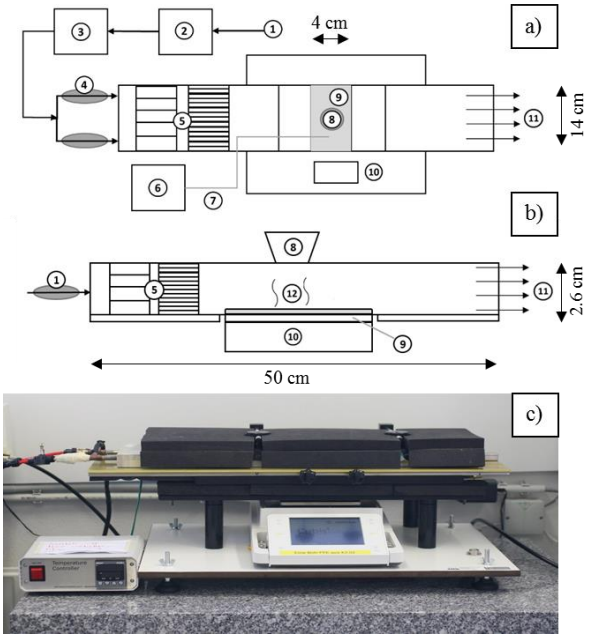

Fig. 5.1. Thin film dryer, with a) schematic top view, b) schematic side view, and c) set-up. 1) air inlet, 2) flow meter, 3) dehumidifier, 4) heating elements, 5) obstacles for air distribution, 6) temperature control, 7) temperature sensor, 8) IR-thermometer, 9) sample tray, 10) mass balance, 11) air outlet, 12) sample.

5.2.3. Thin film rheology

The dried films for rheology were prepared by partial drying of the solutions in an oven at 80°C, followed by an equilibration step in a climate chamber (Memmert, Germany) at 50°C for three days (see Appendix 5.I.). Amplitude and frequency sweeps were performed with a strain-controlled rheometer (MCR 502, Anton Paar), using a parallel-plate geometry with a ribbed probe with a diameter of 24.981 mm, at a temperature of 50°C. Paraffin oil was added to prevent moisture evaporation during the measurement. An amplitude sweep with 25 data points was performed with a strain range of 0.01-100% at an angular frequency of 10 rad·s^{-1}, while keeping the normal force constant at 1N. A frequency sweep with 20 data

points was performed in an angular frequency range of 0.01-100 rad·s^{-1} at a shear strain of 0.05%. Samples were measured in duplicate or triplicate. The dry matter content of the films was measured by overnight drying in an oven at 105°C.

5.3. Results and discussion

The objective of this study was to relate the rheological behavior to the morphology development during spray drying, using thin film drying as a model system. First, skin formation and its effect on drying kinetics was assessed using a custom build thin film dryer. Subsequently, the viscoelastic properties of equilibrated, partially dried films were measured, and finally these results were compared to the morphologies observed in single droplet drying.

5.3.1. Drying kinetics of thin films

As discussed, a thin film drying set-up was built to assess the drying kinetics of thin films while observing the skin formation to provide complementary data to the visual information obtained during single droplet drying. In our previous study on single droplet drying we observed that the initial drying rate for whey protein-maltodextrin mixtures was constant as the drying is limited by the external mass and heat transfer (Both et al., 2018a). It was assumed that the drying enters the falling rate period as soon as a skin is formed, even though this could not be visually confirmed as during this period a rather complex morphology develops.

The total mass and temperature changes of the surface of different drying films are shown in Fig. 5.2: drying of pure water and different 30 w/w% solutions prepared from combinations of whey protein and maltodextrin. Images of the drying films are shown in Figs. 5.3 and 5.4.

Fig. 5.2b shows the drying rates that can be derived from the data in Fig. 5.2a. No clear constant drying rate period can be observed; a continuous declining evaporation rate is seen. This is probably partly due to spatial distribution of the drying behavior along the film length, and due to equilibration of the temperature of the film. During the first minutes of drying, the film temperature decreased to the wet bulb temperature due to evaporative cooling. After 5 minutes, at 0.6 kg/kg water, the evaporation rate decreased even further and the film temperatures started to increase again, due to diffusion limitations inside the film probably due to the formation of a concentrated skin layer. The differences in drying

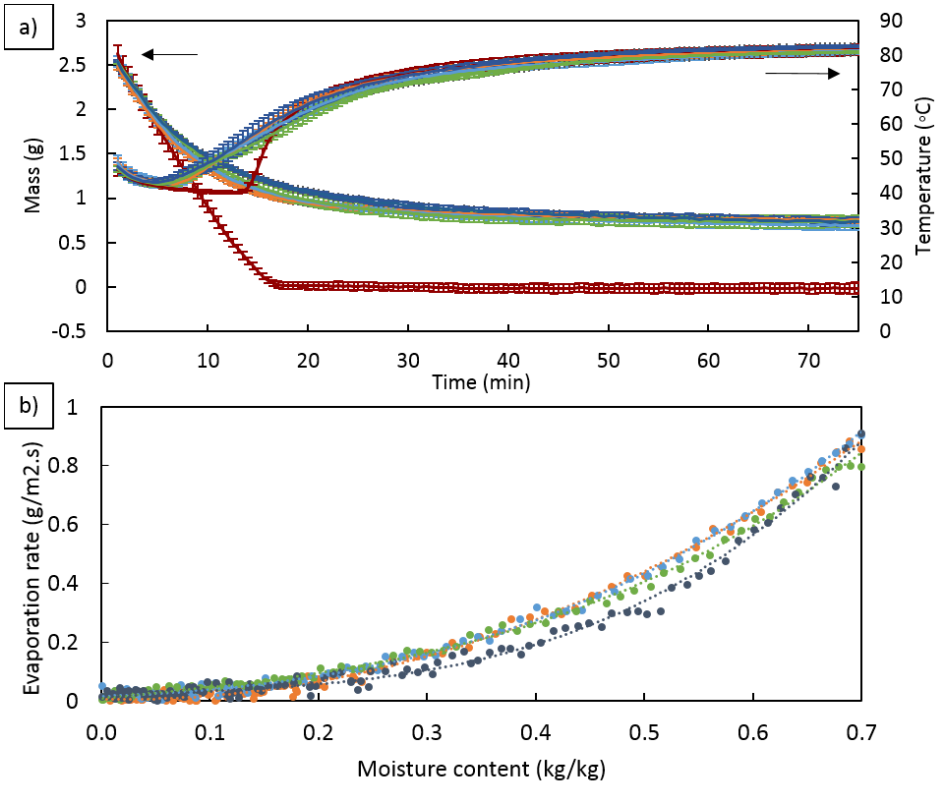

Fig. 5.2. Drying kinetics of thin films, with a) mass decrease (left) and temperature (right) over time and b) evaporation rate (g/m²·s) vs water content (kg/kg), where a moving average is used over 3 points. With (red) water, (orange) 0:100, (light blue) 25:75, (green) 50:50, (dark blue) 75:25 (WP:MD). Films had an initial thickness of 0.8 mm, initial dry matter content of 30 w/w% and were dried at 105°C at 1 m/s air flow. The dotted line is drawn to guide the eye.

rate between the different films suggest influence of film composition on the drying rate. Pure maltodextrin and 25:75 (WP:MD) films showed the highest drying rates for a longer period of time. Adding more whey protein to the film reduced the drying rates, related to a lower moisture diffusivity and a less penetrable skin layer. Final film temperatures were around 82°C, with around 2 w/w% residual moisture in the films.

During thin film drying, detailed pictures were taken after 15 and 30 minutes of drying of a 25:75 (WP:MD) film of a regular and a degassed solution (Fig. 5.3). After 15 minutes the skin is still very much in development, while after 30 minutes about 90% of the water was

evaporated. For a solution that had not undergone vacuum degasification and hence contained dissolved air, a skin developed after 15 minutes (Fig. 5.3a) and the drying was not completely homogenous: at the entrance side of the air flow, a corrugated (probably drier) zone formed. Downstream of the air flow, inhomogeneous drying was observed, with at the top a non-transparent area with cracks and in the middle a zone with air bubble inclusion/nucleation, which is probably less dehydrated than the top area. We expect that some air was dissolved by the mixing during the dissolution procedure. After 30 minutes the films lost approximately 90% of their water and the entire film now was corrugated (Fig. 5.3b). The drier area at the top of the film showed even more cracks, while in the central area air bubbles were visible with some newly developed wrinkles. After 90 minutes the films were white with many cracks at the surface (Fig 5.4c). The whiteness is caused by light diffraction of the air in the cracks.

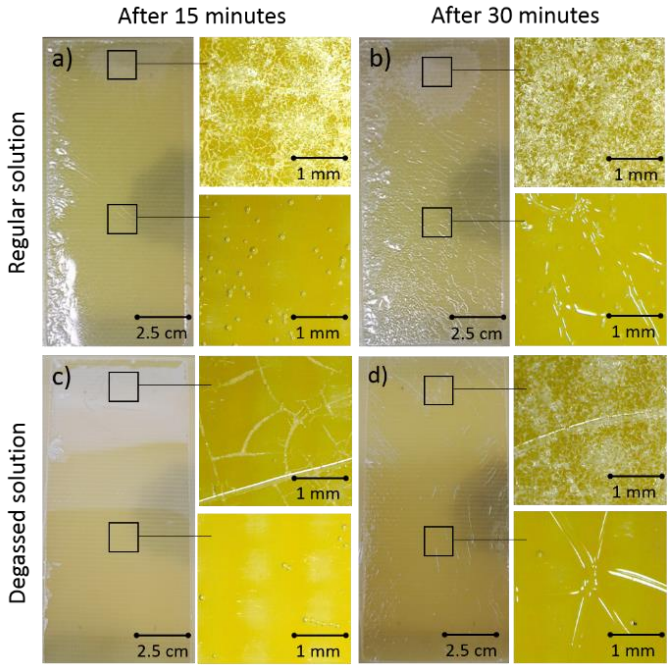

Fig. 5.3. Skin formation in time, with the regular dissolution procedure after a) 15 minutes and b) 30 minutes, or with vacuum degasification after c) 15 minutes and d) 30 minutes. Film composition was 25:75 (WP:MD). Air flow was from left to right.

The air present in the solution was removed by vacuum treatment. After 15 minutes of drying, the degassed film included about five times less air bubbles, and much less cracks were present in the drying zone (Fig. 5.3c). After drying for 30 minutes, this degassed film showed clearly delayed formation of corrugations (Fig. 5.3d). We hypothesize that air bubbles act as weak spots, allowing the deformation of the solution just below the skin, which then makes contraction and wrinkling possible. The effect of air on the skin formation suggest that this would also influence the drying kinetics, possibly leading to faster evaporation. However this has not been studied in detail here.

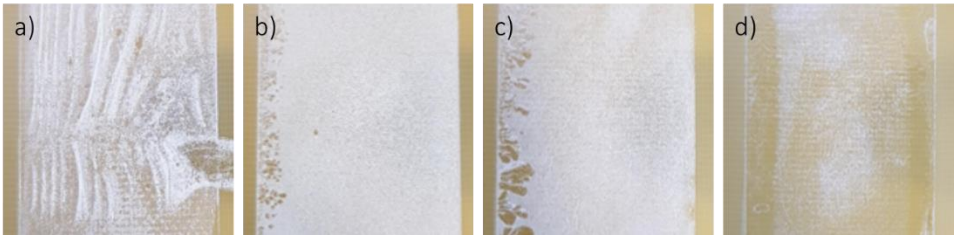

Fig. 5.4. Visual appearance of dried films after 90 minutes, with a) 75:25, b) 50:50, c) 25:75, and d) 0:100 (WP:MD). Air flow was from left to right.

The final appearance of the dried films varied with the WP:MD ratio (Fig 5.4). The film highest in whey protein (75:25 (WP:MD), Fig 5.4a) showed large wrinkles on the surface, and some solution was lost at the downstream side of tray. Furthermore, the final dried film was fragile and small film fragments were blown away by the drying air. Pure whey protein films were so fragile that they could not be studied. The films with the ratios 50:50 and 25:75 showed a smooth surface with many cracks (Fig 5.4b and c), while maltodextrin yielded an opaque film and less cracking (Fig 5.4d).

5.3.2. Rheology

We first report on method development to prepare partially dried thin films that allows rheology analysis. Subsequently, oscillatory rheology results are presented and discussed for films of different whey protein – maltodextrin mixtures.

5.3.2.1. Method development

The dried films for rheology (Fig. 5.5) were prepared by pre-drying the solutions in an oven at 80°C, followed by an equilibration step in a climate chamber at 50°C. The films had to be prepared at specific dry matter contents to allow rheological analysis and transfer of films

without breakage: at too high solids content the films were dry and fragile, while at lower solids contents the films were not rigid enough for transfer. Both extreme situations also complicated the transfer of the films from the preparation cup to the rheometer. The optimum dry matter content varied with composition and thus not all compositions could be tested at the same concentration. Dry matter contents above 60 w/w% are of interest, as the surface concentration of drying droplets is high. The film thickness was also varied, since very thin films lead to instability and breakage during transfer or deformation, while very thick films take too much equilibration time during preparation. The exact sample volume, oven drying times, and relative humidity of the climate chamber were therefore varied per sample to obtain a specific film thickness and dry matter content (see Appendix 5.I.). The targeted film thickness and dry matter content for the ratios 100:0, 75:25 and 50:50 (WP:MD) were 0.72 mm thick and 75 w/w% dry matter, respectively. For 50:50, 25:75, 5:95, and 0:100 (WP:MD) these were 0.45 mm thick and 82 w/w% dry matter, respectively.

The rheological tests were performed in normal force controlled mode at 1N. An amplitude sweep was done to establish the linear viscoelastic range (Fig. 5.6) from which an amplitude of 0.05% was selected to perform subsequent frequency sweep tests.

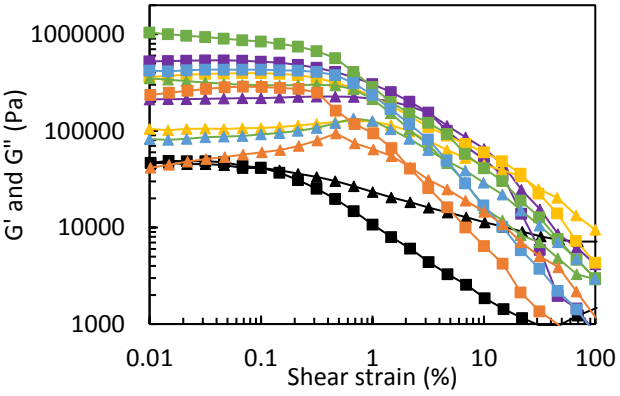

Fig. 5.5. (left) Example of a thin film used in the rheological experiments (25:75 WP:MD).
Fig. 5.6. (right) Amplitude sweep with (orange) 100:0 at 76 w/w%, (blue) 25:75 at 77 w/w%, (green) 50:50 at 77 w/w%, (yellow) 50:50 at 82 w/w%, (purple) 25:75 at 81 w/w%, (black) 0:100 at 81 w/w% (WP:MD). The presented amplitude sweeps are a representative selection of the data set. With (■) storage modulus G' and (▲) loss modulus G".

5.3.2.2. Effect of the composition on the viscoelastic properties

The films high in whey protein, 100:0, 75:25 and 50:50 (WP:MD), were measured at a dry matter content of 75 w/w%, and exhibited a large storage modules over the whole frequency range, which suggests that the material behaves as a solid material (Fig 5.7). Above 0.1 rad·s^{-1} the loss and storage moduli were weakly dependent on the frequency indicating that the system is densely packed. The addition of maltodextrin did not dramatically affect the behavior, except when more than half of the dry matter was replaced by maltodextrin. In that case, the loss modulus increased slightly, resulting in a larger loss factor.

The films high in maltodextrin, 50:50, 25:75, 10:90, 5:95, 1:99 and 0:100 (WP:MD), were measured at a dry matter content of 82 w/w% (Fig. 5.8). The storage moduli of the films with a ratio of 50:50 and 25:75 (WP:MD) were much larger than those of the samples with even more maltodextrin, and in the same order of magnitude as the samples high in protein. This indicates that these films were likely in structural arrest, although the 25:75 film was overall slightly 'softer' indicated by the larger loss modulus and a stronger frequency dependence. The storage moduli of the samples with 1 to 10% protein were much smaller, and similar to each other. This suggests that these samples are in the rubbery state associated with free polymer rheology. Pure maltodextrin films show the same behavior, i.e. at low frequencies the viscous part was dominating (<0.02 rad·s^{-1}), followed by a region of mostly elastic behavior (0.02 to 2 rad·s^{-1}) indicating a rubbery material, while at higher frequencies the viscous part was dominating again (>2 rad·s^{-1}).

Whey protein films at lower solid concentrations (20 to 50 w/w% dry matter) showed viscous behavior, using a cone-plate geometry over a wide ranges of shear rates (Both et al., 2019; Parker et al., 2005). A sharp increase in viscosity at ~50 w/w% was related to jamming of the globular whey proteins. This is in line with earlier observations: oscillatory rheology with just the whey protein bovine serum albumin (BSA) at dry matter contents between 40 and 50 w/w% showed viscous behavior, except for the 50 w/w% which had a crossover from viscous to elastic viscoelastic behavior at around 8 Hz (Brownsey et al., 2003). We here used systems with >70 w/w% solids, which showed predominantly elastic behavior. We therefore pose that the jamming of the whey proteins causes structural arrest; larger concentration does not alter the viscoelastic properties much. Whey proteins are a mixture of proteins with different size and shape, for example BSA is 'heart' shaped

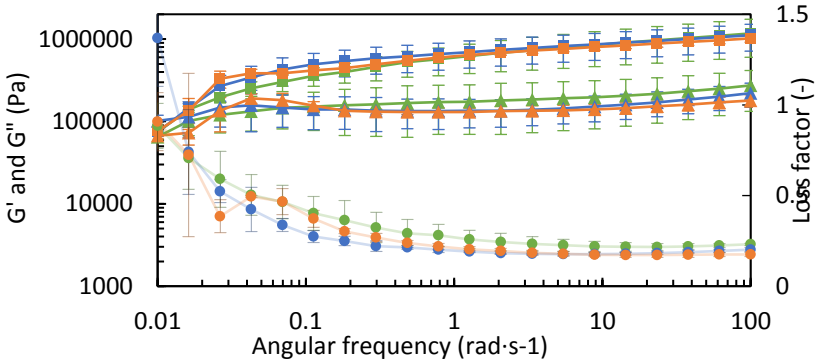

Fig. 5.7. Frequency sweep on films with different composition, with (orange) 100:0, (blue) 25:75, (green) 50:50 (WP:MD). With (■) storage modulus G', (▲) loss modulus G", and (●) loss factor. Films had 75 w/w% d.m. and were 0.72 mm thick

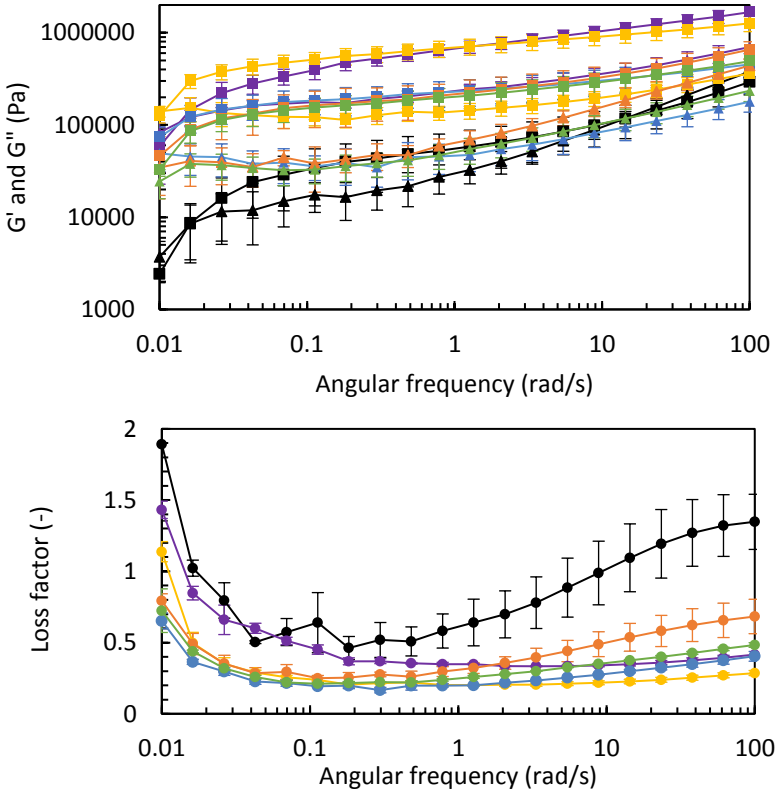

Fig. 5.8. Frequency sweep on films with different composition, with (yellow) 50:50, (purple) 25:75, (green) 10:90, (blue) 5:95, (orange) 1:99, (black) 0:100 WP:MD. With at top (■) storage modulus G' and (▲) loss modulus G", and at bottom (●) loss factor. Films had 82 w/w% d.m. and were 0.45 mm thick.

with a hydrodynamic radius (R_h) of 3.7 nm, whereas BLGs are ellipsoids and form dimers at neutral pH with a R_h of 2.6 to 4.9 nm (Loveday et al., 2007; Parker et al., 2005). We do find that the rheological behavior of whey proteins can be described as that of hard, globular spheres, and thus can be regarded as a colloidal system (Parker et al., 2005). Therefore, the jamming of the proteins can be described as a colloidal glass transition (Weeks, 2017), which explains the viscoelastic properties measured here.

Maltodextrin DE12 is a mostly linear glucose oligomer with on average 7-10 monomers per molecule. Maltodextrin solutions remain liquid up to concentrations of 70 w/w%, and its viscosity can be well described by regular polymer dynamics (Avaltroni et al., 2004; Both et al., 2019). Indeed, we observed this behavior for films with 82 w/w%. The predominantly viscous behavior at low frequencies is possible due to sufficient relaxation of the chains, followed by a 'rubbery' plateau where the elastic part is dominant. A second crossover marks the start of the transition region. At even more extreme angular frequencies, beyond what is measured here, glassy behavior may be observed in polymer systems, as the glass transition temperature is reduced by 6 to 7°C per decade of frequency (Sperling, 2001).

In summary, the behavior of the films composed of both whey protein and maltodextrin was more elastic, indicating structural arrest, even at 75% maltodextrin of the dry matter. This is different from the viscosity measurements by Both et al. (2019), where maltodextrin had a large effect: at more than 25% maltodextrin of the dry matter, the jamming of the whey proteins was hindered by the maltodextrin. Therefore, we concluded that upon addition of maltodextrin the jamming of whey proteins occurs at higher concentrations.

5.3.2.3 Effect of the dry matter content on the viscoelastic properties

During drying the droplets the dry matter content will increase over time. Therefore, we investigated the viscoelastic properties over a wider range of dry matter contents for a 50:50 (WP:MD) mixture (Fig 5.9). At 66 w/w% the viscoelastic response was initially as a solid viscoelastic material, but showed an increase in the loss factor at higher solids content. This is normally associated with viscoelastic behavior, and could therefore indicate that maltodextrin is the continuous phase at these conditions. Upon increasing the concentration towards 72 w/w% different behavior emerged: although the material was still a viscoelastic solid, it was much more deformable and had a larger frequency dependency. Increasing the solids content towards 75 w/w% strongly reduced the loss modulus, while the response did not depend anymore on the frequency above 1 $rad \cdot s^{-1}$.

Further increasing the solids content to 80 w/w% reduced the loss modulus even further, and frequency dependent behavior was only observed below 0.1 rad·s^{-1}.

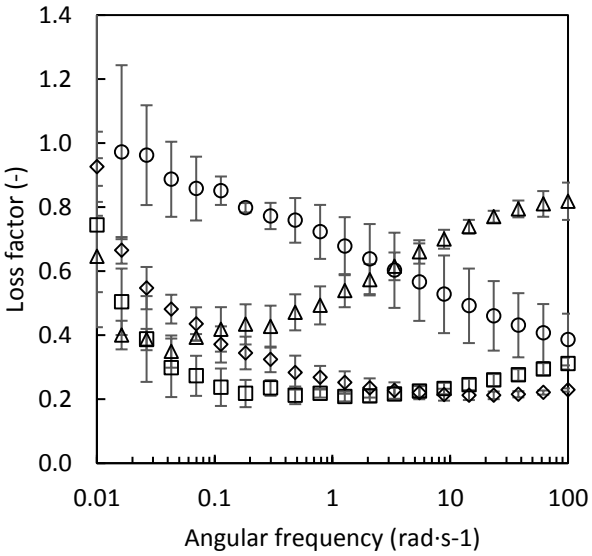

Fig. 5.9. Effect of dry matter on the viscoelastic properties of 50:50 films (WP:MD). With (△) 66 w/w%, (○) 72 w/w%, (◇) 75 w/w%, (□) 80 w/w%. Film thickness was 0.63 mm.

5.3.3. Morphology development during droplet drying

During droplet drying, the concentration of components near the surface increases and a skin is formed (Vehring et al., 2007). This skin does not only lower the evaporation rate, but also mechanically prevents further shrinkage of the droplet. However, the continuing evaporation reduces the pressure inside the droplet (Sugiyama et al., 2006). Due to this pressure, the droplet can either deform when the skin is deformable, or form a vacuole when the skin is rigid (Sadek et al., 2015a). Understanding the resistance of the skin against deformation is necessary to understand this morphology development. Single droplet techniques are not suitable to measure skin deformations, due to the small droplet size and the small forces needed for indentation measurements, so we have to relate these to drying thin films.

5.3.3.1. Morphology development during thin film drying

The drying kinetics monitored during thin film drying showed a faster decline in evaporation rate for films that were rich in whey protein. We showed that whey protein jams during

drying, leading to a rigid skin. This is related to skin formation and morphology development during thin film and single droplet drying. In single droplet drying, the stresses on the skin are reduced by the formation of a vacuole. However, in thin film drying the surface area is fixed. A skin that is rigid can only crack and form local defects, and may even fragment. Therefore, although the phenomena in both systems are different, they originate from similar material behavior and can be related to each other. Visual observation of the skin formation during thin film drying shows that the absence of air in the solution delays the skin formation and subsequent wrinkling or cracking of the film. The exact relation of this phenomenon to particle morphology is still unknown.

5.3.3.2. Relating thin film rheology to droplet drying

Rheological measurements of thin films with high concentrations showed that as little as 1% whey protein of the total dry matter already altered the viscoelastic behavior. This differs from viscosity measurements performed at lower concentrations, where at least 75% protein (of the dry matter) is necessary for a similar influence on the viscoelasticity (Both et al., 2019). We hypothesize that during droplet drying, droplets that are high in maltodextrin still have a flexible skin at intermediate dry matter content (~50-60 w/w%), giving a liquid-like viscoelastic response, allowing wrinkling of the skin. At higher concentrations the skin becomes structurally arrested, no further wrinkling is possible and vacuoles are formed.

In solutions of mostly whey protein, structural arrest occurs at lower solids content, and the vacuoles formed are fewer in number and larger in size, compared to a material where structural arrest occurs at high solids contents, e.g. maltodextrin. This corresponds with the observations of Both et al. (2018a), who observed that droplets high in protein formed smooth particles with one large vacuole (Fig 5.10a), while droplets high in maltodextrin formed wrinkled particles with multiple small vacuoles (Fig 5.10b).

A next step in understanding the skin formation would be to measure the rheological response over a broader concentration range for all components, as was here only done for 50:50 (WP:MD). In this way the dry matter content marking the transition from liquid-like response to structural arrest can be assessed per component, and linked to vacuole formation during droplet drying.

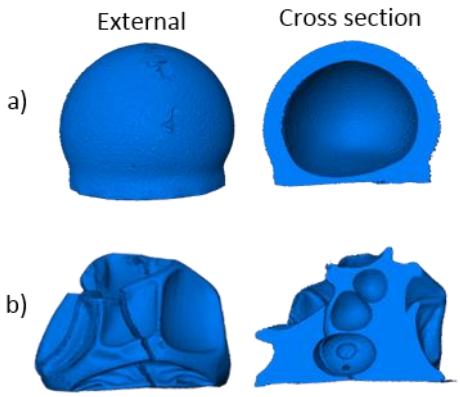

Fig. 5.10. Vacuole formation during single droplet drying, with a) 75:25 (WP:MD) dried at 40°C where one large vacuole was formed, and b) 10:90 (WP:MD) dried at 70°C where 5 small vacuoles were formed (adapted from Both et al. (2018a)).

5.4. Conclusion

We presented a study on thin film drying and rheology to understand droplet drying during spray drying. The effect of skin formation on drying kinetics was shown using a custom-build thin film dryer. Films high in whey protein had lower drying rates. The visual appearance of films was different compared to droplet morphology, but could be well related to it by considering the different system geometry. The rheological data provided insight in the viscoelastic behavior of the whey protein – maltodextrin mixtures at high concentrations, where structural arrest was observed for whey protein-rich (<25%) samples at 75 w/w% dry matter. Conversely, maltodextrin-rich (>75%) films were in a rubbery state and showed typical polymeric behavior at 82 w/w% dry matter. In mixtures of 50:50 (WP:MD) a transition was observed from rubbery behavior to structural arrest when increasing the dry matter content of the films.

This work showed that thin film experiments are complementary to single droplet drying experiments. The combination of both teaches about the formation and properties of the skin, and the subsequent development of particle morphology. More specifically, vacuole formation can be predicted by the occurrence of structural arrest at specific concentrations. With better understanding of the viscoelastic material properties at high dry matter contents, we can therefore more accurately predict spray-dried powder properties. This can contribute to production of less off-spec powder and mitigate undesired processes during spray drying, such as fouling and caking.

Appendix 5.I. Preparation conditions and resulting properties

Table 1. Conditions for sample preparation and the resulting sample properties

	SAMPLE PREPARATION			SAMPLE PROPERTIES	
RATIO (WP:MD)	**Volume (ml)**	**Oven time (min)**	**RH (%)**	**D.M. (w/w%)**	**Thickness (mm)**
0:100[2]	7	115	85	82±0.2	0.46±0.01
1:99[2]	6	100	85	82±0.3	0.47±0.01
5:95[2]	5	100	85	81±0.2	0.47±0.02
10:90[2]	6	100	85	81±1.0	0.56±0.02
25:75[2]	4	55	87	82±0.3	0.43±0.02
50:50[2]	4	55	87	81±0.4	0.48±0.04
50:50[3]	6	85	87	80±0.0	0.67±0.07
50:50[1,3]	6	85	94	75±0.1	0.64±0.02
50:50[3]	6	85	95	72±0.0	0.58±0.01
50:50[3]	6	85	97	66±0.0	0.63±0.07
75:25[1]	5	60	94	76±1.0	0.73±0.08
100:0[1]	5	35	95	73±1.1	0.79±0.02

Used in [1]) figure 5.7, [2]) figure 5.8, and [3]) figure 5.9.

6

General discussion

6.1. Introduction

Spray drying is a process often used in the food industry to make powdered products with an extended shelf life. The liquid feed is dispersed in many minute droplets, which are dried with hot air. During the drying not only water is removed, but the particles also solidify and obtain a morphology, which co-determines the powder quality. The aim of this thesis was to obtain mechanistic understanding of particle morphology development during spray drying. This chapter discusses the main findings of this thesis, combining results from small-scale drying and rheology, relates the main findings to large-scale spray drying experiments, and concludes with an outlook towards future research.

6.2 Main Findings

The drying of sessile droplets consisting of whey protein and maltodextrin was investigated in **chapter 2 and 4**. The initial drying kinetics are, as expected, externally limited, thus only dependent on the drying temperature and not on the particle composition. During drying, dissolved components accumulate near the surface, resulting in skin formation, locking and eventually solidification and morphology development. Droplets consisting of whey proteins (WP), globular proteins, form smooth, spherical particles with one large vacuole. Drying of droplets consisting of maltodextrin DE12 (MD), a random chain carbohydrate polymer, produces wrinkled particles with multiple, small vacuoles. The morphology of droplets of mixtures of the two components could be influenced with the composition, the drying temperature, the initial droplet size and the dry matter content. Confocal Raman microscopy showed the occurrence of phase separation: when droplets were dried at lower temperature, the two polymers became phase separated at least to some extent, and a hollow morphology was formed.

While practically relevant food products such as milk are complex, much of its complexity can also be found in simpler model systems, with whey proteins and casein, and maltodextrin as model components for milk. This was shown in **chapter 3**. In the model solutions the carbohydrates dominate the morphology development, with maltodextrin forming wrinkled particles and lactose dense particles. The added whey protein does not influence the formed morphology, due to the low overall concentrations (max 30% of dry matter). The addition of casein leads to the formation of a more wrinkled particle in the case of maltodextrin – casein particles, and a different morphology of the lactose – casein

particles, if present in sufficiently high amounts. This is due to the flexibility of the casein micelle. In line with these findings, the morphology of complete milk particles was shown to be dominated by the casein micelles present.

In **chapter 4** the viscosities of maltodextrin, whey protein and mixtures thereof were measured and modelled as a function of concentration. Whey protein jams at concentrations of ~50%, whereas maltodextrin remains fluid up to concentrations of ~70%. The jamming of whey protein in the skin during drying provides rigidity to the skin that resists deformation, and therefore hollow particles are formed. Maltodextrin on the other hand is still deformable at high concentration, leading to a wrinkled morphology. To explore skin properties at even higher concentrations, thin films were prepared with a dry matter content of 66% to 82% of which the viscoelastic properties were measured in **chapter 5**. Maltodextrin films show behavior that is typical of random polymers with rubbery behavior, although as little as 1% whey protein (i.e. 1:99 WP:MD) already leads to a drastically increased skin strength. At the measured concentrations, addition of at least 25% protein (i.e. 25:75 WP:MD) results in structural arrest of the films. This was shown to be related to vacuole formation in single droplet drying. Formulations that undergo structural arrest at low concentration, i.e. formulations that are high in whey protein, form fewer but larger vacuoles, compared to formulations that only undergo structural arrest at very high concentration, i.e. formulations high in maltodextrin. It is clear that the rheological behavior over a wide range of concentration is important for understanding the overall morphology development, from initial skin formation, to the occurrence of wrinkling of the surface and/or vacuole formation.

6.3 Pilot-scale spray drying and powder analysis

Single droplet drying was shown to be a suitable method to observe the morphology development of model and complex solutions during drying, however the translation of these results to the actual spray dried droplets is not straightforward. First, in spray drying the wide droplet size distribution and different drying trajectories lead to a wide variation in drying times and behavior. However, the most crucial difference is the smaller droplet diameter employed in spray drying, between 10 and 100μm, whereas the sessile droplets dried in this study were around 1 mm. This difference in size impacts the drying times, which are roughly proportional to the square of the droplet size, and with that possibly the morphology development.

Therefore, a pilot-scale spray drying run was done for whey protein – maltodextrin mixtures, to investigate the correspondence between the morphologies obtained with single droplet drying and with practical spray drying, and to assess the possibility of steering the powder properties on pilot scale. A single stage pilot-scale spray dryer (DW1000 Spray dry work, Netherlands) was used, which had a maximum evaporation capacity of 80 kg/h. The effect of the composition on the morphology was studied by drying maltodextrin DE12 (Roquette, France), whey protein isolate (Volac, United Kingdom), and mixtures with a ratio of 75:25 and 50:50 (WP:MD). The drying conditions were varied by changing the inlet air temperature, 140°C, 150°C or 190°C, and the relative humidity of the outlet air (RH_{out}), 8% or 15%. The RH_{out} was changed by varying the nozzle pressure, which influenced the feed rate. The outlet air humidity was the main control parameter, and not temperature, as this provides a fairer comparison between the samples using a Mollier diagram. The exact drying conditions per sample are given in table 1 in Appendix 6.I.

The produced powders were analyzed on visual appearance, particle size distribution, and bulk density. A selection of the powders was analyzed on morphology with a Malvern Morphologi 4 system. 11 mm^3 of powder was distributed on a glass plate; the individual particles were photographed, and the particle circumference, width, length, and light intensity, were measured and converted into descriptive parameters such as the circularity and the CE diameter. This was repeated 2 to 4 times until sufficient particles were scanned, i.e. between 8 900 and 24 000 particles per sample. Filters were then applied to classify particles based on one or more parameters, as described in table 2 in the Appendix 6.I. Particles below 5 or above 100 µm were excluded the classification, which amounted to 5 – 25% of the total and were mostly small particles.

6.3.1 Morphology of spray dried powders

The effect of the composition on the morphology was studied by drying all formulations at T_{in} = 190°C and RH_{out} = 8%. Large differences in the morphology within the batches were observed (Fig. 6.1a – d), but the overall appearance is clear: maltodextrin and 50:50 (WP:MD) powder contained more wrinkled particles, whey protein more hollow and fragmented, and the 75:25 (WP:MD) powder has both characteristics. This is most clearly visible through quantitative analysis (with a Malvern Morphologi 4 particle characterization system). Three groups were differentiated: hollow particles, wrinkled particles and other particles. The first two groups resemble the morphologies that were observed with single

droplet drying, while the latter group is a mixture of fragmented or agglomerated particles without a distinctive morphology. This classification indeed shows that the maltodextrin and 50:50 (WP:MD) powder contained more wrinkled particles than the 75:25 (WP:MD) and whey protein powder, and less hollow particles (Fig. 6.1e). Whey protein powder and the mixtures also contained a large fraction of other particles. Once dried, the hollow particles are more fragile than wrinkled (compact) particles, and fragment more easily upon wall collision, such that they end in the 'other' category. This confirmed by the observation that many particles created with WP showed many cracks in the shell of the hollow particles, indicative of their susceptibility to shattering

The quantitative results were classified according to particle size. Small particles (between 5 and 20µm) are more often hollow, while larger particles (between 20 and 100µm) are more often wrinkled. Smaller droplets have a higher heat and mass transfer coefficient, as described in the Ranz-Marshall equation (Ranz and Marshall, 1952), thus have a faster evaporation rate (Tran et al., 2016), which leads to faster crust formation and thus probably to formation of more hollow particles.

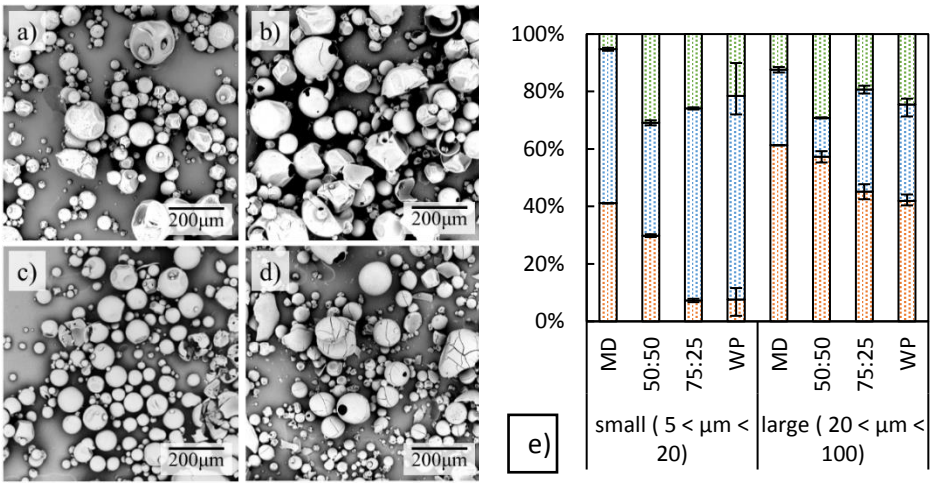

Fig. 6.1. Effect of composition of spray dried powders on morphology, with SEM images: a) maltodextrin (MD), b) 50:50 (WP:MD), c) 75:25 (WP:MD) and d) whey protein (WP), and d) the results of the Morphologi 4 with % wrinkled (orange), % hollow (blue) and % other (green), divided in two size groups: between 5 and 20µm and between 20 and 100µm. Categories are described in the appendix. The formulations were dried at 190°C inlet temperature and 8% outlet humidity. The error bars represent the absolute error.

The effect of the drying conditions on the morphology was studied for a 75:25 (WP:MD) mixture, dried at five different conditions. Here the visual differences between the samples were small (Fig. 6.2a – e); all samples contained both hollow and wrinkled particles. Quantitative morphological classification 4 yielded a significant difference in particle morphology however: a higher inlet temperature leads to less wrinkled particles, with ~ 6% wrinkled particles at T_{in} 190°C, 15% at T_{in} 150°C, and 20% at T_{in} 140°C (small particles, RH_{out} 15%), while the number of hollow particles increases with higher inlet temperatures. The number of particles that could not be classified as hollow or wrinkled was larger, especially at lower inlet temperatures. This might be due to particle stickiness and subsequent agglomeration, or due to particle fragmentation. Increasing the outlet humidity did not have a pronounced effect on the morphology development. Again, a large effect of the droplet size was observed: smaller particles are more often hollow, caused by faster drying kinetics as discussed before.

This indeed demonstrates that it is possible to control the morphology of mixtures by adapting the drying conditions: a lower inlet temperature yields more wrinkled particles, and thus less hollow particles. The outlet humidity is not an important parameter. The inlet temperature is important during the initial drying, where most evaporation takes place and skin formation is initiated, while the outlet temperature is only important at the final stage of drying, where most water has already evaporated, and most morphological changes have already taken place.

6.3.2. Relation to observations in single droplet drying

The morphologies obtained with pilot-scale drying were similar to those obtained with single droplet drying. Single droplet drying yields wrinkled particles with maltodextrin, 75:25 (WP:MD) and hollow particles with whey protein, while for 50:50 (WP:MD) it depended on the drying conditions (**chapter 2**). This corresponds to the overall observations in the pilot trial, although this gave much more variation in morphology. This demonstrates the usefulness of the single droplet drying approach despite the different time scales of drying.

The whey protein isolate used in pilot-scale study was obtained from a different supplier than the whey protein used in the rest of this thesis. The WPI used here contained some insoluble components, probably denatured protein, of which preliminary single droplet drying experiments showed irregularities on the surface of the particles. The insoluble

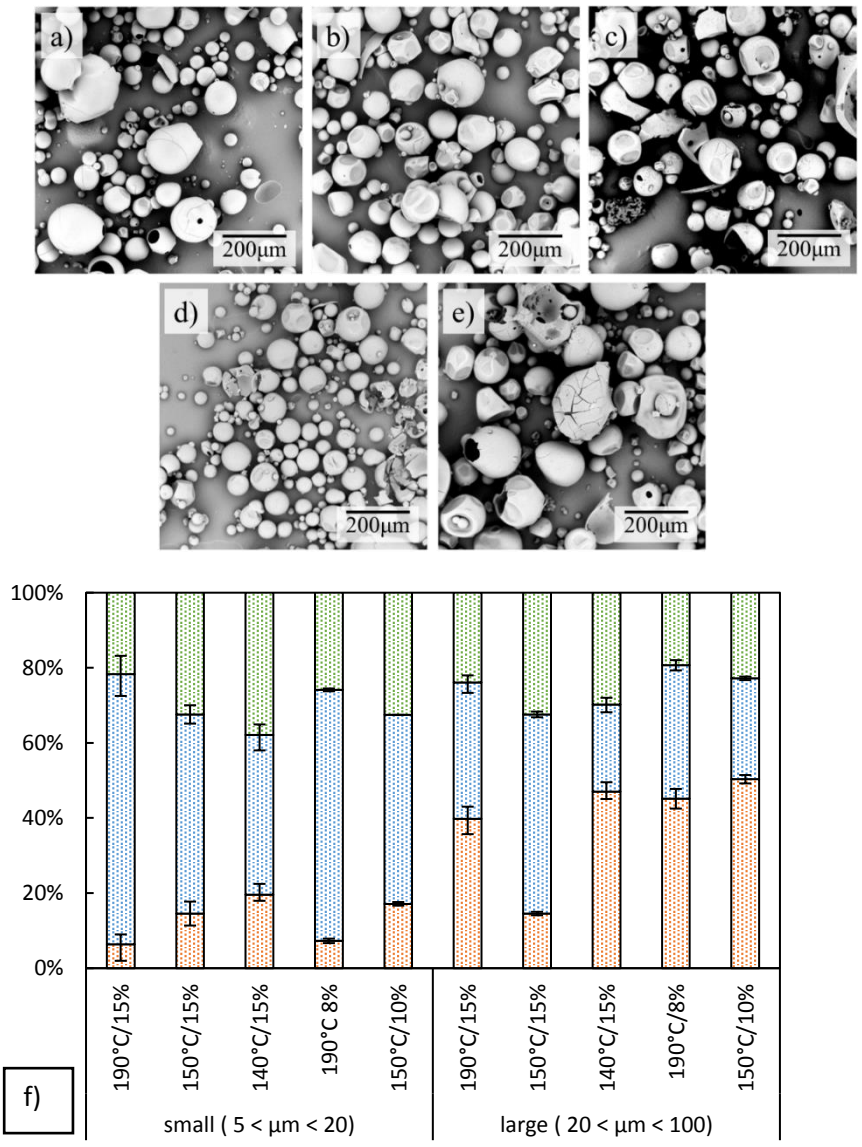

Fig. 6.2. Effect of drying conditions on 75:25 (WP:MD) spray dried powders on morphology, with SEM images: a) 190°C/15%, b) 150°C/15%, c) 140°C/15%, d) 190°C/8%, e) 150°C/10%, and f) the results of the Morphologi 4 with % wrinkled (orange), % hollow (blue) and % other (green) divided in two size groups: between 5 and 20µm and between 20 and 100µm. Categories are described in the appendix. The error bars represent the absolute error.

components can be removed by centrifugation before drying, after which smooth particles are formed (data not shown). These insoluble components are likely to have also influenced the morphologies observed in the pilot-scale drying.

The effect of the droplet size on the obtained morphology was opposite between the methods: larger droplets were wrinkled in pilot-scale, and smaller particles were hollow, in single droplet drying this was the other way around (**chapter 4)**. This can be explained by the different phenomena taking place. In single droplet drying the larger droplets have more time to phase separate due to the longer drying times, which has a pronounced effect of the whey protein present. This promotes the formation of hollow particles. In pilot-scale drying, however, drying times are very short, and phase separation is unlikely to occur. Smaller droplets will dry faster, due to faster heat and mass transfer, and therefore have an earlier locking point. This leads to the formation of hollow particles. During single droplet drying, lower drying temperatures lead to more extensive phase separation within the droplet, and more hollow particles are formed (**chapter 2**). In spray drying a lower temperature leads to later locking, and therefore more wrinkling. Therefore, the time scale of drying has to be taken into account. This suggests the need for single droplet drying methods that can be operated with smaller droplets at higher air temperatures.

6.3.3. Relation between morphology and powder properties

The relation between particle morphology and the macroscopic powder properties is not yet well established. The importance of the size and shape of the individual particles on the flow behavior of a powder was shown for lactose (X. Fu et al., 2012), and for glass spheres, calcium carbonate crystals, and plate-shaped talc (Bumiller et al., 2002). The effect of the particle surface area, bulk density and porosity, on the reconstitution behaviour was also shown for maltodextrin powders (Takeiti et al., 2010). However, the effect of the drying conditions on morphology and subsequent powder properties is still not fully understood and therefore of interest here. Therefore, the bulk density and particle size distribution of the produced powders were analyzed and compared to the morphology (Fig. 6.3).

The effect of the drying conditions on bulk density was studied by varying the operating conditions during drying of systems with compositional ratio 75:25 (WP:MD) (Fig. 6.3a). There is a clear link between morphology and bulk density. Powders that contained more hollow particles, also had a lower bulk density, which may be explained by the larger porosity of the hollow particles. At the same time the number mean diameter (D[1,0])

remained constant. We compare here to the number mean particle size as the percentage of hollow particles is also number-based. At the same time, the volume mean particle size increases with smaller percentage of hollow particles – the fact that the number mean diameter remains constant, indicates a much wider distribution with less hollow particles. We expect that this is because of more agglomeration and the presence of a few large agglomerates when drying at lower inlet air temperature (especially 140 °C). The formation of these agglomerates may be due to the particles being dried at a slower rate, and therefore remaining sticky for a longer time. The agglomeration may either prevent the primary particles from becoming hollow, or may lead to collapse of initially hollow primary particles, due to rewetting by the agglomerate, which remains wet for a longer time than individual primary particles, due to its much smaller surface-to-volume ratio.

The maltodextrin powder had a much higher bulk density (>450 g/L) compared to formulations containing whey protein (Fig. 6.3c), while the particle size was comparable to other formulations dried at the same drying conditions (Fig. 6.3d). The differences between the other formulations were smaller, but present nonetheless. Whey protein and 50:50 (WP:MD) powder had similar bulk densities (350 – 400 g/L), while the powder with a ratio of 75:25 (WP:MD) had a slightly lower bulk density (340 – 370 g/L at similar drying conditions). Similarly as for 75:25 (MD:WP) powder (Fig. 6.3a), the ratio 50:50 (WP:MD) shows that the bulk density can be increased by decreasing the inlet temperature. Although morphological analysis was not done for these samples, it is expected that this corresponds to an increase in percentage of wrinkled and decrease in percentage of hollow particles. The two mixed formulations dried here show that the bulk density can indeed be influenced by adapting the inlet temperature.

An important process parameter is the nozzle pressure, which determines the feed rate and with that the outlet conditions of the spray tower. Moreover, it influences the droplet size of the spray, which in its turn influences the drying kinetics and final particle size. Higher nozzle pressure can be expected to generate smaller droplets, which affects the morphology development. However, the final particle size appears to be randomly distributed with nozzle pressure for the majority of the samples (Fig. 6.3b). The large average particle size of the 75:25 (WP:MD) powder produced at 20 bar might be caused by agglomeration due to stickiness of the drying droplets, which is caused by the low drying temperature (140°C). Only the powders produced at the highest nozzle pressure (>70 bar)

gave a slightly smaller particle size. Therefore, the nozzle pressure has only a small effect on the powder characteristics. The relation between the droplet size and the particle size is not evident, however: it depends on the shrinkage before solidification, which in its turn depends on the droplet composition and drying conditions.

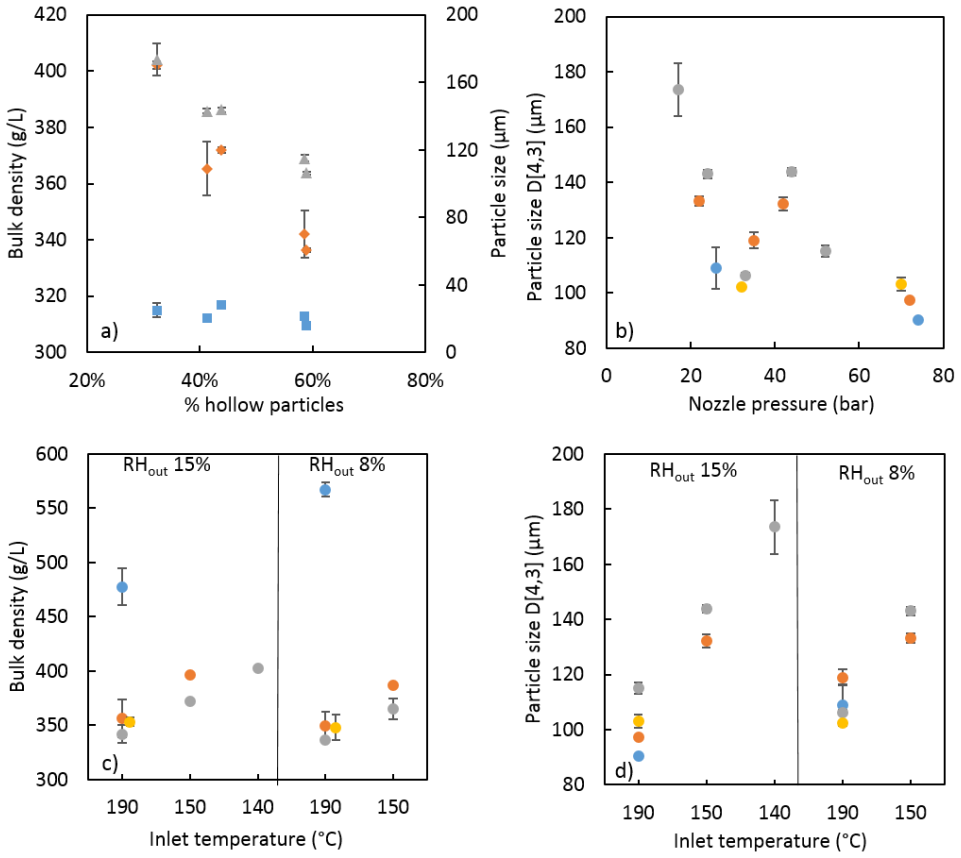

Fig. 6.3. Analysis of the spray dried powder, with a) powder with a 75:25 (WP:MD) ratio with the % hollow particles as a function of (◆) bulk density (g/L), (■) number mean diameter D[1,0] (µm), and (▲) volume mean diameter D[4,3] (µm), and b) the effect of nozzle pressure on particle size, c) the powder bulk density (g/L) as a function of drying conditions, and with d) volume mean diameter D[4,3] (µm) as a function of inlet conditions. With (●) maltodextrin DE12, (●) whey protein, (●) 50:50 (WP:MD), and (●) 75:25 (WP:MD).

Ultimately, it is desired to produce powders with fast reconstitution and high flowability. However, the relation of these macroscopic properties and the particle morphology is not yet fully understood. This is complicated by the fact that powders are normally agglomerated to improve these properties, and a combined effect is expected. Previous studies show a relation between the morphology of the agglomerates and the instant properties of a powder (Ji et al., 2015; Turchiuli et al., 2005). The flowability and reconstitution of the powder produced in our pilot experiments were not measured, as the powders were not agglomerated and thus not optimized for these properties.

6.3.4. Conclusions of pilot-scale spray drying

The results from the pilot-scale experiments showed that overall the morphologies observed could be very well compared to the single droplet drying results, despite the effect of the different time scales of drying. However, the wide particle size distribution combined with the large effect of size on morphology created much variation in morphology with the powders produced on pilot scale, which made visual distinction between samples difficult. Quantitative assessment of the powder morphology is therefore very important.

The drying conditions can increase the number of wrinkled particles from 19% to 34% for a 75:25 (WP:MD) powder, while reducing the number of hollow particles from 59% to 32%. This is done by operating the spray dryer at very low inlet temperatures and/or low outlet humidity, which reduces the capacity of the tower significantly. Therefore, the drying conditions used here are normally not used in industrial processes. Therefore, this trial should be seen as a 'proof of principle' that morphology can indeed be steered by changing conditions, and should investigated further for feasibility on larger scale. The larger process costs may be acceptable for specific high-quality products, but may not be feasible for bulk applications.

Although the single droplet drying results are representative for spray drying at pilot-scale, it is still important to further develop the single droplet drying methods. First of all, the droplet size in the currently available set-ups is a factor 10 larger than during spray drying. Drying at the proper droplet size is relevant, shown by the effect of size in the pilot-scale experiments. Secondly, realistic drying temperatures, and especially the rapid initial drying (when the droplet is exposed to a high inlet air temperature up to 220°C) should be simulated in an experimental single droplet drying set-up. Currently, the entire drying

process operates at typical spray drying outlet temperatures of around 80°C, which slows down the initial drying rates tremendously. Developing better single droplet drying methods will provide a better insight in spray drying.

6.4 Outlook for future research

The results from the pilot-scale drying demonstrated the value of combined single droplet drying and rheology measurements. The next step is to create guidelines for morphology development, by answering the following questions:

1. Does the formulation undergo structural arrest, and if so at what dry matter content?
   Method: measure the rheological properties at high dry matter content (50 to 80 w/w%)

From the rheological experiments on whey protein – maltodextrin films it was hypothesized that formulations that undergo structural arrest at low concentration form fewer but larger vacuoles, compared to formulations that will only undergo structural arrest at very high concentration. However, these measurements were here done with only a few, relatively simple formulations. Following the procedure of **chapter 5** this range could be extended, and the hypothesis checked for validity over a wider range of formulations. For example, micellar casein was found to deform even after initial locking (Dahbi et al., 2010), which should be taken into account in the prediction of the morphology.

2. What is the critical concentration in the skin for morphology development?
   Method: compare rheological data to single droplet drying data

The rheological properties of the skin at the locking point determine the particle morphology, however the concentration in the skin at locking is as yet unknown, and will not be similar for each formulation. Measuring the rheological properties as a function of dry matter content can provide insight in the critical skin concentration. For example, a droplet with 50:50 (WP:MD) formed a wrinkled morphology (**chapter 2**), and therefore the skin concentration was most likely below 72 w/w%, such that the rheological behavior was still rubbery (**chapter 5**). Knowing the critical concentration for morphology development narrows the window for rheological experiments.

3. Can the morphology of new formulations be predicted?
   Method: create a numerical model for morphology development

Once the critical skin concentration and rheological behavior at that concentration is known, these data should be captured in integrated models for coupled heat and mass transfer and rheology. Subsequently these (numerical) models may be used to predict the morphology. Ultimately, guidelines should be developed from numerical modelling results, which can be applied in industrial practice.

4. Can we steer towards a desired particle morphology?

   Method: altering drying conditions (pilot-scale) and component properties (lab-scale)

Ideally, we can indeed steer spray drying processes to produce a specific desired morphology. Indirectly, this would allow control of powder properties. This may be done by changing the drying conditions or by adjustment of the ingredient properties. In the case of for whey proteins this can be done by altering the protein-protein interactions (Fig. 6.4). Near neutral pH (pH 5 – 8), the particles had a smooth surface and a large internal vacuole, due to jamming of the whey proteins upon concentration. However, the droplet wrinkled when a solution was dried with a pH close to the isoelectric point of the whey proteins (pH 4.5), due to reduced intermolecular repulsion. At pH 4 and 9 the droplet did form a vacuole, although the surface was not smooth. Possibly at these extreme pH conditions the whey protein unfolded and might even have been aggregated. The addition of salt yielded similar results: at neutral pH (6.2) and salt concentrations higher than 0.5M NaCl or 0.1M $CaCl_2$ the particles were wrinkled, similar to drying at pH 4.5 (data not shown). Similarly, the addition of carbohydrates with different chain length alters the rheological properties, and may be used in a similar way to steer the morphology.

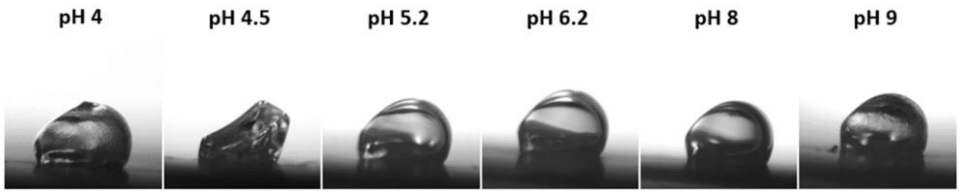

Fig. 6.4. The effect of pH on the morphology of dried whey protein particles. The droplets were dried on the sessile single droplet drying platform as described in Perdana et al. (2011), with an initial dry matter content of 30 w/w% and an initial diameter of 1 mm, at an air temperature of 90°C, RH of 1% and an air flow of 0.3 m/s.

6.5 General conclusion

In this thesis, single droplet drying, thin film drying and rheology were combined for better understanding of the mechanisms that determine the morphology of powder particles that are obtained with spray drying. The component properties have the strongest effect, and rheological measurements can shed much light on the effects that are important in this. This was shown for whey protein, maltodextrin and mixtures thereof, and could explain whether a particle would wrinkle or not, and what the size and number of vacuoles are. Understanding the drying behavior of model components lead to a better understanding of the drying of a complex formulation like milk. Finally, the morphologies observed in single droplet drying were similar to pilot-scale drying. Therefore, the that was obtained can lead to a better understanding of particle morphology development during spray drying, and with that to the production of better quality products, with a lower environmental impact.

Appendix 6.I. Experimental set-up

Table 6.I.1. Drying conditions

Inlet temperature	Outlet temperature	Outlet humidity	Composition	Nozzle pressure
190°C	93°C	8%	MD	26
			WP	32
			50:50	35
			75:25	33
	80°C	15%	MD	74
			WP	70
			50:50	72
			75:25	52
150°C	83°C	10%	50:50	22
			75:25	24
	73°C	15%	50:50	42
			75:25	44
140°C	70°C	15%	75:25	17

Table 6.I.2. Categories used in Morphologi 4 analyzer:

		HS Circularity**		
		< 0.85	0.85 ≤ x < 0.93	≥ 0.93
Intensity mean*	< 50	Other	Wrinkled	Hollow
	≥ 50		Hollow	Hollow

* Intensity mean: the average of the pixel greyscale levels in the object ranging from 0 (black) to 255 (white)

** HS Circularity: $\frac{4*\pi*Area}{Perimeter^2}$

R

References

Adhikari, B., Howes, T., Bhandari, B.R., Langrish, T.A.G., 2009. Effect of addition of proteins on the production of amorphous sucrose powder through spray drying. J. Food Eng. 94, 144–153. doi:10.1016/j.jfoodeng.2009.01.029

Adhikari, B., Howes, T., Bhandari, B.R., Troung, V., 2017. Surface Stickiness of Drops of Carbohydrate and Organic Acid Solutions During Convective Drying : Experiments and Modeling 3937. doi:10.1081/DRT-120021689

Adhikari, B., Howes, T., Bhandari, B.R., Truong, V., 2000. Experimental studies and kinetics of single drop drying and their relevance in drying of sugar-rich foods: A review. Int. J. Food Prop. 3, 323–351. doi:10.1080/10942910009524639

Adhikari, B., Howes, T., Lecomte, D., Bhandari, B.R., 2005. A glass transition temperature approach for the prediction of the surface stickiness of a drying droplet during spray drying. Powder Technol. 149, 168–179. doi:10.1016/j.powtec.2004.11.007

Alamilla-Beltrán, L., Chanona-Pérez, J.J., Jiménez-Aparicio, A.R., Gutiérrez-Lopez, G.F., 2005. Description of morphological changes of particles along spray drying. J. Food Eng. 67, 179–184. doi:10.1016/j.jfoodeng.2004.05.063

Andersson, I.M., Glantz, M., Alexander, M., Millqvist-fureby, A., Paulsson, M., Bergenståhl, B., 2018. Impact of surface properties on morphology of spray-dried milk serum protein / lactose systems. Int. Dairy J. 85, 86–95. doi:10.1016/j.idairyj.2018.04.011

Anese, M., Shtylla, I., Torreggiani, D., Maltini, E., 1996. Water activity and viscosity—relations with glass transition temperatures in model food systems. Thermochim. Acta 275, 131–137. doi:10.1016/0040-6031(95)02712-2

Avaltroni, F., Bouquerand, P.E., Normand, V., 2004. Maltodextrin molecular weight distribution influence on the glass transition temperature and viscosity in aqueous solutions. Carbohydr. Polym. 58, 323–334. doi:10.1016/j.carbpol.2004.08.001

Berenschot, 2017. Electrification in the Dutch process industry, http://www.ispt.eu/media/Electrification-in-the-Dutch-process-industry-final-report-DEF_LR.pdf.

Both, E.M., Karlina, A.M., Boom, R.M., Schutyser, M.A.I., 2018a. Morphology development during sessile single droplet drying of mixed maltodextrin and whey protein solutions. Food Hydrocoll. 75, 202–210. doi:10.1016/j.foodhyd.2017.08.022

Both, E.M., Nuzzo, M., Millqvist-Fureby, A., Boom, R.M., Schutyser, M.A.I., 2018b. Morphology development during single droplet drying of mixed component formulations and milk. Food Res. Int. 109, 448–454. doi:10.1016/j.foodres.2018.04.043

Both, E.M., Siemons, I., Boom, R.M., Schutyser, M.A.I., 2019. The role of viscosity in

morphology development during single droplet drying. Food Hydrocoll. 94, 510–518. doi:10.1016/j.foodhyd.2019.03.023

Bouman, J., Venema, P., de Vries, R.J., van der Linden, E., Schutyser, M.A.I., 2016. Vacuole and hole formation during drying of sessile whey protein droplets. Food Res. Int. 84, 16. doi:10.1016/j.foodres.2016.03.027

Brask, A., Ullum, T., Thybo, P., Andersen, S., 2007. High-temperature ultrasonic levitator for investigating drying kinetics of single droplets, in: 6th International Conference on Multiphase Flow. Leipzig, Germany.

Brownsey, G.J., Noel, T.R., Parker, R., Ring, S.G., 2003. The glass transition behavior of the globular protein bovine serum albumin. Biophys. J. 85, 3943–3950. doi:10.1016/S0006-3495(03)74808-5

Bumiller, M., Carson, J., Presscott, J.., 2002. A preliminary investigation concerning the effect of particle shape on powder's flow properties. In world congress on particle technology 4 Sydney, Australia.

Bylaitë, E., Venskutonis, P.R., Mapdpierienë, R., 2001. Properties of caraway (Carum carvi L.) essential oil encapsulated into milk protein-based matrices. Eur. Food Res. Technol. 212, 661–670. doi:10.1007/s002170100297

Castro, N., Durrieu, V., Raynaud, C., Rouilly, A., 2016. Influence of DE-value on the physicochemical properties of maltodextrin for melt extrusion processes. Carbohydr. Polym. 144, 464–473. doi:10.1016/j.carbpol.2016.03.004

Che, L., Li, D., Chen, X.D., 2012. Convective Drying Kinetics of Single Droplets of Aqueous Glucose. Dry. Technol. 30, 1029–1036. doi:10.1080/07373937.2012.663844

Chew, J.H., Liu, W., Fu, N., Gengenbach, T., Chen, X.D., Selomulya, C., 2014. Exploring the drying behaviour and particle formation of high solids milk protein concentrate. J. Food Eng. 143, 186–194. doi:10.1016/j.jfoodeng.2014.07.004

Chronakis, I.S., Kasapis, S., Richardson, R.K., 1996. Small deformation rheological properties of maltodextrin-milk protein systems. Carbohydr. Polym. 29, 137–148. doi:10.1016/0144-8617(96)00014-8

Couchman, P.R., Karasz, F.E., 1978. A Classical Thermodynamic Discussion of the Effect of Composition on Glass-Transition Temperatures. Macromolecules 11, 117–119. doi:10.1021/ma60061a021

Dahbi, L., Alexander, M., Trappe, V., Dhont, J.K.G., Schurtenberger, P., 2010. Rheology and structural arrest of casein suspensions. J. Colloid Interface Sci. 342, 564–570. doi:10.1016/j.jcis.2009.10.042

deWit, J.N., Klarenbeek, G., 1984. Effects of Various Heat Treatments on Structure and Solubility of Whey Proteins. J. Dairy Sci. 67, 2701–2710. doi:10.3168/jds.S0022-0302(84)81628-8

Dokic, P., Jakovljevic, J., Dokic-baucal, L., 1998. Molecular characteristics of maltodextrins and rheological behaviour of diluted and concentrated solutions 141, 435–440. doi:10.1016/S0927-7757(97)00118-0

Donev, A., Cisse, I., Sachs, D., Variano, E.A., Stillinger, F.H., Connelly, R., Torquato, S., Chaikin, P.M., 2004. Improving the Density of Jammed Disordered Packings Using Ellipsoids. Science (80-.). 303, 990 LP-993. doi:10.1126/science.1093010

Dörr, A., Sadiki, A., Mehdizadeh, A., 2013. A discrete model for the apparent viscosity of polydisperse suspensions including maximum packing fraction. J. Rheol. (N. Y. N. Y). 57, 743–765. doi:10.1122/1.4795746

Fäldt, P., Bergenståhl, B., Carlsson, G., 1993. The surface coverage of fat on food powders analyzed by ESCA (electron spectroscopy for chemical analysis). Food Struct. 12, 225–234.

Foerster, M., Gengenbach, T., Woo, M.W., Selomulya, C., 2016. The impact of atomization on the surface composition of spray-dried milk droplets. Colloids Surfaces B Biointerfaces 140, 460–471. doi:10.1016/j.colsurfb.2016.01.012

Fu, N., Woo, M.W., Chen, X.D., 2011. Colloidal transport phenomena of milk components during convective droplet drying. Colloids Surf. B. Biointerfaces 87, 255–66. doi:10.1016/j.colsurfb.2011.05.026

Fu, N., Woo, M.W., Chen, X.D., Fu, N., Woo, M.W., Chen, X.D., 2012a. Single Droplet Drying Technique to Study Drying Kinetics Measurement and Particle Functionality: A Review. Dry. Technol. 30, 1771–1785. doi:10.1080/07373937.2012.708002

Fu, N., Woo, M.W., Moo, F.T., Chen, X.D., 2012b. Microcrystallization of lactose during droplet drying and its effect on the property of the dried particle. Chem. Eng. Res. Des. 90, 138–149. doi:10.1016/j.cherd.2011.06.016

Fu, N., Woo, M.W., Selomulya, C., Chen, X.D., Patel, K., Schuck, P., Jeantet, R., 2012c. Drying kinetics of skim milk with 50 wt.% initial solids. J. Food Eng. 109, 701–711. doi:10.1016/j.jfoodeng.2011.11.018

Fu, X., Huck, D., Makein, L., Armstrong, B., Willen, U., Freeman, T., 2012. Effect of particle shape and size on flow properties of lactose powders. Particuology 10, 203–208. doi:10.1016/j.partic.2011.11.003

Griesing, M., Grosshans, H., Hellwig, T., Sedelmayer, R., Gopireddy, S.R., Pauer, W., Gutheil, E., Moritz, H.-U.U., 2016. Influence of Air Humidity on the Particle Formation of Single

Mannitol-Water Droplets during Drying. Chemie Ing. Tech. 88, 929–936. doi:10.1002/cite.201500087

Haene, P.D., Liederkerke, B. Van, 1996. Viscosity Prediction of Starch Hycirolysates from Single Point Measurements.

Haque, M., Roos, Y., 2004. Water Plasticization and Crystallization of Lactose in Spray-dried Lactose / Protein Mixtures. J. Food Sci. 69.

Haque, M.A., Chen, J., Aldred, P., Adhikari, B., 2015. Drying and denaturation characteristics of whey protein isolate in the presence of lactose and trehalose. Food Chem. 177, 8–16. doi:10.1016/j.foodchem.2014.12.064

Jakubczyk, D., Kolwas, M., Derkachov, G., Kolwas, K., Zientara, M., Jakubczyk, D., 2012. Evaporation of Micro-Droplets : the Radius-Square-Law Revisited 122, 1–23.

Ji, J., Cronin, K., Fitzpatrick, J., Fenelon, M., Miao, S., 2015. Effects of fluid bed agglomeration on the structure modification and reconstitution behaviour of milk protein isolate powders. J. Food Eng. 167, 175–182. doi:10.1016/j.jfoodeng.2015.01.012

Loveday, S.M., Creamer, L.K., Singh, H., Rao, M.A., 2007. Phase and rheological behavior of high-concentration colloidal hard-sphere and protein dispersions. J. Food Sci. 72, 101–107. doi:10.1111/j.1750-3841.2007.00452.x

Lucassen-Reynders, E.H., Benjamins, J., Fainerman, V.B., 2010. Dilational rheology of protein fi lms adsorbed at fl uid interfaces. Curr. Opin. Colloid Interface Sci. 15, 264–270. doi:10.1016/j.cocis.2010.05.002

Maas, S.G., Schaldach, G., Littringer, E.M., Mescher, A., Griesser, U.J., Braun, D.E., Walzel, P.E., Urbanetz, N.A., 2011. The impact of spray drying outlet temperature on the particle morphology of mannitol. Powder Technol. 213, 27–35. doi:10.1016/j.powtec.2011.06.024

Malafronte, L., Ahrné, L., Schuster, E., Innings, F., Rasmuson, A., 2015. Exploring drying kinetics and morphology of commercial dairy powders. J. Food Eng. 158, 58–65. doi:10.1016/j.jfoodeng.2015.02.029

Manoj, P., Kasapis, S., Chronakis, I.S., 1996. Gelation and phase separation in maltodextrin-caseinate systems. Food Hydrocoll. 10, 407–420. doi:10.1016/S0268-005X(96)80019-1

Meerdink, G., van't Riet, K., 1995. Modeling segregation of solute material during drying of liquid foods. AIChE J. 41, 732–736. doi:10.1002/aic.690410331

Meng, F., Doi, M., Ouyang, Z., 2014. Cavitation in Drying Droplets of Soft Matter Solutions. Phys. Rev. Lett. 113, 098301. doi:10.1103/PhysRevLett.113.098301

Moejes, S.N., Visser, Q., Bitter, J.H., van Boxtel, A.J.B., 2018. Closed-loop spray drying solutions for energy efficient powder production. Innov. Food Sci. Emerg. Technol. 47, 24–37. doi:10.1016/j.ifset.2018.01.005

Molinero, V., Çağin, T., Goddard, W.A., 2003. Sugar, water and free volume networks in concentrated sucrose solutions. Chem. Phys. Lett. doi:10.1016/S0009-2614(03)01170-9

Mujumdar, A.S., 2015. Handbook of Industrial Drying, Drying Technology. CRC press. doi:10.1080/00222338708074452

Nuzzo, M., Millqvist-Fureby, A., Sloth, J., Bergenstahl, B., 2015a. Surface Composition and Morphology of Particles Dried Individually and by Spray Drying. Dry. Technol. 3937, 141217112010003. doi:10.1080/07373937.2014.990566

Nuzzo, M., Sloth, J., Bergenståhl, B., Millqvist-fureby, A., 2017. The morphology and internal composition of dried particles from whole milk — From single droplet to full scale drying. Food Struct. 13, 35–44. doi:10.1016/j.foostr.2017.02.001

Nuzzo, M., Sloth, J., Brandner, B., Bergenstahl, B., Millqvist-Fureby, A., 2015b. Confocal Raman microscopy for mapping phase segregation in individually dried particles composed of lactose and macromolecules. Colloids Surfaces A Physicochem. Eng. Asp. 481, 229–236. doi:10.1016/j.colsurfa.2015.04.044

Parker, R., Noel, T.R., Brownsey, G.J., Laos, K., Ring, S.G., 2005. The Nonequilibrium Phase and Glass Transition Behavior of β-Lactoglobulin. Biophys. J. 89, 1227–1236. doi:10.1529/biophysj.105.064246

Pauchard, L., Couder, Y., 2004. Invagination during the collapse of an inhomogeneous spheroidal shell. Europhys. Lett. 66, 667–673. doi:10.1209/epl/i2003-10242-8

Perdana, J., Bereschenko, L., Fox, M.B., Kuperus, J.H., Kleerebezem, M., Boom, R.M., Schutyser, M.A.I., 2013a. Dehydration and thermal inactivation of Lactobacillus plantarum WCFS1: Comparing single droplet drying to spray and freeze drying. Food Res. Int. 54, 1351–1359. doi:10.1016/j.foodres.2013.09.043

Perdana, J., Fox, M.B., Schutyser, M.A.I., Boom, R.M., 2013b. Mimicking Spray Drying by Drying of Single Droplets Deposited on a Flat Surface. Food Bioprocess Technol. 6, 964–977. doi:10.1007/s11947-011-0767-4

Perdana, J., Fox, M.B., Schutyser, M.A.I., Boom, R.M., 2011. Single-Droplet Experimentation on Spray Drying: Evaporation of a Sessile Droplet. Chem. Eng. Technol. 34, 1151–1158. doi:10.1002/ceat.201100040

Perdana, J., van der Sman, R.G.M., Fox, M.B., Boom, R.M., Schutyser, M.A.I., 2014. Measuring and modelling of diffusivities in carbohydrate-rich matrices during thin film

drying. J. Food Eng. 122, 38–47. doi:10.1016/j.jfoodeng.2013.08.033

Qiu, J., Boom, R.M., Schutyser, M.A.I., 2018. Agitated thin-film drying of foods. Dry. Technol. 0, 1–10. doi:10.1080/07373937.2018.1458037

Ranz, W.E., Marshall, W.R., 1952. Evaporation from drops - Part 1. Chem. Eng. Prog. doi:10.1016/S0924-7963(01)00032-X

Rogers, S., Duo, W., Xu, S., Lin, Q., Dong, X., 2012. Particle shrinkage and morphology of milk powder made with a monodisperse. Biochem. Eng. J. 62, 92–100. doi:10.1016/j.bej.2011.11.002

RVO, 2015. Best Practice Droogprocessen, https://www.rvo.nl/sites/default/files/2015/10/Best practise Droogprocessen oktober 2015.pdf.

Sadek, C., Li, H., Schuck, P., Fallourd, Y., Pradeau, N., Le Floch-Fouéré, C., Jeantet, R., 2014. To What Extent Do Whey and Casein Micelle Proteins Influence the Morphology and Properties of the Resulting Powder? Dry. Technol. 32, 1540–1551. doi:10.1080/07373937.2014.915554

Sadek, C., Pauchard, L., Schuck, P., Fallourd, Y., Pradeau, N., Le Floch-Fouéré, C., Jeantet, R., 2015a. Mechanical properties of milk protein skin layers after drying: Understanding the mechanisms of particle formation from whey protein isolate and native phosphocaseinate. Food Hydrocoll. 48, 8–16. doi:10.1016/j.foodhyd.2015.01.014

Sadek, C., Schuck, P., Fallourd, Y., Pradeau, N., Jeantet, R., Le Floch-Fouéré, C., 2016. Buckling and collapse during drying of a single aqueous dispersion of casein micelle droplet. Food Hydrocoll. 52, 161–166. doi:10.1016/j.foodhyd.2015.06.016

Sadek, C., Schuck, P., Fallourd, Y., Pradeau, N., Le Floch-Fouéré, C., Jeantet, R., 2015b. Drying of a single droplet to investigate process–structure–function relationships: a review. Dairy Sci. Technol. 95, 771–794. doi:10.1007/s13594-014-0186-1

Sadek, C., Tabuteau, H., Schuck, P., 2013. Shape, Shell, and Vacuole Formation during the Drying of a Single Concentrated Whey Protein Droplet. Langmuir.

Schuck, P., Blanchard, E., Dolivet, A., Méjean, S., Onillon, E., Jeantet, R., 2005. Water activity and glass transition in dairy ingredients. Open acces. doi:10.1051/lait

Schuck, P., Jeantet, R., Bhandari, B., Chen, X.D., Tuler, Í., Carvalho, A.F. De, Fenelon, M., Kelly, P., 2016. Recent advances in spray drying relevant to the dairy industry : A comprehensive critical review 3937. doi:10.1080/07373937.2016.1233114

Schutyser, M.A.I., Both, E.M., Siemons, I., Vaessen, E.M.J., Zhang, L., 2018. Gaining insight on spray drying behavior of foods via single droplet drying analyses. Dry. Technol. 0,

1–10. doi:10.1080/07373937.2018.1482908

Schutyser, M.A.I.I., Perdana, J., Boom, R.M., 2012. Single droplet drying for optimal spray drying of enzymes and probiotics. Trends Food Sci. Technol. 27, 73–82. doi:10.1016/j.tifs.2012.05.006

Sman, R.G.M. Van Der, Meinders, M.B.J., 2013. Moisture diffusivity in food materials 138, 1265–1274.

Sman, R.G.M. Van Der, Meinders, M.B.J., 2012. Supplementary Material to : Moisture diffusivity in food materials 1–11.

Soesanto, T., Williams, M.C., 1981. Volumetric Interpretation of Viscosity for Concentrated and Dilute Sugar Solutions 3338–3341. doi:10.1021/j150622a026

Sopade, P.A., Halley, P., Bhandari, B., D'Arcy, B., Doebler, C., Caffin, N., 2003. Application of the Williams-Landel-Ferry model to the viscosity-temperature relationship of Australian honeys. J. Food Eng. 56, 67–75. doi:10.1016/S0260-8774(02)00149-8

Sperling, 2001. Introduction to physical polymer science, 3rd ed. Wiley.

Spurlin, H.M., Martin, A.F., Tennent, H.G., 1946. Characterization of cellulose derivatives by solution properties: plasticizers as solvents. J. Polym. Sci. Part A Polym. Chem. 1, 63–74.

Sugiyama, Y., Larsen, R.J., Kim, J.-W., Weitz, D. a, 2006. Buckling and crumpling of drying droplets of colloid-polymer suspensions. Langmuir 22, 6024–30. doi:10.1021/la053419h

Takeiti, C.Y., Kieckbusch, T.G., Collares-Queiroz, F.P., 2010. Morphological and Physicochemical Characterization of Commercial Maltodextrins with Different Degrees of Dextrose-Equivalent. Int. J. Food Prop. 13, 411–425. doi:10.1080/10942910802181024

Tourneur, T., Broqueville, A. de, Wilde, J. De, 2018. Experimental and CFD study of multi-zone vortex chamber spray dryers, in: International Symposium on Chemical Reactor Engineering-ISCRE 25.

Tran, T.T.H., Avila-Acevedo, J.G., Tsotsas, E., 2016. Enhanced methods for experimental investigation of single droplet drying kinetics and application to lactose/water. Dry. Technol. 34, 1185–1195. doi:10.1080/07373937.2015.1100202

Tran, T.T.H., Jaskulski, M., Avila-Acevedo, J.G., Tsotsas, E., 2017. Model parameters for single-droplet drying of skim milk and its constituents at moderate and elevated temperatures. Dry. Technol. 35, 444–464. doi:10.1080/07373937.2016.1182548

Tsapis, N., Dufresne, E.R., Sinha, S.S., Riera, C.S., Hutchinson, J.W., Mahadevan, L., Weitz, D.A., 2005. Onset of buckling in drying droplets of colloidal suspensions. Phys. Rev. Lett. 94, 1–4. doi:10.1103/PhysRevLett.94.018302

Turchiuli, C., Eloualia, Z., El Mansouri, N., Dumoulin, E., 2005. Fluidised bed agglomeration: Agglomerates shape and end-use properties. Powder Technol. 157, 168–175. doi:10.1016/j.powtec.2005.05.024

Ullum, T., Sloth, J., Brask, A., Wahlberg, M., 2017. Predicting Spray Dryer Deposits by CFD and an Empirical Drying Model Predicting Spray Dryer Deposits by CFD and an Empirical Drying Model 3937. doi:10.1080/07373931003799319

van der Sman, R.G.M., Meinders, M.B.J., 2011. Prediction of the state diagram of starchwater mixtures using the Flory–Huggins free volume theory. Soft Matter 7, 429–442. doi:10.1039/C0SM00280A

Vehring, R., 2008. Pharmaceutical particle engineering via spray drying. Pharm. Res. 25, 999–1022. doi:10.1007/s11095-007-9475-1

Vehring, R., Foss, W.R., Lechuga-Ballesteros, D., 2007. Particle formation in spray drying. J. Aerosol Sci. 38, 728–746. doi:10.1016/j.jaerosci.2007.04.005

Walstra, P., Jenness, R., Badings, H.T., 1984. Dairy chemistry and physics. Wiley.

Walton, D.E.E., Mumford, C.J.J., 1999. The Morphology of Spray-Dried Particles. Chem. Eng. Res. Des. 77, 442–460. doi:10.1205/026387699526296

Weeks, E.R., 2017. Introduction to the colloidal glass transition. ACS Macro Lett. 6, 27–34. doi:10.1021/acsmacrolett.6b00826

Williams, M.L., Landel, R.F., Ferry, J.D., 1955. The Temperature Dependence of Relaxation Mechanisms in Amorphous Polymers and Other Glass-forming Liquids. J. Am. Chem. Soc. 77, 3701–3707. doi:10.1021/ja01619a008

Wu, W.D., Liu, W., Gengenbach, T., Woo, M.W., Selomulya, C., Chen, X.D., Weeks, M., 2014. Towards spray drying of high solids dairy liquid: Effects of feed solid content on particle structure and functionality. J. Food Eng. 123, 130–135. doi:10.1016/j.jfoodeng.2013.05.013

Yarin, A.L., Brenn, G., Kastner, O., Rensink, D., Tropea, C., 1999. Evaporation of acoustically levitated droplets 399, 151–204.

S

Summary

Spray drying is widely applied in food industry to convert liquid formulations into powders to facilitate transport and extend their shelf-life. Spray dried powders have superior quality due to their excellent reconstitution behavior and the relative mild drying process which preserves product quality. One of the key factors in determining product quality is the morphology of the primary powder particle, which influences reconstitution behavior and flowability. However, the complex phenomenon of morphology development, especially as function of material composition and drying conditions, has not been topic of in-depth scientific study. Better understanding of morphology development is expected not only to contribute to improved powder quality, but also to improved efficiency of spray drying operations. Specifically, lack of control on particle formation and stickiness behavior increases risk of fouling in spray drying towers, which leads to extended downtime and loss of material. The main objective of the research in this thesis was thus to create mechanistic understanding of morphology development of drying droplets, which was divided in two main research questions:

1) How are skin formation and subsequent morphology development affected by the drying conditions or product formulation?
2) Can the rheological properties of components at high concentration explain the morphology development during drying?

To answer these research questions multiple methods were employed. Single droplet drying was used to observe morphology development, thin film drying was used to study skin formation and its effect on drying kinetics, and rheology was used to measure properties of model components. Finally, pilot-scale experiments were done to translate findings of this research to larger-scale spray drying.

In **chapter 2** the influence of drying temperature and droplet composition on the formed particle morphology was studied for model components whey protein and maltodextrin DE12. It was observed that after a period of constant drying rate, the particle morphologies evolve in interaction with droplet composition and drying temperature. Droplets with a high concentration of protein yielded smooth and hollow particles, whereas particles with more maltodextrin were wrinkled and had multiple smaller vacuoles. Particles dried at lower temperatures were more likely to form hollow particles, whereas particles dried at higher temperature had the tendency to become wrinkled with fixed ratio of maltodextrin to whey

protein. It was hypothesized that hollow particle formation at lower temperatures is related to phase separation of the individual components. This was confirmed by Confocal Raman Imaging, where it was observed that at lower temperatures (40°C) demixing occurred and at higher temperature (90°C) the system was well mixed.

This work was extended with the drying of micellar casein and lactose, and eventually to the drying of whole milk in **chapter 3**. It was found that the influence of carbohydrates (lactose and maltodextrin DE12) and proteins (micellar casein or whey protein) on morphology development is very different, since upon concentration protein systems will jam and undergo a colloidal glass transition, whereas carbohydrate systems will gradually increase in viscosity as a consequence of the concentration. Whey protein gives relatively rigid shells due to jamming of the 'hard sphere' proteins, while casein micelles behave as 'soft spheres' that can deform after jamming, which gives flexibility to the shell during drying. The influence of the carbohydrates on the final morphology was found much larger than the influence of the proteins. Caseins influenced morphology only in mixtures with lactose at higher concentrations due to its high voluminosity. Similar observations were done for whole milk, where fat appeared to have no influence and the morphology was mainly determined by the presence of casein. In casein and maltodextrin mixtures it was observed that maltodextrin subtly influenced particle morphology via the shape and smoothness of wrinkles.

In **chapter 4** the work on maltodextrin and whey protein was continued, however this time the effect of initial droplet size and dry matter content was studied. Especially, the latter provided insight on the skin formation during drying, and therefore these results were combined with viscosity measurements. Shear rate sweeps showed jamming of the whey protein at concentrations of ~50% (w/w), whereas maltodextrin remained liquid-like up to concentrations of ~70% (w/w). Morphology development of the latter components during single droplet drying showed that it could be influenced by altering initial droplet size and dry matter content. If droplets had a high initial dry matter (50% (w/w) morphology development started immediately, and the formed morphology could be related to the rheological behavior of the mixture at that concentration. This indicated that measuring the rheological properties at high concentrations can provide insight in morphology development.

In **chapter 5** a different approach was chosen to understand the drying behavior, using thin films as a model system. First, the drying kinetics were measured using a specially developed thin film dryer. Subsequently, the viscoelastic properties of nearly dried films were studied. Drying kinetics of thin films were monitored in a custom-built drying equipment. Subsequently, the rheological properties of equilibrated thin films were assessed by oscillatory shear measurements at relevant high dry matter contents (66-82 w/w%). During drying, the samples high in whey protein formed brittle films and had lower evaporation rates, compared to films high in maltodextrin. From rheology analysis it was observed that for whey protein rich (>25%) systems, the samples were in structural arrest at the dry matter contents measured. Maltodextrin on the other hand showed typical viscoelastic polymer behavior, although as little as 1% addition of whey protein altered the viscoelastic properties drastically. Lastly, these properties were related to vacuole formation during single droplet drying: samples that undergo structural arrest at a lower dry matter content, i.e. high in whey protein, will form less and larger vacuoles compared to samples that undergo structural arrest only at high concentration, i.e. high in maltodextrin.

Finally, the results from our single droplet drying research were compared with the morphology development in a pilot scale spray dryer in **chapter 6**. This showed the importance of looking at drying from a product perspective, and emphasized the industrial relevance of the project. A pilot scale single stage spray dryer was used with a maximum evaporation capacity of 80 kg/h. The effect of composition on morphology was studied by drying maltodextrin DE12, whey protein, and mixtures thereof with a ratio of 75:25 and 50:50 (WP:MD). The analysis was carried out with the Malvern Morphologi 4 analyzer. The morphologies observed in pilot scale drying were similar to the observations seen in single droplet drying, which showed the usefulness of this method, despite the different time scales of drying. This shows that component properties and interactions play a more important role than the drying conditions, and shows the relevancy of the single droplet drying methods for observing morphology development. Moreover, altering the drying conditions (specifically reducing the inlet air temperatures) could increase the number of wrinkled particles from 19% to 34% for a 75:25 (WP:MD) powder, which showed that morphology could be steered by the drying conditions.

In summary, the combined approach of single droplet drying and rheology showed great value in understanding morphology development in spray drying, despite the longer drying times in single droplet versus spray drying. Using this approach it was shown that morphology depended greatly on the component properties, and could be steered by altering the drying conditions. This knowledge can be applied in industry to steer their spray drying operations better on powder morphology and thus resulting powder properties. This know-how can also be exploited to develop new strategies to mitigate risk of fouling, where for example earlier locking influences stickiness. Outlook for further research could be directed at developing single droplet drying methods with small droplet size, relating the morphology to powder properties using pilot-scale spray drying studies, and modifying protein properties to steer powder functionality.

Acknowledgements

I cannot believe that I am now writing my acknowledgements. The past years have gone by so quickly and now my PhD life is almost over. I am very proud on the work done, but I cannot take all the credits. So, I would like to thank the many people who helped me! First of all I would like to thank my promotors. Maarten, thank you for guiding me in becoming an independent scientist and for keeping me on track. I have learned so much from you! Remko, your enthusiasm and ideas were always an inspiration (and sometimes a distraction).

Martin, the droplet dryer only worked when you were in the lab, so thank you for all your help! I could not have developed the thin film dryer without Jos and the team of the technical workshop, in particular Eric and Johan. Thank you Maurice for your help with microscopy, and Jan-Eise for your help with Matlab. Wouter, Jarno, Marjan and Ilona, thank you for the numerous little things you have arranged for me! I would also like to thank ISPT and the involved company representatives; your critical questions and expertise have made this project better. Marine Nuzzo, Anna Fureby, and Birgit Brandner thank you for the pleasant collaboration. And of course I would like to thank all of my thesis students for their help with the experimental work: Loes, Tim, Eva, Ruixi, Danica, Ruurd, Aysha, Bart, Sabien, Marit and Saskia. I have really enjoyed supervising you!

To my dear colleagues at FPE: you have made my time here very enjoyable and I have learned a lot from you. PhD life would not have been the same without the discussions with my roommates, group meetings, lunch walks, borrels, help in the lab, game nights, and much more. So thank you all! Isabel, your enthusiasm when starting your PhD reminded me of mine, so working with you has been a great pleasure!

Lastly I would like to thank my family and friends for their support; I am happy I could share my successes and frustrations with you. Dear Joep, thank you for being so supportive and I am so excited to spend the rest of my life with you!

About the author

Eline Verbaanderd-Both was born on May 5 1990 in Emmen, the Netherlands. She attended Hondsrug College in Emmen, where she obtained her VWO diploma in 2008. After this she started her bachelor studies in Food Technology at Wageningen university. Eline conducted her bachelor thesis in the laboratory of Food Process Engineering (FPE) on the extraction of isoflavones from okara, and with that completed the bachelor program in 2011.

In 2011 she continued with the master Food Technology with a specialization in Sustainable Food Process Engineering. For the master thesis Eline returned to the FPE group, where she worked on membrane filtration. For her internship she moved to Melbourne, Australia, to work on Simulated Moving Bed Chromatography at CSIRO. After this Eline completed a second master thesis on blood coagulation in microchannels at the Stone group of Princeton University, USA. She obtained her master diploma in 2014, and started as a PhD candidate in the FPE group of Wageningen University. During this research Eline worked on understanding morphology development during spray drying, and the results of this research are described in this thesis.

Contact: eline.both@gmail.com

List of publications

Both, E.M., Karlina, A.M., Boom, R.M., Schutyser, M.A.I., 2018. Morphology development during sessile single droplet drying of mixed maltodextrin and whey protein solutions. Food Hydrocoll. 75, 202–210.

Both, E.M., Nuzzo, M., Millqvist-Fureby, A., Boom, R.M., Schutyser, M.A.I., 2018. Morphology development during single droplet drying of mixed component formulations and milk. Food Res. Int. 109, 448–454.

Schutyser, M.A.I., **Both, E.M.,** Siemons, I., Vaessen, E.M.J., Zhang, L., 2018. Gaining insight on spray drying behavior of foods via single droplet drying analyses. Dry. Technol. 0, 1–10.

Both, E.M., Siemons, I., Boom, R.M., Schutyser, M.A.I., 2019. The role of viscosity in morphology development during single droplet drying. Food Hydrocoll. 94, 510–518.

Both, E.M., Tersteeg, S.M.B., Boom, R.M., Schutyser, M.A.I., Drying kinetics and viscoelastic properties of concentrated thin films as a model system for spray drying. *Submitted for publication.*

Both, E.M., Boom, R.M., Schutyser, M.A.I., Controlling particle morphology and powder properties during spray drying of maltodextrin and whey protein mixtures. *Submitted for publication.*

Overview of completed training activities

Discipline specific activities

Courses

Spray, fluid bed and belt drying (IP&D, Amersfoort, NL)	2014
Multivariate analysis for food sciences (VLAG, Wageningen, NL)	2014
Numerical methods for chemical engineers (OSPT, Eindhoven, NL)	2015
15th European school on Rheology (KU Leuven, Leuven, BE)	2015
Modelling and Simulation of Food School (Viprofood, Capri, IT)	2016
Membrane concentration (NIZO, Ede, NL)	2017

Conferences

NWGD symposium (Wageningen, NL) [a,b]	2014-2018
Droplets (Enschede, NL) [a]	2015
Eurodrying (Liège, BE) [b]	2017
NIZO Dairy conference (Papendal, NL) [c]	2017
Food Structure and Functionality Forum (Montreal, CA) [c]	2018
International Drying symposium (Valencia, SP) [a]	2018

General courses

PhD week (VLAG)	2015
Effective behaviour in your professional surroundings (WGS)	2015
Mobilizing your scientific network (WGS)	2015
Supervising students (ESD)	2016
Scientific writing (WGS)	2017
PhD workshop carousel (PR)	2017
Process Economics and cost engineering (OSPT)	2017
Career perspectives (WGS)	2018

Optional courses and activities

FPE weekly meetings [b]	2014-2019
PhD study tour Germany and Switzerland [a,b]	2016
PhD study tour Canada [c]	2018

[a] Poster presentation, [b] Oral presentation, [c] Pitch and poster presentation;
NL: the Netherlands, BE: Belgium, IT: Italy, CA: Canada, SP: Spain.

The work presented in this thesis has been carried out in the framework of the Institute of Sustainable Process Technology (ISPT) under the project “DR-20-04: Droplets modelling”

Cover design by Tim Jacobs || Identim
Printed by Digiforce || ProefschriftMaken